

Comparing the latest galaxy observations with current dark matter models

Victor Hugo Robles Sánchez

CINVESTAV

September 22, 2015

“The freedom of thought is key to be creative”.

Victor H. Robles

AGRADECIMIENTOS

- A mis padres Julio Robles Lara y Ofelia Sánchez González, así como a mis hermanos que me han apoyado en mi carrera.
- A mi director de tesis, Dr. Tonatiuh Matos Chassin, por su todo su apoyo que llevo a la realización de esta tesis.
- A CONACyT por proveer los recursos necesarios para realizar este trabajo.
- A la Escuela Superior de Física y Matemáticas (ESFM) del IPN por brindarme las bases del conocimiento que me permitieron seguir adelante.
- Al Departamento de Física del Centro de Investigación y de Estudios Avanzados (CINVESTAV) del IPN por brindarme la formación científica.
- A James S. Bullock y Philip Hopkins por darme la oportunidad de formar parte de su grupo de trabajo.
- A todos mis compañeros, amigos, profesores, colegas nacionales y en el extranjero, y a mis familiares que han contribuido a mi actual desarrollo personal y profesional.

VICTOR HUGO ROBLES SÁNCHEZ

Contents

Resumen	V
Abstract	VIII
1 Introduction	1
The Friedmann equations	3
Overview of dark matter models	8
2 Current status of the ΛCDM model	11
Initial fluctuations in the matter-dominated era	11
Large scale structure in CDM	14
Testing CDM with dwarf galaxies	18
2.3.1 Cusp-core problem	18
2.3.2 Missing satellite problem	22
2.3.3 The Local Group: Too-Big-to-Fail	24
2.3.4 Alignment of satellite galaxies in MW and M31	26
Baryons to the rescue, or not?	27
3 Scalar field dark matter	33
The quantum dark matter paradigm	33

Cosmology in SFDM	36
3.2.1 Cosmological evolution of a scalar field with $V(\Phi) = m^2\Phi^2/2$	40
3.2.2 Cosmological evolution of a SF with self-interactions.	41
Density perturbations	47
Linear growth of scalar field perturbations	53
Halo Mass function and Power Spectrum	55
Spontaneous symmetry break	62
3.6.1 Quantum and thermal corrections in Minkowski space-time	65
3.6.2 Thermal corrections in FRW universe	69
3.6.3 Analytical solution for SFDM halos	70
4 Consequences of SFDM in galaxies	75
SFDM halos in equilibrium	75
LSB and dwarf galaxies	80
Tidal Stripping in SFDM halos	87
Rings and shells in early type galaxies	95
Galaxy formation scenario in SFDM haloes	98
5 Self interacting dark matter	101
Satellites in SIDM halos	102
Too-Big-to-Fail in SIDM	106
6 Conclusions	115

RESÚMEN

La cosmología actual se encuentra en una etapa de observaciones de alta precisión capaces de poner a prueba nuestro conocimiento acerca de la formación y evolución de las galaxias. Gracias a los avances numéricos se pueden simular procesos astrofísicos como explosiones de supernovas, radiación por vientos estelares, formación estelar entre otros. Así mismo permiten estudiar la dinámica entre la componente visible de materia y la presunta materia oscura responsable de mantener estables a las galaxias. Recientemente las observaciones han revelado algunas discrepancias difíciles de explicar de acuerdo con lo esperado teóricamente del modelo estándar de materia oscura fría, esto ha dado entrada a reconsiderar nuevas alternativas de materia oscura en busca de una solución a los problemas del modelo que a su vez sea compatible con los éxitos del modelo estándar, por ejemplo, la materia oscura con auto interacción o el modelo de materia oscura como un campo escalar ultra ligero. En esta tesis se abordan las consecuencias sobre los perfiles de densidad y distribución de materia en galaxias de diferente morfología que resultan de asumir un campo escalar ultra ligero como materia oscura. Se propone un modelo semi analítico de formación de halos y se estudia numéricamente los efectos en la evolución del gas alrededor de galaxias tardías debidos a la naturaleza cuántica del campo escalar que conforma los halos en los que éstas residen. Se comparan nuestros resultados con las últimas observaciones en galaxias y determinamos la validez del modelo de materia oscura escalar como alternativa, además se estudian algunas soluciones propuestas a las discrepancias en el contexto de materia oscura auto interactuante. Ante la gran atención que ha recibido el modelo por reproducir exitosamente las observaciones de estructura a gran escala, es relevante estudiar y probar la consistencia del modelo en escalas galácticas así como proveer una descripción de las discrepancias que siguen presentes en el modelo estándar en donde las soluciones dependen fuertemente de procesos astrofísicos que aun son fuente de debate, en vista de la gran cantidad de datos de mayor precisión en misiones futuras enfocadas al estudio de la evolución de galaxias es importante conocer si el modelo de materia oscura escalar ofrece explicaciones a las actuales observaciones y seguir no solo como un candidato viable de la materia oscura, si no incluso mejorar el conocimiento actual sobre la formación de nuestro universo.

ABSTRACT

Current cosmology is facing an epoch where high resolution observations and large data sets can be used to test our actual understanding of galaxy formation and their evolution. Numerical simulations are now able to track different astrophysical processes such as feedback from stellar evolution, radiation pressure, star formation among others. At the same time they serve to study the interplay of visible matter component and the assumed dark matter required to form galaxies. Recently, some observations have revealed discrepancies from the expected results found in the standard cold dark matter model, this has led to reconsider new dark matter alternatives that share the successes of the standard model and that offer attractive solutions to such discrepancies, for instance, the self-interacting dark matter and the ultra light scalar field dark matter model. In this thesis we focus on the consequences of assuming an ultra light scalar field as the dark matter on the density profiles and matter distribution in galaxies of different morphology. We propose a semi-analytic model for halo formation and study numerically the effects due to the quantum nature of the scalar field on the surrounding gas in late type galaxies that reside in scalar field dark matter halos. We compare our results with recent galaxy observations and determine the viability of the scalar field model as a dark matter alternative, we also study some proposed solutions in the context of self-interacting dark matter. Given the attention that the model has received for the successful description of the large scale structure, it is relevant to study and test the consistency of the scalar field model in the galactic scale as well as to provide a description to the problems that persist in the standard model of cosmology where the solutions are strongly dependent in astrophysical processes that are still subject to debate. In the advent of high-precision data sets from several galaxy surveys it is the time to assess the explanations offered by the scalar field dark matter model if it wants not only to continue as a viable dark matter candidate that describes our universe.

CHAPTER 1

INTRODUCTION

One of the great mysteries of the universe is how galaxies came to be as we observe them now. For a long time this question has triggered the curiosity of several scientists, through time the acquisition of data at different scales became larger and more precise that now a fair amount of evidence from observations of supernovae, galaxy rotation curves, gravitational lensing, offset in mass and light distribution, large scale structure, and the cosmic microwave background (CMB) seem to indicate that there exist other forms of matter besides the one we can directly observe, one is the dark matter responsible of galaxy formation, and the second is dark energy believed to drive the current accelerated expansion of the universe.

The observations support the *Cosmological Principle*(CP), which states that the universe is homogeneous and isotropic at sufficiently large scales, from the CMB we observe that deviations from isotropy are of order 10^{-5} . In order to obtain such degree of homogeneity we require to assume *Inflation*, a phase of exponential expansion in the early universe($\approx 10^{-35}$ seconds after the big bang) that smooths out any previous inhomogeneities. If we add to these hypotheses the assumption of an initial Gaussian field to generate the initial primordial perturbations that will expand enough to form the seeds that will lead to the large-scale structure and galaxies, then we end with the standard model of cosmology known as cold dark matter¹(CDM).

The standard model is complemented with a galaxy formation scenario known as the hierarchical model. In this model galaxies are assembled by mergers, that is, massive galaxies accrete less massive galaxies and grow in size and mass, this galactic cannibalism

¹The standard model also takes into account the cosmological constant Λ , we will simply denote it as CDM.

repeats several times in the lifetime of the most massive galaxies, the rate of accretion and galaxy interactions depend on the environment surrounding a given initial overdensity region, it is then expected that galaxies in denser regions undergo collisions with galaxies of different masses more frequently. To get a more realistic description of how galaxies evolve in time we require getting as much information as possible of the factors that determine its evolution, for instance, the total mass of gas and stars, stellar supernovae feedback, its angular momentum etc., in order to account for all these complex processes we need to have numerical simulations that are able to track the interplay of all these aspects. It is important to notice that the implementation of algorithms that mimic the above astrophysical processes are still in development and strongly depend on our current understanding on the given process. With this in mind, the results of galaxy formation from numerical simulations should be interpreted with caution.

On the other hand, on large scales the numerical simulations of galaxy formation have been able to reproduce the observed web-like galaxy distribution when the dark matter is assumed to be collisionless and with negligible velocity dispersion which gives the name of “cold” dark matter. Reproducing the large-scale structure is one of the main successes of CDM (see Figure 1). At scale of ≈ 150 Mpc the Sloan Digital Sky Survey (SDSS) has found irregularities in the galaxy density on the level of a few percent[Hogg et al. (2005)], however, the geometry of the universe shows only small deviations from the homogeneous and isotropic background at the scale of few Mpc, so that large scales² can be safely considered as few Mpc. At this scale the baryonic processes do not play a major role to determine the evolution of the universe, what drives the expansion is the total matter content, as we will mention below the visible matter doesn’t seem to be the dominant mass component and for this reason baryons³ are frequently neglected in cosmological simulations.

Given the importance in cosmology of the CMB and large-scale structure distributions, they provide a means to test different models. The important statistic for these two cases is the *two-point function*, called the *power spectrum* in Fourier space. If \bar{n} is the mean

²In cosmology a convenient unit of distance is parsecs with $1 \text{ pc} = 3.261 \text{ light years} = 3.085 \times 10^{16} \text{ m}$.

³As a convention, baryons, hadrons and charged leptons are all termed *baryons*, this is a short name for the known particles of the standard model of elementary particles.

density of the galaxies, then we can characterize the inhomogeneities with $\delta(\mathbf{x}) = (n - \bar{n})/\bar{n}$ or $\tilde{\delta}(\mathbf{k})$. The power spectrum $P(k)$ is defined

$$\langle \tilde{\delta}(\mathbf{k})\tilde{\delta}(\mathbf{k}') \rangle = (2\pi)^3 P(k) \delta^3(\mathbf{k} - \mathbf{k}'). \quad (1.1)$$

The angular brackets denote average over the whole distribution, δ^3 is the Dirac delta function which constrains $\mathbf{k} = \mathbf{k}'$. Equation (1.1) indicates that the power spectrum is the spread, or variance, in the distribution, then it will be small if the distribution is smooth, whereas it is large if there are several extremely under- and overdense regions. It gives information about the clumpiness on scales $k \propto 1/(\text{length})$. In Fig. 1.1 we observe that dark matter is necessary to describe observational data.

§1.1 The Friedmann equations

Our universe can be described by a four-dimensional spacetime (M, g) given by a pseudo-Riemannian manifold M with metric g . The CP implies that the spacetime admits a slicing into homogeneous and isotropic, maximally symmetric, 3-spaces. This selection gives a preferred geodesic time coordinate t , called cosmic or physical time, such that the 3-spaces of constant time are maximally symmetric spaces, hence spaces of constant curvature. The metric with these properties is the Robertson-Walker metric

$$ds^2 = -c^2 dt^2 + a^2(t) \left[\frac{dr^2}{1 - Kr^2} + r^2(d\theta^2 + \sin^2\theta d\varphi^2) \right]. \quad (1.2)$$

The function $a(t)$ is called the scale factor and K is the curvature of the 3-space. For a different sign of K the space is locally isometric to a 3-Sphere ($K > 0$), a three-dimensional pseudo-sphere ($K < 0$) or a flat Euclidean space ($K = 0$). We will follow the convention to normalize the scale factor such that today $a_0 = 1$. Another frequently used time coordinate is called the conformal time, τ , and it is related to t by $a dt = d\tau$, so that the metric becomes

$$ds^2 = a^2(\tau) \left[-c^2 dt^2 + \frac{dr^2}{1 - Kr^2} + r^2(d\theta^2 + \sin^2\theta d\varphi^2) \right]. \quad (1.3)$$

This metric can be used to describe the observed expanding Universe along with the Einstein's equations of general relativity that determine the evolution of the Universe

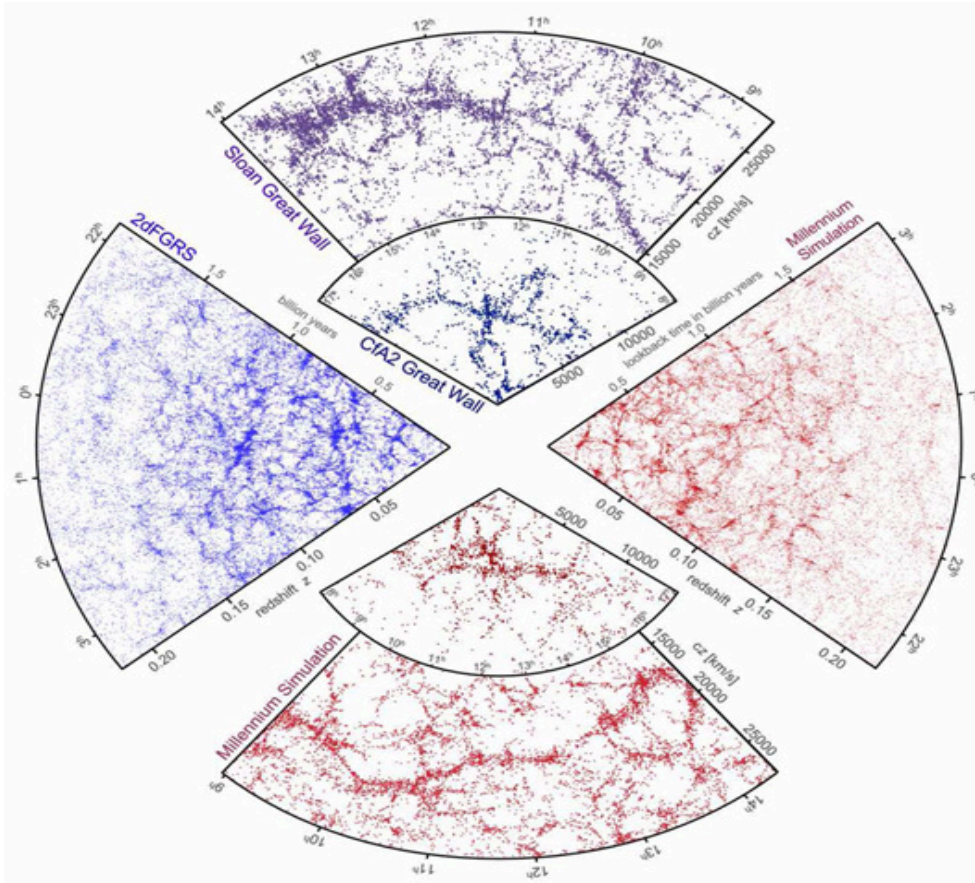


Figure 1.1: The galaxy distribution obtained from spectroscopic redshift surveys and from mock catalogues constructed from cosmological simulations. The top slice shows the immense galaxy filament, one of the largest known superstructures in the observable universe, known as the “Great Wall” , with the Coma cluster at the center. Also shown is a small section of the Sloan Digital Sky Survey (SDSS), in which an even larger “Sloan Great Wall” has been identified, containing over 10,000 galaxies and stretching over more than 1.37 billion light years. On the left it is shown one-half of the Two-degree-Field Galaxy Redshift Survey (2dFGRS), which determined distances to more than 220,000 galaxies in the southern sky out to a depth of 2 billion light years. The SDSS has a similar depth but a larger solid angle and currently includes over 650,000 observed redshifts in the northern sky. For comparison, the bottom and right panels show mock galaxy surveys from the "Millennium" simulation constructed using semi-analytic techniques to simulate the formation and evolution of galaxies within the evolving dark matter distribution, these patches were selected with matching survey geometries and magnitude limits[Springel et al.(2006)]

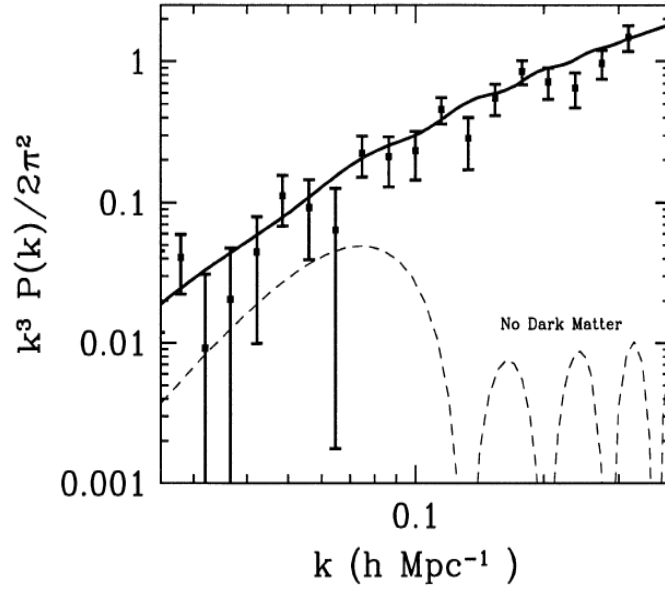


Figure 1.2: Variance $\Delta^2 := k^3 P(k)/2\pi^2$ of the Fourier transform of the galaxy distribution as a function of scale. The solid line is the theoretical prediction of the standard model including Λ and perturbations generated by inflation. Dashed line is a theory where no dark matter is considered. Data are shown with error bars taken from the IRAS Point Source Catalog Redshift (PSCz) Survey.(Figure taken from [Dodelson (2003)].)

according to the matter that it contains, we call a solution of this system a Friedmann-Robertson-Walker(FRW) universe.

$$G_{\mu\nu} = R_{\mu\nu} - \frac{1}{2}g_{\mu\nu} R = \frac{8\pi G}{c^4}T_{\mu\nu} - g_{\mu\nu}\Lambda, \quad (1.4)$$

$R_{\mu\nu}$ is the Ricci curvature tensor, $g_{\mu\nu}$ is the metric tensor, Λ is the cosmological constant, G is Newton's gravitational constant, c is the speed of light in vacuum, R is the scalar curvature, and $T_{\mu\nu}$ is the energy-momentum tensor that due to the symmetry of space-time it can only be diagonal with non-zero components $T_{00} = -\rho c^2 g_{00}$ and $T_{ij} = pg_{ij}$. It is not necessary to assume that the matter content of the Universe is an ideal fluid to get this from of $T_{\mu\nu}$, it is simply a consequence of the homogeneity and isotropy of the universe and it is verified for scalar field matter, a viscous fluid or free-streaming particles in a FRW universe. The energy density ρc^2 and the pressure are defined as the time and space-like eigenvalues of $(T_{\mu\nu})$.

The Einstein or Friedmann equations for the FRW universe become

$$H^2 := \left(\frac{\dot{a}}{a}\right)^2 = \frac{8\pi G}{3c^2}\rho - \frac{kc^2}{a^2} + \frac{\Lambda c^2}{3} \quad (1.5)$$

$$\frac{\ddot{a}}{a} = -\frac{4\pi G}{3}\left(\rho + \frac{3p}{c^2}\right) + \frac{\Lambda c^2}{3} \quad (1.6)$$

$$\dot{\rho} = -3H\left(\rho + \frac{p}{c^2}\right). \quad (1.7)$$

Where the last equation is also a consequence of the energy conservation $T_{;\mu}^{\mu\nu} = 0$, and it is a consequence of the contracted Bianchi identities. H is the Hubble ‘‘constant’’ or Hubble parameter⁴ We parametrize the Hubble parameter by $H = 100h \text{ km s}^{-1} \text{ Mpc}^{-1}$, where observations show that $h_0 \approx 0.70 \pm 0.1$ [Komatsu et al. (2011)].

From equation (1.7) we can obtain simple solutions if $w = p/\rho c^2 = \text{constant}$. One finds that

$$\rho = \rho_0(a_0/a)^{3(1+w)} \quad (1.8)$$

⁴The Hubble parameter in cosmic time is related to the comoving Hubble parameter $H(\tau)$ by $H(t) = H(\tau)/a^{-1}$. A comoving coordinate system is a system of coordinates fixed with respect to the overall expansion of the universe, so that a given galaxy's location in comoving coordinates does not change as the Universe expands. This allows distances, locations, etc. in an expanding homogeneous and isotropic cosmology to be related solely in terms of the scale factor.

where ρ_0 and a_0 denote the values of the energy density and the scale factor at the present time t_0 . Unless otherwise stated, the subscript 0 refers to quantities evaluated at present time.

If the energy density is dominated by one component with $w = \text{constant}$ and we neglect the curvature K , then we different scale factors depending on the dominant component. For non-relativistic matter, usually refer as dust, $p_m = 0$, for radiation (photons or any kin of massless particles) $p_r = \rho_r c^2/3$. A cosmological constant corresponds to $p_\Lambda = -\rho_\Lambda c^2$, inserting these in eq. (1.8) we obtain

$$\rho_m \propto a^{-3}, \quad a \propto t^{2/3} \propto \tau^2 \quad w = 0, \quad (\text{dust}), \quad (1.9)$$

$$\rho_r \propto a^{-4}, \quad a \propto t^{1/2} \propto \tau \quad w = 1/3, \quad (\text{radiation}), \quad (1.10)$$

$$\rho_\Lambda = \text{const.}, \quad a \propto \exp(Ht) \propto 1/|\tau| \quad w = -1, \quad (\text{cosmol. const.}), \quad (1.11)$$

One can define the adiabatic sound speed c_s as

$$c_s^2 = \frac{\dot{p}}{\dot{\rho}} \quad (1.12)$$

where the derivative is taken respect to cosmic time. From eq. (1.5) we can define a critical value for the energy density for vanishing curvature and cosmological constant

$$\rho_c(t) = \frac{3H^2 c^2}{8\pi G}, \quad (1.13)$$

where $\rho_c(t)$ is called the critical density. The ratio $\Omega_X = \rho_X/\rho_c$ is the ‘‘density parameter’’ of the component X , it indicates the fraction that the component X contributes to the expansion of the universe. For the different components we get $\Omega_m(t_0) = \rho_m(t_0)/\rho_c(t_0)$, $\Omega_r(t_0) = \rho_r(t_0)/\rho_c(t_0)$, $\Omega_\Lambda(t_0) = \Lambda c^2/3H_0^2$, and $\Omega_K(t_0) = -Kc^2/(a_0^2 H_0^2)$.

We can separate $\Omega_m = \Omega_{dm} + \Omega_b$, where Ω_{dm} is the dark matter component and Ω_b is the baryonic density parameter, for the radiation we can separate in photons and neutrinos $\Omega_r = \Omega_\gamma + \Omega_\nu$. Current constrains for all these cosmological parameters come principally from the CMB combined with large scale structure data given $h_0^2 \Omega_{m,0} = 0.134$, $h_0^2 \Omega_{b,0} \approx 0.023$, $h_0^2 \Omega_{dm,0} \approx 0.111$, $h_0^2 \Omega_{\Lambda,0} \approx 0.357$, $h_0^2 \Omega_{r,0} = 4.15 \times 10^{-5}$, $h_0^2 \Omega_{\gamma,0} = 2.47 \times 10^{-5}$, $h_0^2 \Omega_{\nu,0} = 1.68 \times 10^{-5}$, with the fiducial value $h_0 = 0.7$ [Massimo(2008), Spergel et al.(2007), Page et al. (2007)] we get $\Omega_{m,0} = 0.27$, $\Omega_{b,0} \approx 0.046$, $\Omega_{dm,0} \approx 0.22$, $\Omega_{\Lambda,0} \approx 0.73$, $\Omega_{\gamma,0} \approx 5.04 \times 10^{-5}$, $\Omega_{\nu,0} \approx 3.42 \times 10^{-5}$, $\Omega_{r,0} \approx 8.47 \times 10^{-5}$.

This suggests that $\Omega_K \approx 0$, therefore the geometry of the universe is remarkably flat and this parameter will be neglected in calculations. Assuming $K=0$, the age of the universe is of 13.69 Gyr. We observe that baryons constitute only $\sim 5\%$ of the total energy density and that there is strong evidence of an unknown component.

§1.2 Overview of dark matter models

The standard model assumes dark matter behaves as dust, there is no particular information on its nature. There are several particle candidates for the dark matter thoroughly reviewed in [Bertone et al. (2005), Feng (2010), Martin et al.(2008)], depending on its the general properties they can be classified as cold dark matter, self-interacting dark matter, warm dark matter, ultra light scalar field dark matter, etc.

One of the preferred candidates of cold dark matter are Weakly Interacting Massive Particles (WIMP) whose mass range is typically from $10 \text{ GeV}/c^2$ to $1 \text{ TeV}/c^2$, these kind of dark particles interact in the weak sector with ordinary matter. These particles became the default CDM candidates and are studied in great detail given that their cross section yields a value of Ω_{dm} fairly close to the one observed. Another candidate widely discussed as a CDM candidate is the axion with mass in the range $10^{-3} - 10^{-6} \text{ eV}/c^2$ [Sikivie & Yang (2009)], this particle originates from the breaking of the Peccei-Quinn symmetry in the early universe [Peccei & Quinn (1977)] which solves the CP problem of strong interactions. In the context of warm dark matter are the sterile neutrinos, their mass scale is $\sim \text{keV}/c^2$ and they are thermal relics with a higher velocity dispersion than CDM candidates (hence warm dark matter) and they follow Fermi-Dirac statistics. However recent cosmological constraints to the mass of the sterile neutrino seem to create tension for this candidate [Villaescusa-Navarro & Dalal (2011), Viel et al.(2013), Souza et al.(2013), Macció et al.(2012)].

The other contenders that will be treated in more detail in this thesis are the ultra light scalar fields and self-interacting dark matter, the main motivation to study these models stems from the accurate descriptions offered to explain some of the problems encountered at the level of galaxies in the CDM model, in addition to retaining the successful description at large scales.

The above list is not limited to the these classes of dark matter and there exists other models that can agree with current data, but ultimately there is a trend to apply the *Occam's razor*⁵, our best bet is to keep acquiring higher resolution observations at all scales that let us assess our current theoretical models and eventually we get to unravel some of the mysteries of the universe.

We have provided the bases of the current standard model of cosmology that will be the benchmark when comparing results in other alternative dark matter models. As we mentioned, the standard model struggles to solve some issues at the level of galaxies that will be discussed in the next chapter in more detail, we also present the current status of the proposed solutions. In Chapter 3 we explore thoroughly the ultra light scalar field dark matter pay close attention to the expected properties of the dark matter halos that result from the model and examine their impact on the visible matter in galaxies. Due to the increasing interest in the self-interacting dark matter model we dedicate Chapter 4 to expose the status of this model.

Throughout the thesis several quantities are given in solar units and will always be denoted by a subscript \odot . We will use units where $c = 1$, Planck constant $\hbar = 1$, except in some cases where they help to make the discussion clearer.

⁵Occam's razor is a principle devised by William of Ockham. The principle states that among competing hypotheses, the one with the fewest assumptions should be selected. Other, more complicated solutions may ultimately prove correct, but in the absence of certainty the fewer assumptions that are made, the better.

CURRENT STATUS OF THE Λ CDM MODEL

§2.1 Initial fluctuations in the matter-dominated era

We can measure the position of an object in the sky from its angular coordinates, but in order to know how far away it is from us we can use as the third coordinate the *redshift* z experienced by photons emitted from the object. A spectral line with intrinsic wavelength λ is redshifted due to the expansion of the universe, if it is emitted at some time t an observer on Earth will see it today with wavelength $\lambda_0 = \lambda a_0/a(t) = (1+z)\lambda$, this leads to the definition of the cosmic redshift

$$z(t) + 1 = \frac{a_0}{a(t)}. \quad (2.1)$$

For small redshifts $z \ll 1$ Hubble found that objects at a physical distance $d = a_0 r$ away from us, it recedes with speed $v = H_0 d$, this is called the Hubble's law. This law can be related to redshift z approximately by making a Taylor series expansion to lowest order in z : $a(t_0) \approx a(t) + \dot{a}(t_0 - t)$, if in addition the distance to the object is not too large then the time interval is simply the distance divided by the speed of light $t_0 - t = d/c$, therefore

$$1 + z \approx 1 + \frac{\dot{a}}{a}(t_0 - t) \approx 1 + H_0 \frac{d}{c}$$

from where it follows that $cz = H_0 d = v$, valid at low redshifts. This is the method usually applied to measure the Hubble constant. In cosmology it is typical to deal with object far away from us, this makes the redshift a suitable coordinate to identify the time at which events take place.

As mentioned in the introduction the deviations from the homogeneous cosmic microwave background and the large scale structure suggest we need to go beyond the standard model

of elementary particles(normal matter) to explain the structure of the universe, one of the implications is the addition of a new dark matter(DM) component.

The temperature we see today of the CMB photons is 2.725 K, as photons are massless and behave as radiation their temperature decreases with the adiabatical expansion of the universe as $T = a_0 T_0 / a(t)$, at the temperature $T_{dec} \sim 3000$ K the mean free path of the photons grows larger than the Hubble scale, this means that they effectively decouple from baryonic matter and the universe becomes transparent to them, by eq. (2.1) this corresponds to $z_{dec} \simeq 1100$, at this time the universe was $t \simeq 10^5$ yr old. From this point, the small perturbations in the density of baryons can grow to form the galaxies we observe today. Anisotropies in the CMB tell us how the universe looked like when it was some hundred thousand years old being excellent probes of the perturbations and a good reference point for numerical studies.

On the other hand, the non-relativistic dark matter will clump and form overdensity regions, the standard CDM stops interacting with the rest of the particles at an earlier epoch than z_{dec} , the DM overdensities can start growing before the decoupling of photons from baryons so that by the time photons travel freely baryons follow the gravitational potential wells previously generated by the cold dark matter. In fact, from eqs. (1.9),(1.10) it follows that after a certain time the matter will start dominating over the energy density of radiation, from the observed values of the density parameters of matter and radiation this happens at a redshift

$$1 + z_{eq} = \frac{a_0}{a_{eq}} = \frac{h_0^2 \Omega_{m,0}}{h_0^2 \Omega_{r,0}} = 3228.91 \left(\frac{h_0^2 \Omega_{m,0}}{0.134} \right), \quad (2.2)$$

that is $z_{eq} \simeq 3000 > z_{dec}$, after this time of matter-radiation equality the universe is effectively dominated by non-relativistic matter until the moment dark energy starts being dominant ($z \approx 0.7$), during this epoch DM fluctuations can grow. Eventually, at relatively recent times, perturbations in the matter ceased to be small and become the nonlinear structure we see today. Thus, photons decouple from baryons when the universe is already well into the matter-dominated era, we have seen that the visible matter contributes a small fraction to Ω_m and it is then reasonable to consider that the main component that determines the evolution of matter fluctuations will be the dark matter, hence a first approach to study the evolution of density fluctuations consists on analyzing the dark

matter growth and its distribution. In order to follow the spatial and time evolution of the density perturbations up to the time where they collapse to form virialized gravitational configurations it is necessary to rely on numerical simulations.

In the standard model, dark matter configurations grow and collapse before galaxies as the latter decouple from photons at a later time, in their evolution DM fluctuations will cluster and form even larger under- and overdense regions, these large structures strongly attract more baryons that much later produce stars and form the observed galaxies surrounded by the large dark matter halos. We can get insight into the galaxy distribution from the dark matter one as we expect that baryons move according to the underlying dark matter potentials.

For this reason, a first step that is taken to study the growth of DM perturbations in cold dark matter simulations consists in neglecting baryons, in order to compare with galaxy surveys it is required to use semi-analytical models describing the baryonic physics and use matching techniques to link galaxies with the dark matter background distribution. Recalling that baryons aren't the dominant component in Ω_m , we see that taking the approach of first studying only the dark matter evolution, it is possible to get an idea of what to expect for the galaxy distribution, as seen in Fig 1.1 it is an excellent approximation.

It is important to notice that the DM distribution depends on the dark matter properties (cold, warm, etc.). Assuming it is cold and collisionless at all scales results in dark matter halo formation at practically all scales. A direct consequence of these hypotheses is that DM halos will form accreting other halos several times increasing their masses and their sizes, as more massive structures are assembled, smaller halos in the neighborhood will also be accreted turning this merging process quite chaotic. Nevertheless, once the merger rate slows down, the number of halos that survive and the orbiting subhalos that remain bounded within a given distance from the final massive host can be compared with observations applying techniques like abundance matching that relates the galaxy stellar mass to the halo mass, we should always consider similar environmental conditions as galaxies that are in more isolated regions present different structural properties.

The above discussion displays the relevance of the CMB in the study of structure formation, the catch is that it offers a detailed map of the building blocks that will give rise to the observable universe. A detailed discussion of how the primordial fluctuations arise from

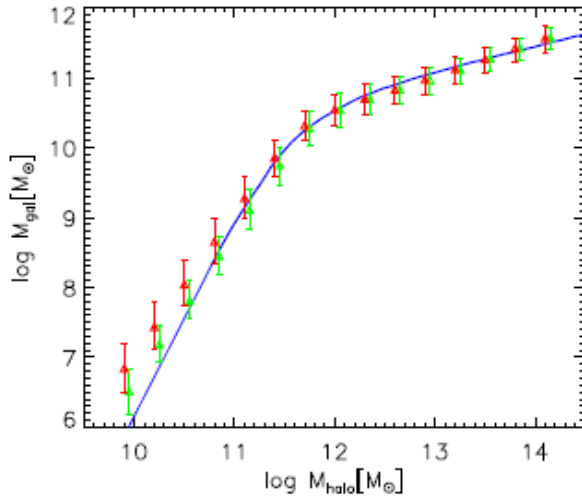


Figure 2.1: Relation between the halo mass and the stellar mass using the abundance matching technique for the Millenium Simulation(MS) and Millenium II(MS-II), taken from [Guo et al(2011)]. The halo mass is taken as the maximum mass that the halo ever attained in the simulation. Green symbols are for central galaxies, while red symbols are for satellites. The blue curve is the relation derived directly from the SDSS stellar mass function and from subhalo abundances in the MS and the MS-II under the assumption that the two quantities are monotonically related without scatter [Guo et al(2010)].

inflation can be found in [Liddle & Lyth (2000)] and i will not pursue it further because it would get us sidetracked from our main focus, galaxies and dark matter. Below we describe how simulations make use of the CMB to evolve linear perturbations up to the nonlinear regime.

§2.2 Large scale structure in CDM

There is evidence from the CMB that the primordial fluctuations are well described by an initial random gaussian distribution, there are codes[Hahn & Abel(2011)] in the literature that allow to generate initial conditions with these characteristics. Evolving the CMB density field since $z_{dec} \sim 1100$ becomes extremely time consuming in

terms of computing time and memory (although recent technological advances are making this goal feasible). Knowing that the fluctuations evolve linearly far later than $z \sim 120$, it is desirable to begin a simulation much later than z_{dec} but still in the linear regime, fortunately there are codes like CAMB and CMBFast[Seljak & Zaldarriaga(1996), Zaldarriaga, Seljak, & Bertschinger(1998), Zaldarriaga & Seljak(2000)] for calculating the linear cosmic microwave background anisotropy spectra based on integration over the sources along the photon past light cone. Using these codes allow us to obtain the initial conditions for the fluctuations for a given set of cosmological parameters compatible with observations and that can be used in CDM simulations, most of the latter are taken to start at $z = 120$ which is still in the linear regime and run until $z = 0$.

Due to the collisionless nature of the cold dark matter, a successful numerical implementation to describe this type of dark matter bases on calculating the interactions of N particles of a given mass, simulations that use a code based on this implementation are called N -body simulations. One of the most reknown codes of this type is called GADGET[Springel(2005)], this has been modified and optimized through the years with the latest version being GADGET-3, the code have been expanded to include hydrodynamics, it can simulate the gravitational interaction of gas, stars and dark matter as well as several astrophysical processes that are involved during the galaxy formation process(stellar feedback, gas cooling, stellar metallicity, star formation, etc.).

The advantage of simulations is the possibility to study the nonlinear regime, that is, once the initial fluctuations become massive enough that their gravitational pull counters the expansion of the universe they stop expanding and start collapsing under its own gravity, this time is called the *turnaround*. The study of the collapse of a given CDM halo has to be followed numerically due to the nonlinear effects that enter during its virialization process.

One of the great successes of the CDM model is the astonishing parallel of the large scale structure resulting from simulations and the current observations of galaxies in the universe. This extraordinary reproduction of the cosmic structure in CDM N -body simulations is one reason to place it as the benchmark. There has been several cosmological simulations with different degrees of resolution and all of them find similar results on large scales, one the most recent ones is The Bolshoi simulation measuring one billion cubic light-

years compared to the Milky Way that is only about 100,000 light-years long or the Local Group of just 10 million light-years in diameter. The simulation covered a massive portion of the universe, and it simulated the interactions of 8.6 billion dark matter particles. Starting from the relatively smooth dark matter distribution of the early universe discerned from the CMB, the Bolshoi simulation tracked the universe's evolution to the present epoch assuming the CDM model. In similarity to lower resolution simulations, it displays knots of dark matter, long filaments and clusters of galaxies, all gravitationally dominated by dark matter. These structures are also found in DM-only simulations, but they do not directly predict anything about the galaxies themselves, requiring an extra step in order to bridge the gap with observations. Two dominant approaches have been used to establish the link: (1) the technique of semi-analytical modeling, whereby baryonic physics are modeled at the scale of an entire galaxy, and applied in post-processing on top of DM simulations, and (2) hydrodynamic simulations, whereby the evolution of the gaseous component of the universe is treated using the methods of computational fluid dynamics. The latter approach enables the complex interaction of the different baryonic components (gas, stars, black holes) to be treated at a much smaller scale, ideally yielding a self-consistent and powerfully predictive calculation. Hydrodynamical cosmological simulations have a high computational cost and have usually targeted specific problems, only very recently have several groups started projects following approach (2), one of them is the Illustris simulation. The technical details of the simulation can be found in the webpage¹ and some introductory articles are [Vogelsberger et al.(2014), Vogelsberger et al.(2014b), Genel et al.(2014)], given the massive data sets that it produced the project is still ongoing and much of the analysis has yet to be done, it is worth pointing out these type of projects may change some of the previous results that were obtained following approach (1), but in the meantime, it is worth discussing the known results that were obtained using the link (1).

One useful technique to link the number DM halos and the galaxy population in the universe assuming they should match is called abundance matching, it essentially links the observed galaxies in the expected dark matter halo according to semi-analytical models which imposed a set of rules based on observed properties of gas and stars in galaxies that are then implemented by hand in simulations[Guo et al(2011)]. A relevant parameter is

¹<http://www.illustris-project.org/>

the efficiency with which halos are able to condense gas at their centers and form stars and is called “galaxy efficiency”. Abundance matching models suggest that this galaxy efficiency depends strongly on halo mass, for systems like the Milky Way (MW) with halo mass of $M_{200} := M(r = r_{200}) \sim 1 \times 10^{12} M_{\odot}$ (r_{200} is the radius in which the density is 200 times the critical cosmological density ρ_c), about 20% of the available baryons are turned to stars. For halos of an order of magnitude smaller this number drops quickly to $\sim 5\%$, and plumpers to even less than 1% for dwarf galaxies inhabiting halos with mass $M_{200} < 1 \times 10^{10} M_{\odot}$ (see Fig. 2.1). Dwarf galaxies is a general term for galaxies that are faint, they can have stellar masses at least two orders of magnitude below the stellar mass of a Milky Way-like galaxy. There are several dwarfs with luminosities as low as $L \sim 1 \times 10^3 L_{\odot}$. Two of the most massive dwarfs nearby are the small and large Magellanic Clouds visible by the naked eye on dark nights from the Southern Hemisphere.

Unfortunately, observing these faint objects is challenging, the galaxy luminosity function² is only reliably measured for dwarfs with stellar masses $\log(M_*) \sim 8.5$ and above, not fainter. Thus, if we are interested on dimmer dwarfs, like dwarf spheroidals or ultra faint dwarfs, we have to make an extrapolation of the halo mass-galaxy mass relation observed towards faint dwarfs, assuming that the stellar mass-halo mass relation is correct, then for all dwarfs with measured stellar mass we know the halo they live in, in fact from Fig. 2.1, we expect that all dwarfs with stellar masses larger than $M_* \sim 1 \times 10^6 M_{\odot}$ live in halos with virial mass $M_{200} = 1 \times 10^{10} M_{\odot}$ and larger. We require more data to confirm the validity of extrapolating the abundance matching (AM) relation to the faint end of the luminosity function, the potential candidates that will provide this confirmation are expected to be dwarf and ultrafaint dwarf galaxies, moreover, if we consider these are systems that are dominated by dark matter, we would expect baryons to move according to the underlying potential, therefore it would be reasonable to expect that the kinematics of the gas and stars are almost completely determined by the DM halo distribution. This can be checked by comparing the circular velocity profile predicted by such dark halo with the measured rotation curve of the dwarf, as the baryons are considered to have a

²The luminosity function gives the number of stars or galaxies per luminosity interval. The luminosity is the total amount of energy emitted by a star, galaxy, or other astronomical object per unit time. It is related to the brightness, which is the luminosity of an object in a given spectral region.

minor contribution to the total mass, hence acting as tracers of the much more dominant dark matter potential, the observed profiles should be remarkably similar to the DM only profile. Despite the accuracy of AM for MW like galaxies or larger, it was found that its extrapolating to lower masses breaks, meaning that there exist more scatter for the low mass dwarfs.

There has been a great deal of work trying to explain why most of the dwarfs of $\log(M_*/M_\odot) = 10^6-10^7$ are inconsistent with the expected $M_{200} > 1 \times 10^{10} M_\odot$ and seem to be better described with lower mass halos. Unfortunately, lowering the mass also translates into a lower stellar mass leading to a characteristic density divergent profile that is in tension with the flatter profiles found in observed dwarfs. The success of AM in galaxies of $\log(M_*) \geq 8.5$ is undeniable, what remains fuzzy is the cause of the discrepancy of CDM predictions and the low mass galaxies. This conundrum is just one of the cornerstones that motivates exploring other dark matter models.

§2.3 Testing CDM with dwarf galaxies

2.3.1 Cusp-core problem

Analyzing a statistical sample of CDM halos from the high resolution simulations, there exists some common structural properties in the DM distribution of such collapsed structures despite the chaotic history associated to the formation of each halo. One such property is the universal density profile known as Navarro-Frenk-White (NFW) profile [Navarro et al.(1996)]. The NFW profile emerges from numerical simulations that use only CDM and are based on the Λ CDM model [Navarro et al.(1996), Navarro et al.(1997)]. Its density profile is

$$\rho_{NFW}(r) = \frac{\rho_i}{(r/R_s)(1 + r/R_s)^2} \quad (2.3)$$

ρ_i is related to the density of the universe at the moment the halo collapsed and R_s^2 is a characteristic radius. We notice that in collisionless CDM the inner region of DM halos show a density distribution described by a power law $\rho \sim r^\alpha$ with $\alpha \approx -1$, such behaviour

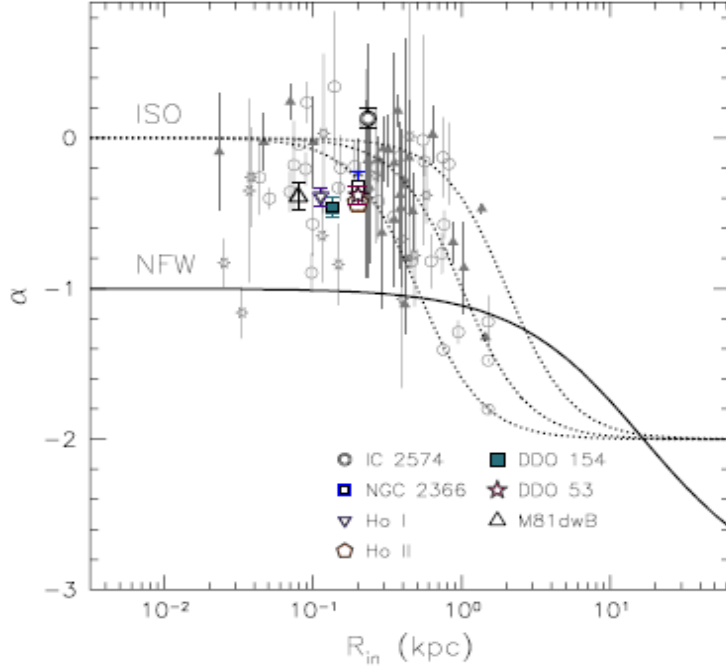


Figure 2.2: The inner slope of the dark matter density profile plotted against the radius of the innermost point. The inner density slope α is measured by a least squares fit to the inner data point as described in the small figure. The inner-slopes of the mass density profiles of the 7 THINGS dwarf galaxies are overplotted with earlier papers and they are consistent with previous measurements of LSB galaxies. The pseudo-isothermal model with its characteristic core seems to provide a better fit to the data than the NFW model. Gray symbols: open circles [de Blok et al.(2001)]; triangles [de Blok & Bosma(2002)]; open stars [Swaters et al.(2003)].

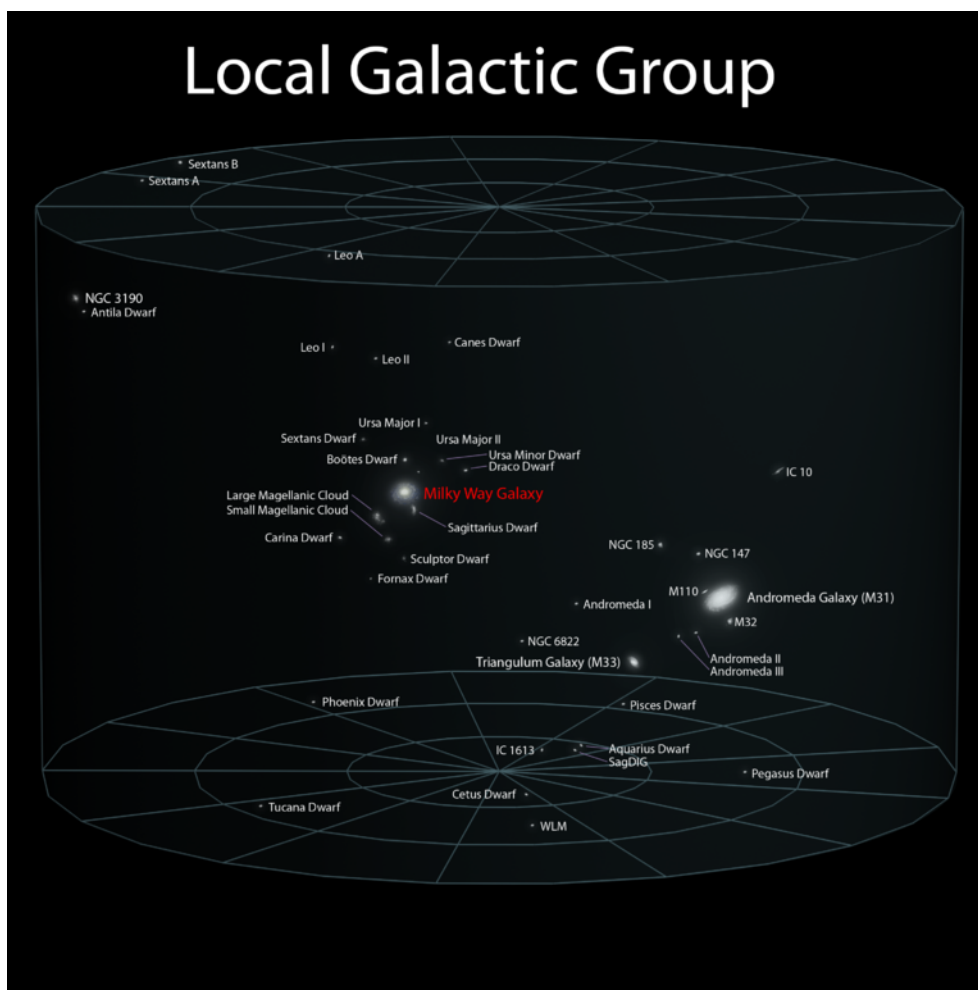


Figure 2.3: Observed galaxies in the Local Group shown in proportion to their measured distances. The most massive galaxies in the group are our Milky Way and M31 (Andromeda galaxy). Image by Andrew Z. Colvin “5 Local Galactic Group (ELitU)”.

is what is called a “cusp”. The associated rotation curve³ (RC) for a NFW halo is

$$V_{NFW} = V_{200} \sqrt{\frac{\ln(1 + cx) - cx/(1 + cx)}{x[\ln(1 + c) - c/(1 + c)]}} \quad (2.4)$$

where $x = \frac{r}{r_{200}}$, the concentration parameter is $c = r_{200}/R_s$, and is related to the circular velocity V_{200} , measured at a radius r_{200} , the usage of this radius stems from the similarity to the virial radius. V_{200} and c are related by

$$\log V_{200} = 3.22 - \log[g(c)] - \log\left(\frac{h}{2}\right) \quad (2.5)$$

where

$$g(c) = \frac{c^2}{\ln(1 + c) - c/(1 + c)} \quad (2.6)$$

and $h_0 = H_0/100 \text{ km s}^{-1} \text{ Mpc}^{-1}$.

Observations in the central region of luminous galaxies often lack the resolution to accurately determine the density slope, specially as the visible matter also contributes to the mass budget in a non negligible way for small radii. On the other hand, the cusp or divergent behavior of the density profile is always maintained in DM-only simulations, in fact, for halos that accrete smaller halos with steeper slopes in their density profiles, the final merged halo will reform its cusp [Binney & Tremaine (2008)]. This property is found at all scales, from scales of massive galaxy clusters with halo masses $M_h \sim 10^{14-15} M_\odot$ to the less massive dwarf halos with $M_h \sim 10^{10} M_\odot$.

Given the omission of baryons in the above simulations, it is sensible to compare the results with galaxies where baryons are not dominant, the suitable candidates that satisfy this condition are dwarf and low surface brightness (LSB) galaxies. Startlingly, high resolution observations in nearby galaxies seem to be better described by a profile with a shallower central density going as $\rho \sim r^0$ within $r \leq 1$ kpc (see figure 2.2). This discrepancy between observation and the CDM model received the name of cusp-core problem. It is worth noting that even in state-of-the-art N-body simulations with much higher resolution adequate to

³The rotation(velocity) curve of a galaxy is a plot of the magnitude of the orbital velocities of the particles that move in that galaxy versus their radial distance from that galaxy’s centre. As galaxies are inside dark matter halos, in general the total rotation curve is the result of the dark matter component and the baryonic matter rotation curve.

resolve the inner kpc the resulting density profile is still cuspy. Adding baryons may reduce the problem, but as we see below this is not the only issue that seems to require baryons to agree with observations.

2.3.2 Missing satellite problem

In the hierarchical galaxy formation scenario a large number of halos are consumed by more massive ones, however, there are still many dark matter substructures that are not disrupted and that remain orbiting a massive halo, these surrounding structures are called subhalos and the central massive one is called the host halo. The number of subhalos can be predicted by CDM simulations, in particular, it is found that the low mass halos are always more numerous, given the apparent universal NFW profile these halos don't suffer strong tidal stripping so as to be completely destroyed, resulting in host with a large population of low mass subhalos. This picture also appears at larger scales, in galaxy clusters the gravitational potential is stronger and can capture more subhalos, given the above properties of CDM halos there will be also a great abundance of dwarf halos, some are associated to a particular host but some others are not, the latter are called field halos (galaxies) in the field, simply representing that they are somewhat isolated and are not satellites that belong to a specific host.

It is straightforward to compare the number of observed satellites to the predicted subhalos using AM. As the more precise observations are in our local neighborhood, an obvious candidate is our own Milky Way or the Andromeda galaxy (M31) and their respective satellite galaxies. One way to proceed is to choose a MW mass halo from a cosmological simulation that resembles as close as possible our environmental conditions, it is frequent to have more than a Milky Way analogue in these simulations, this suggests that we have to count the subhalos of all these MWs and give a statistical result. Another way is to simulate with a much higher resolution an isolated MW like system with much more detail so that it can have a closer resemblance to our observed Via Lactea, such systems are chosen from large simulated boxes that allow the formation of at least one halo of $M_h \sim 10^{12} M_\odot$. Among the most famous simulations that study MW halos is the Aquarius project [Navarro et al. (2010), Springel et al. (2008)]. The Aquarius simulations study an

isolated halo similar in mass to that of the Milky Way at various resolutions, about 200 million particles at r_{200} and one at even higher resolution with almost 1.5 billion particles within this radius. These simulations are being used to understand the fine-scale structure predicted around the Milky Way by the standard structure formation model.

A problems emerged when the abundance of satellites expected from CDM simulations was found to be overpredicting the number of dwarf satellite galaxies in the MW and M31, this mismatch was initially of an order of magnitude larger[Klypin et al.(1999)] and called the “missing satellite problem” (MSP), nowadays, the discovery of more ultra faint dwarfs (UFD) within the MW halo has reduced the missing satellite problem (e.g.[Simon & Geha(2007)]),The problem can be rephrased by saying that there are more subhalos with circular velocities $V_{circ} < 30$ km/s than observed satellites around MW and M31.

There are solutions to this problem that based on redefining the MSP, for instance, considering only the mass within 600 pc $M_{0.6}$ [Strigari et al.(2007)], doing this it was found that models where the brightest satellites correspond to the earliest forming subhalos or the most massive accreted objects both reproduce the observed mass function.

Another possibility is that despite the existence of DM subhalos, most of them will not host galaxies, hence, aren’t observed. This solution relies on the efficiency of star formation, which requires baryons to be included forcing us to use hydrodynamical simulations. It is likely that dwarfs are the most affected by reionization, the epoch where the neutral hydrogen get ionized, at early times the smallest galaxies first dominate but given their small gravitational potentials their own star formation blows out their primordial gas through their own supernovae and heating of their environment. Therefore, they stop forming stars for not much longer after reionization and if the star formation was very inefficient at that time, only the DM halo will remain today and no galaxy will be observed. Three year WMAP data found that reionization began at $z = 11$ and the Universe ionized by $z=7$.[Spergel et al.(2007)]. Assuming the unrealistic case of an instantaneous reionization, the combination of results from the Planck mission, WMAP polarization, CMB and BAO measurements yield a redshift of $z_{reio} = 11.3 \pm 1.1$.[Ade et al. (2007)]. Although a value of 7 is in much better agreement with the quasar data. In view of the uncertainty of z_{reio} the baryonic solution to the MSP is still uncertain. Moreover, if dwarf galaxies

are the primary source of ionizing photons during the epoch of reionization they will be star forming, but this continual star formation will again overproduce the abundance of the Via Lactea's satellites at $z=0$ [Boylan-Kolchin et al. (2014)].

Incorporating baryons in current simulations seems to be mandatory, but the required fraction of baryons to dark matter has to be carefully controlled, as pointed in Peñarrubia et al. (2012), solving the cusp-core problem with strong stellar feedback may result in luminosities at odds with those of MW satellites. Before jumping to result from hydrodynamic simulations let us see a more recent issue related to the above discrepancies.

2.3.3 The Local Group: Too-Big-to-Fail

Our galaxy resides in a group of galaxies that spans a diameter of 3 Mpc termed the Local Group (LG). The group's most massive members are the Milky Way and M31(Andromeda) galaxies, these two spiral galaxies have a system of satellite galaxies. The LG comprises around 78 galaxies[Pawlowski et al.(2013)]. The group itself is a part of the larger Virgo Supercluster (i.e. the Local Supercluster[Tully (1982)]). In fig. 2.3 we see the distribution of most of the galaxies in the LG.

In the spirit of abundance matching, it is prudent to expect that the most massive satellites of the MW reside in the most massive subhalos that are found in simulations, a similar situation is natural for other hosts with their respective galaxies. As mentioned, observations of nearby dwarfs suggest high mass-to-light ratios($10-1000M_{\odot}/L_{\odot}$) so the kinematics of stars are good tracers of the DM halo distribution.

By carefully studying the results of CDM simulations that emulate the MW, it was found that the central densities of MW dSph galaxies are required to be significantly lower than the densities of the largest subhalos found in collisionless DM simulations to agree with the observed data(Boylan-Kolchin et al. 2011; Garrison-Kimmel et al. 2014). CDM simulations of the Aquarius Project suggest that the MW-size halos should inhabit at least eight subhalos with maximum circular velocities exceeding 30 km/s, while observations indicate that only three satellite galaxies of the MW possess halos with maximum circular velocities > 30 km/s. This discrepancy is not particular of the MW, it is expected for M31 and even in galaxies outside the LG. This issue differs from the MSP in that there

are multiple subhalos that have no visible counterpart, from the above results, out of the 8 subhalos with similar masses, only 3 have a visible pair even though the remaining 5 are just as massive to cool hydrogen, form stars and eventually host a galaxy, so why do we observe only three galaxies when we should see eight? These subhalos would be massive“failures” because they fail to form galaxies, and this issue is known as the Too-big-to-fail(TBTF) problem.

In virtue of the hierarchical model, we could expect that the presence of our close companion M31 may change our results since it is as massive as the MW and at a distance of 775 kpc. If we are more strict we should consider the Large Magellanic Cloud (LMC) that is $\sim 41kpc$ from us. In the search of a fair comparison a first approach was to analyze pair of galaxies resembling the MW and M31. This was done in the ELVIS⁴ suite[Garrison-Kimmel et al. (2014a)].

The analyses reveal that the TBTF persists within the virial radius of each host, in fact, it is also present at the scale of the LG (see fig. 2.4). In their study the authors found that within 300 kpc of the Milky Way, the number of unaccounted-for massive halos ranges from 2 - 25 over their full sample. Moreover, this “too big to fail” count grows as the comparison is extended to the outer regions of the Local Group: within 1.2 Mpc of either giant(the MW and M31) they find that there are 12-40 unaccounted-for massive halos. This count excludes volumes within 300 kpc of both the MW and M31, and thus they conclude that these systems should be largely unaffected by any baryonically-induced environmental processes. According to abundance matching, all of these missing massive systems should have been quite bright, with $M_* > 10^6 M_\odot$. This outcome was to be expected as more massive hosts will attract more dark matter that can also end as DM subhalos.

An evident solution would be to consider tidal stripping, although this seems plausible for galaxies that are in orbits with close pericenter distance to their host it is unclear that this mechanism is the main reason to reach agreement with current data, principally because several studies have shown that tidal stripping of CDM halos with cuspy profiles

⁴ELVIS is a suite of high-resolution, cosmological zoom-in simulations. The suite contains 48 halos, each with up to 15 million particles within the virial radius and 53 million particles within an uncontaminated sphere centered on each halo. Half of these halos exist in Local Group-like configurations, chosen to mimic the Milky Way and Andromeda in mass and phase space configuration.

is not effective enough to destroy the subhalos, however, we need to include baryons in the studies to assess this solution, in the end what we observe are galaxies. Notice that the TBTF problem remains for galaxies in the field where tidal stripping is subdominant.

2.3.4 Alignment of satellite galaxies in MW and M31

Until very recently, the peculiar distribution of satellites around the MW and M31 caught the attention of several astronomers. Dark matter simulations predict the accretion of various subhalos around massive hosts, but statistically its distribution tends to be isotropic. Unexpectedly, the observed nearby satellites of our galaxy and those in M31 show a certain degree of spatial arrangement. Both galaxies of the Local Group are surrounded by thin planes of mostly co-orbiting satellite galaxies, the vast polar structure (VPOS) around the Milky Way and the Great Plane of Andromeda (GPoA) around M31 [Ibata et al.(2013)]. This issue is further review in [Pawlowski et al.(2013)].

Some of the proposed scenarios trying to explain the LG galaxy structures as either originating from cosmological structures or from tidal debris of a past galaxy encounter. On large scales, the cosmic web consists of massive clusters that are connected with dark matter “filaments”, these filaments serve as fountains of particles that feed dark matter to massive concentrations of halo clusters and superclusters, it is quite similar to networks of neurons in our brain, in fact, it is outstanding that the large scale structure of the universe presents such similarity to the micro scale in our brains, whether this apparent coincidence hides a deeper meaning is an interesting question that may deserve to be subject to further scrutiny, for now i will leave it as a side comment. Getting back to the satellites, one of the scenarios concentrates on how the satellite distribution is correlated to the direction of filaments, mainly in intersections of the filamentary structure. During the formation of a MW-mass host, part of the dark matter flows along the filament so that as DM clumps and halos form in such filament, their peculiar velocities can share a preferential direction, as a result, when they become bounded to a massive host they can possess a particular orientation that today give the pattern of a plane [Pawlowski et al.(2013), Ibata et al.(2013), Pawlowski & McGaugh (2014)]. This scenario can explain the orientation of the satellites in one host galaxy, under the same

framework we would expect that the satellites in M31 and our galaxy, both being relatively close and part of the LG, share a particular direction in one plane, what is observed is that each set of satellites has its own plane implying that they don't originate in the same filament. Looking at the vast cosmic structure in principle it should be possible to find two hosts with the desired satellite distribution, in contrast, it has proven difficult to find pairs of hosts whose satellites are in planes with the observed inclinations. There exists the uncertainty that the MW and M31 are cosmologically rare, it may be that the criteria to look for akin systems in simulations needs to be redefined or simply that there is a different formation mechanism tied to the halo shape that is not fully understood. Also explored is that they are tidal debris of a past galaxy encounter, the details and feasibility of this solution requires a more convoluted study. Although it is worth noting that because of the proximity of M31 and MW to us, it is possible to obtain accurate measurements of these systems, however this doesn't imply that such pairs are statistically significant. There currently exists no full detailed model which satisfactorily explains the existence of the thin symmetric LG planes.

§2.4 Baryons to the rescue, or not?

The above issues led to much effort in improving the resolution of simulations so that regions of order kpc could be resolved and the results are not biased by numerical errors due to a lack of convergence. The problem that attracted most of the attention is the cusp-core issue. This results undoubtedly change when astrophysics are involved, due to the large concentration of DM particles in the center of subhalos, we need to identify an energetic process capable of efficiently expelling the DM and disperse to a more uniform distribution to form a core. This naturally points to supernova feedback, each supernova type II comes along a massive explosion injecting $\sim 10^{51} \text{ergs}$ to the surrounding gas, after several of these events the dark matter which interacts gravitationally will be modified and in the best scenario a core will be formed. Under this picture most hydrodynamical simulations have focused on modeling supernovae feedback (FB) to accurately implement it into numerical simulations.

Reproducing the general properties of dwarfs in a cosmological setting has been quite chal-

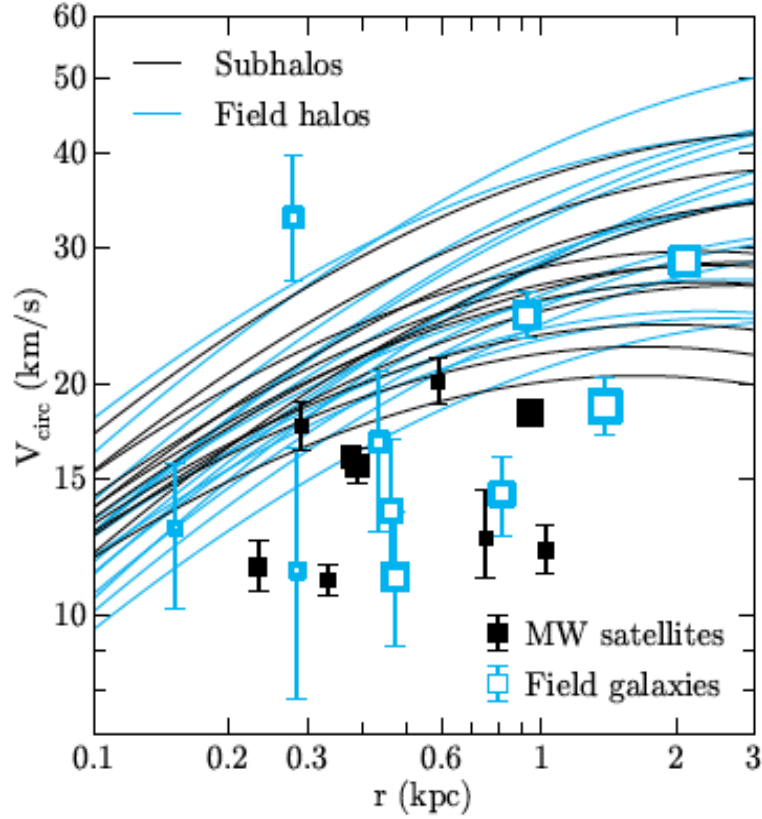


Figure 2.4: Plotted are the rotation curves for all halos identified as massive failures around one of the simulated ELVIS pairs, both within 300 kpc (black lines) and in the Local Field surrounding it (light blue lines), along with constraints on the dwarf galaxies in each region (black squares denote MW satellites and open light blue squares indicate field galaxies (sizes are proportional to M_*)). Not shown are halos with $V_{\text{peak}} < 30 \text{ km s}^{-1}$. Image from [Garrison-Kimmel et al. (2014b)].

lenging. So far the relation of stellar mass and halo mass inferred from local galaxy counts implies a suppression of galaxy formation by a factor of $\sim 10^3$ [Garrison-Kimmel et al. (2014b), Brook et al.(2014)], if stellar feedback is the main ingredient to achieve the desired effect we need to get a physically realistic model that so far has proven difficult.

As for a feedback-driven core formation, there is still debate. One of the most successful simulations at producing cores in dwarf galaxies with supernova feedback have suggested a transition mass of $M \sim 10^7 M_\odot$ below which core formation becomes difficult [Governato et al.(2012)]. Using a slightly different approach, [Di Cintio et al.(2013)] find similar results, where the cusp-core transition should be most effective when the ratio of stellar mass to dark matter halo mass is relatively high, they find cores in massive dwarfs with $M \sim 10^8 M_\odot$ and $M_{vir} \sim 3 \times 10^{10.5} M_\odot$. It may be that at some mass scale, galaxy formation becomes stochastic (e.g., [Boylan-Kolchin et al.(2011), Power et al.(2014)]). Recent work by [?], however, suggests that stochasticity may appear at lower mass scales ($M_{vir} \sim 10^9 - 10^{9.5} M_\odot$). The results of Di Cintio et al. (2013) and Governato et al. (2012) agree reasonably well, in contrast, results from a different set of high resolution simulations with a simpler implementation of stellar feedback have not produced cores in dwarf galaxy halos at any mass ([Vogelsberger et al.(2014)]), even though a number of other observables are well matched. One caveat of these simulations is that the sub-grid inter stellar medium (ISM) and star formation (SF) model leads to SF histories smoothed in time, compared to the bursty star formation found in the above models or in the highly resolve explicit feedback models ([Hopkins et al.(2014)]).

Until now, feedback has needed ad-hoc approximations due to the lack of resolution of molecular clouds where star formation takes place, for instance, turning off cooling for material heated by SNe. It is then unclear that the sub-grid feedback recipes capture the expectations from stellar evolution models and end forming large cores. To this end, [Oñorbe et al.(2015)] simulated two typical isolated dwarfs with $M \sim 10^{10} M_\odot$ using a more realistic explicit implementation of feedback using the code GIZMO [Hopkins (2014)]. They found that their simulated dwarfs present bursty star formation, in the event that it continues until late times a core of ~ 1 kpc can form and at the same time the dwarf galaxy can sit on the M_* vs M_{vir} relation to match the LG stellar mass function via abundance matching. The success depends strongly on the star formation histories, indeed,

they conclude that the presence of cores in galaxies with $M_{*} = \sim 10^6 - 10^7 M_{\odot}$ requires substantial late time star formation. It is also questionable if subsequent accretions could reform the cusp.

Although the cusp-core issue remains an open question, we can conclude that in hydrodynamical CDM simulations transforming a cusp into a core seem to be strongly dependent on bursty periods of star formation and a steady supernovae feedback to avoid the cusp regeneration. Recently [Trujillo-Gomez et al.(2015)] found in their simulations that radiation pressure from massive stars is the most important source of core formation, not thermal feedback from supernova, which has been the primary mode used by other groups that have produced cores. This approach may seem promising, but from the experience with feedback models, forming a core may result in a mismatch with other galaxy properties, it remains to be seen whether the radiation pressure model is consistent with other observables such as the stellar metallicity-stellar mass correlation [Gallazzi et al.(2005), Kirby et al.(2013)]. Regarding the MSP and the TBTF, many attempts to decrease the subhalo population focus on the interaction of the satellites with the galactic disk. In general, the closer the subhalos are to the disk, the larger the influence and their destruction. Simulations studying the dynamics of several dwarf subhalos in different orbits with and without the presence of a disk component in the host show that halos that are accreted possessing an initial cuspy profile will always leave a remnant, they are not fully destroyed even if its outer envelope is heavily dispersed. For subhalos in orbits whose pericenters are smaller than the disk length, the effects are enhanced such that only a compact structure remains losing almost 90% of its initial mass [Peñarrubia et al.(2010), Łokas et al.(2012)]. CDM simulations don't predict cores naturally and baryons must be taken into account, but for comparison, the tidal stripping effects were also studied assuming a CDM halo with an empirical core profile, it was found that subhalos with initial core profiles that fully dive inside the disk several times are completely torn down, whereas they can survive if their pericenter distances are larger than the disk's size albeit with more mass lost than their cuspy analogues. These simulations have considered controlled orbits, the results look promising to get a lower abundance of satellites even though some subhalos may still be present after the mass lost from the disk they will be devoid of stars, it remains to be seen that orbits that come from cosmological simulations fall into the same regime of close

disk-subhalo interactions as these idealized simulations.

The potential success of tidal stripping in dwarfs led to consider a combined model of feedback and tidal stripping in the hope that the circular velocities are reduced and alleviate the tension suggested in the TBTF issue. This combination of effects was studied in high resolution cosmological hydrodynamical simulations of Milky Way-massed disk galaxies[Zolotov et al.(2012), Brooks & Zolotov (2014)], they found that supernovae feedback and tidal stripping lower the central masses of bright ($-15 < M_V < -8$) satellite galaxies, the bursty star formation can reduce dark matter densities forming shallower inner density profiles in the massive satellite progenitors ($M_{vir} \geq 10^9 M_\odot$, $M \geq 10^7 M_\odot$) compared to DM-only simulations. In the progenitors of the lower mass satellites are unable to maintain bursty star formation histories, due to both heating at reionization and gas loss from initial star forming events, preserving the steep inner density profile predicted by DM-only simulations. After infall (when galaxies enter the virial radius of the host galaxy), tidal stripping further reduces the central densities of the luminous satellites, particularly those that enter with cored dark matter halos, consistent with the expected results where each effect is treated separately. It seems that an over simplification of the MW potential where the disk is not taken into account may be the source of the discrepancies in DM-only simulations, even taking this solution at face value, it would imply that if cores are indeed present in galaxies in the field, where interactions with the disk are of minor importance, supernovae feedback will be left as the most efficient agent contributing to core formation, as mentioned in the cusp-core issue, forming cores in CDM simulations is often correlated to late bursty star formation but at the same time we require a strong suppression of star formation in low-mass haloes in order to explain the small number of visible satellites, unifying the solutions may require some tuning or a better understanding of the dark-baryons coupling as well as the galaxy formation process itself.

We have seen that including hydrodynamics into CDM simulations has provided different scenarios that could explain the long standing problems of DM-only simulations. Up until now there is not unanimity in the cause of these conflicts, it may seem that supernova feedback seen as the main mechanism to form cores in dwarfs requires detailed modeling so as not to aggravate the fit to other observations. Curiously, the few cases that have simulated DM halos with pre assumed flat inner profiles seem to lead to simpler descriptions,

specially since no fine tuning of stellar feedback is needed, although cores are not naturally produce in CDM they can arise in alternative dark matter models, this in turn leads to study in more detail the explanations that these other models offer. Unquestionably, dwarf galaxies will be a key factor to unravel the properties of dark matter.

The list of issues that I have presented in this chapter forms just part of other puzzling observations, such as the how statistically significant is the “Bullet cluster” in simulations [Hayes et al.(2006), Lee & Lim(2010)], the details of the relation between the specific angular momentum distribution of DM halos and the one observed in the gas component[Bullock et al. (2001), van den Bosch et al. (2001)], why there are less observed galaxies in the local void than in simulations[Peebles & Nusser (2010)], the formation of rings and shells in early type elliptical galaxies in non interacting environments, etc.

[Hau & Forbes (2006), Taehyun et al. (2012), Koprolin & Zeilinger (2000)].

All these observations are intriguing enough to explore the outcome from modifications to the CDM model, mainly at small scales given its extraordinary success at large scales, as it appears that the non appearance of core profiles in CDM halos is tightly related to all the problems, in the next chapter we will then explore one model in which the core formation is simply a natural consequence of the dark matter properties, this type of solution is usually preferable to invoking poorly understood astrophysical processes

SCALAR FIELD DARK MATTER

§3.1 The quantum dark matter paradigm

In CDM there are several dark matter candidates, many of them proposed from extensions of the standard model of particles, among which the most popular ones at present are in the form of weakly interacting massive particles (WIMPs), see [Goodman & Witten (1985), Scherrer & Turner(1986), Drukier et al. (1986)]. The main characteristics that identify the WIMPs are being collisionless and massive ($> \text{GeV}$).

Furthermore, current dark matter detection experiments, both direct and indirect ones, have not yet discovered any compelling signals of WIMPs [Bauer et al. (2013)]. As a matter of fact, while WIMPs are mostly expected to be the lightest supersymmetric particle in the Minimal Supersymmetric Standard Model(MSSM), [Griest & Kamionkowski (2000)], recent data from the Large Hadron Collider has found no evidence of a deviation from the standard model of particles on GeV scales, significantly restricting the allowed region of MSSM parameters [Aad et al.(2013)]. It is clear that the microscopic nature of dark matter is sufficiently unsettled as to justify the consideration of alternative candidates for the CDM paradigm.

One of these assumptions is to assume that the dark matter particles are described by a spin-0 scalar field(SF) with a possible self-interaction and a very small mass. There are several scalar fields that have been predicted by a variety of unification theories, e.g., string theories and other multi dimensional theories [Carroll (1998), Arkani et al. (1999)]. The bosonic particles we are envisaging are typically ultralight, with masses down to the order of $10^{-33}\text{eV}/c^2$. This small mass suggests the possibility of formation of a Bose-Einstein

condensate (BEC), i.e., a macroscopic occupancy of the many-body ground state. In principle, for a fixed number of (locally) thermalized identical bosons, a BEC will form if $n\lambda_{deB}^3 \gg 1$, where n is the number density and λ_{deB} is the de Broglie wavelength. This is also equivalent to the existence of a critical temperature T_c , below which a BEC can form.

Recently the idea of the scalar field has gained interest, given the uncertainty in the parameters the model has adopted different names in the literature depending on the regime that is under discussion, for instance, if the interactions are not present and the mass is $\sim 10^{-22}\text{eV}/c^2$ this limit was called fuzzy dark matter[Hu, Barkana & Gruzinov(2000)] or more recently wave dark matter[Schive et al.(2014)], another limit is when the SF self-interactions are described with a quartic term in the scalar field potential and dominate over the mass(quadratic) term, this was studied in [Goodman (2000), Slepian & Goodman] and called repulsive dark matter or fluid dark matter by[Peebles(2000)].

Notice that for a scalar field mass of $\sim 10^{-22}\text{eV}/c^2$ that is non-relativistic the critical temperature of condensation for the field is $T_{\text{crit}} \sim m^{-5/3} \sim \text{TeV}$, which is very high, if the temperature of the field is below its critical temperature it can form a cosmological Bose Einstein condensate, if it condenses it is called Bose-Einstein condensed(BEC) dark matter[Colpi,Shapiro,& Wasserman(1986), Guzmán & Matos(2000), Matos & Ureña(2001), Bernal et al.(2010), Harko(2011), Chavanis & Harko (2012), Robles & Matos(2013)]. One type of bosonic particle suggested as a major candidate for dark matter is the QCD axion. It is the pseudo-Nambu-Goldstone boson in the Peccei-Quinn mechanism, proposed as a dynamical solution to the strong CP-problem in QCD. For the axion to be CDM, it has to be very light, $m \sim 10^{-5} \text{ eV}/c^2$ ([Sikivie(2012)]). More recently [Sikivie & Yang (2009)] mentioned that axions could also form Bose-Einstein condensates, however, the result was contested in [Davidson & Elmer(2013)], this suggest that the condensation process should be study in more detail to confirm it can remain as BEC dark matter.

In [Ureña-Lopez(2009)], it was found that complex scalar field with $m < 10^{-14}\text{eV}/c^2$ that decoupled being still relativistic will always form a cosmological Bose-Einstein condensate described by the ground state wavefunction, this does not preclude the existence of bosons with higher energy, particularly in dark matter halos. A fully relativistic treatment($k_B T \gg mc^2$) of Bose-Einstein(BE) condensation was given by [Kapusta (1981),

Haber & Weldon (1982)], including the relationship between BE condensation and symmetry breaking of a scalar field. Those authors showed that, for an ultra relativistic ideal charged boson gas, described by a complex scalar field,

$$T_c = \frac{(\hbar^3 c)^{1/2}}{k_B} \left(\frac{3q}{m} \right)^{1/2} \quad (3.1)$$

where q is the charge per unit proper volume. This does not take self-interactions into account. In [Haber & Weldon (1982)] it was shown that, in the case of an adiabatically expanding boson gas, if the scalar field has a generic quartic self-interaction, then the bosons must either be condensed at all temperatures (i.e. at all times) or else never form a BEC. In this case, the charge per unit comoving volume, Q ($Q = qa^3$), and entropy per unit comoving volume, S , are both conserved. In their work they establish the condition for the formation of a BEC

$$\frac{Q}{S} = \frac{5}{4\pi k_B} \left(\frac{\hat{\lambda}}{4} \right)^{1/2} \quad (3.2)$$

where $\hat{\lambda}$ is the dimensionless coupling strength of the quartic self-interaction, in natural units. The SF is assumed to have essentially zero entropy per unit comoving volume and for the typical boson masses we are interested, $m < 10^{-14} \text{eV}/c^2$, the conserved charge density in the comoving frame, Q , is extremely high, given the observed dark matter energy density today $\rho_{dm,0}$, for $Q \approx \rho_{dm,0}/(mc^2)$. Therefore, inequality (3.2) would be satisfied and thus almost all of the bosons occupy the lowest available energy state. It is important to notice, that the condensation process requires Bose-Einstein statistics in the first place, i.e., local thermalization [Sikivie & Yang (2009), Erken et al.(2012)], it has been argued that thermal decoupling within the bosonic dark matter can occur when the expansion rate exceeds its thermalization rate, without disturbing the condensate, however, just like with QCD axions the thermalization might break with the expansion of the universe, although a large number of dark matter bosons would stay in the ground state and the classical field remains a good description, it will no longer be completely BEC dark matter, this is still something that remains to be seen.

From the above discussion we see that the smallness of the boson mass is its characteristic property and cosmological condensation is a likely consequence. The preferred mass of the scalar field dark matter(SFDM) lies close to $\sim 10^{-22} \text{eV}/c^2$ satisfying the above constraint,

although there are still uncertainties on the mass parameter, in order to avoid confusion with the already known axion and help with the identification in future works, we find it useful and appropriate to name the scalar field dark matter candidate, given the above characteristics we can define it as a particle with mass $m < 10^{-14} \text{eV}/c^2$, being commonly described by its wavefunction, we have named this DM candidate *psyon*.

It is worth emphasizing that despite the variety of names given to the model the main idea mentioned above remains the same, it is the quantum properties that arise due to the small mass of the boson that characterize and distinguishes this paradigm, analogous to the standard cosmological model represented by the CDM paradigm whose preferred dark matter candidates are the WIMPs (weakly interacting massive particles), we see that all the above regimes SFDM, Repulsive DM, Axion DM, or any other model assuming an ultra light bosonic particle comprise a single class of paradigm, which we call *Quantum Dark Matter* (QDM) paradigm.

As pointed before, in the QDM paradigm the small mass of the dark matter boson leads to the possibility of forming cosmological condensates, even for axions which are non-thermally produced and have masses in $10^{-3} - 10^{-6} \text{eV}/c^2$ [Sikivie & Yang (2009)], from here we can obtain a characteristic property that distinguishes these dark matter candidates from WIMPs or neutrinos, namely, the existence of *bosons in the condensed state*, or simply *BICS*, from our above discussion the axion and psyon are included in the BICS.

Now that we have given a classification of the variants and regimes of QDM it is of particular interest for us the SFDM alternative with psyons of typical mass $m \sim 10^{-22} \text{eV}/c^2$ such that its de Broglie wavelength is of order $\sim \text{kpc}$, relevant for galactic scales and cosmological scales. Indeed, the quantum behavior of the field has created much interest in the model due to its success to account for some CDM discrepancies with dark matter properties only, for example, the small mass keeps the central density from increasing indefinitely due to the uncertainty principle in contrast to CDM simulations where supernova feedback is required [Governato et al.(2010), Governato et al.(2012), Pontzen & Governato(2012), Scannapieco et al.(2012)].

§3.2 Cosmology in SFDM

The study of scalar fields in cosmology has been widely explored in the context of inflation, dark energy and dark matter. As it is known from quantum mechanics one intrinsic property of particles is its spin, in particular scalar fields correspond to the spin-0 fields. If the SF is complex it has a corresponding particle and antiparticle, whereas for a real scalar field there is only one particle associated to the field, being itself its own antiparticle. Remembering that at large scale our universe satisfies the cosmological principle, we begin the study of the cosmological expansion of the different components (radiation, matter, cosmological constant, etc.) by first deriving the Friedmann equations in the context of SFDM. In the following we use $c=1$.

The Lagrangian density of a real scalar field Φ minimally coupled to gravity¹ is

$$L_{\Phi} = -\frac{1}{2}g^{\mu\nu}\partial_{\mu}\Phi\partial_{\nu}\Phi - V(\Phi), \quad (3.3)$$

where $g^{\mu\nu}$ is the space-time metric. The kinetic energy term is $K_{\Phi} := -\frac{1}{2}g^{\mu\nu}\partial_{\mu}\Phi\partial_{\nu}\Phi$, $V = V(\Phi)$ is the potential of the SF that encompass all the information about the mass and self-interaction. Thus, the gravitational interaction with the field is accounted for through the metric $g^{\mu\nu}$, and the Lagrangian density for the metric is given by the Einstein-Hilbert form

$$L_{EH} = \frac{R}{2\kappa^2} \quad (3.4)$$

where $\kappa^2 = 8\pi G$ and R is the Ricci scalar which is obtained by the contraction of the Ricci tensor ($R_{\mu\nu}$) as $R = R^{\mu}_{\mu}$. The total Lagrangian is then

$$L = L_{EH} + L_{\Phi} \quad (3.5)$$

The action to derive the equations of motion is then

$$S = \int_M L\sqrt{-g}dx^4 \quad (3.6)$$

where M is the four-dimensional manifold and $g := \det(g_{\mu\nu})$ is the determinant of the metric, we are using the $(-, +, +, +)$ metric signature, applying the principle of least action $\delta S = 0$ yields the Einstein field equations varying respect to $g_{\mu\nu}$ and when the variation

¹The field is not coupled to other fields or to the scalar curvature or Ricci scalar R , e.g., there are no terms of the form ΦR or similar products.

is respect to the SF Φ it yields the evolution equation for the scalar field, specifically :

$$G_{\mu\nu} := R_{\mu\nu} - \frac{1}{2}g_{\mu\nu}R = \kappa^2 T_{\mu\nu}(\Phi), \quad (3.7)$$

where $G_{\mu\nu}$ is called the Einstein tensor and $T_{\mu\nu}(\Phi)$ is the energy-momentum tensor for the SF defined as

$$T_{\mu\nu}(\Phi) := -2\frac{\delta L_\Phi}{\delta g^{\mu\nu}} + g_{\mu\nu}L_\Phi = \partial_\mu\Phi\partial_\nu\Phi - g_{\mu\nu}\left[\frac{1}{2}g^{\alpha\beta}\partial_\alpha\Phi\partial_\beta\Phi + V(\Phi)\right]. \quad (3.8)$$

In case a cosmological constant is included the right hand side(rhs) of (3.7) is modified as in (1.4). For the scalar field equation,

$$\square\Phi + V_{,\Phi} = 0, \quad (3.9)$$

$\square = g^{\alpha\beta}\nabla_\alpha\nabla_\beta$ is d'Alembertian operator, with

$$\nabla_\alpha\nabla_\beta\Phi = \partial_\alpha\partial_\beta\Phi - \Gamma_{\alpha\beta}^\sigma\partial_\sigma\Phi$$

where the connection coefficients of an affine connection in a coordinate basis are the Christoffel symbol $\Gamma_{\alpha\beta}^\sigma$ defined

$$\Gamma_{\beta\gamma}^\alpha = \frac{1}{2}g^{\alpha\beta}\left(\frac{\partial g_{\rho\gamma}}{\partial x^\beta} + \frac{\partial g_{\beta\rho}}{\partial x^\gamma} - \frac{\partial g_{\beta\gamma}}{\partial x^\rho}\right). \quad (3.10)$$

The comma in $V_{,\Phi}$ is the derivative respect to the scalar field and

$$\square\Phi = -\frac{1}{\sqrt{-g}}\partial_\mu[\sqrt{-g}g^{\mu\nu}\partial_\nu\Phi]. \quad (3.11)$$

As noted in the introduction the $T_{\mu\nu}(\Phi)$ is diagonal and can be written

$$T_{\mu\nu}(\Phi) = (\rho_\Phi + p_\Phi)u_\mu u_\nu + pg_{\mu\nu} \quad (3.12)$$

if we make the analogy with a perfect fluid we can define the 4-velocity u^μ , from (3.8) we get

$$\rho_\phi = -\frac{1}{2}\partial^\mu\Phi\partial_\mu\Phi + V(\Phi), \quad (3.13)$$

$$p_\Phi = -\frac{1}{2}\partial^\mu\Phi\partial_\mu\Phi - V(\Phi), \quad (3.14)$$

$$u^\mu = -\frac{\partial^\mu\Phi}{\sqrt{-\partial^\mu\Phi\partial_\mu\Phi}}. \quad (3.15)$$

For a cosmological SF that evolves in a FRW universe $u^0=1$ and $u^i=0$ and we have²

$$\rho_\phi = \frac{1}{2}\dot{\Phi}^2 + V(\Phi), \quad (3.16)$$

$$p_\phi = \frac{1}{2}\dot{\Phi}^2 - V(\Phi), \quad (3.17)$$

the field has no dependence on the spatial coordinates \mathbf{x} , indeed, as a consequence of the cosmological principle $\Phi(t, \mathbf{x}) = \Phi(t)$. The Klein-Gordon equation for the scalar field in a FRW universe reads

$$\ddot{\Phi} + 3H\dot{\Phi} + V_{,\Phi} = 0. \quad (3.18)$$

or in conformal time

$$\Phi'' + 2H(\eta)\Phi' + V_{,\Phi} = 0. \quad (3.19)$$

Following the standard notation of an equation of state, we can relate the pressure and density of the SF defining $p = \omega_\Phi \rho$ with

$$\omega_\Phi = \frac{\frac{1}{2}\dot{\Phi}^2 - V(\Phi)}{\frac{1}{2}\dot{\Phi}^2 + V(\Phi)}. \quad (3.20)$$

From (3.20) we notice that

1. if $\dot{\Phi}^2 \gg V$, then $p \simeq \rho$: in this regime the scalar field behaves as a stiff fluid;
2. if $V \gg \dot{\Phi}^2$, then $\omega \simeq -1$: in this regime the scalar field is an inflation candidate.

From the conservation of the energy-momentum tensor $T_{\Phi;\nu}^{\mu\nu} = 0$, we get for $\mu = 0$

$$\dot{\rho}_\Phi + 3H(\rho_\Phi + p_\Phi) = 0. \quad (3.21)$$

The above equation describes the cosmological evolution of the field which is assumed to describe the dark matter. Baryons, photons, neutrinos and the cosmological constant if included, may be treated as perfect fluids with a barotropic equation of state $p_\theta = (\theta - 1)\rho$, for baryons $\theta_b = 1$, for photons and neutrinos $\theta_\gamma = \theta_\nu = 4/3$, and $\theta_\Lambda = 0$. Thus the system

²Notice that (1.3) can also be written as $ds^2 = a^2(\eta)[-d\eta^2 + \delta_{ij}(x^k)dx^i dx^j]$ with δ_{ij} the Kronecker delta, spatial indices denoted by latin letters run from 1 to 3, while greek letters run from 0 to 4.

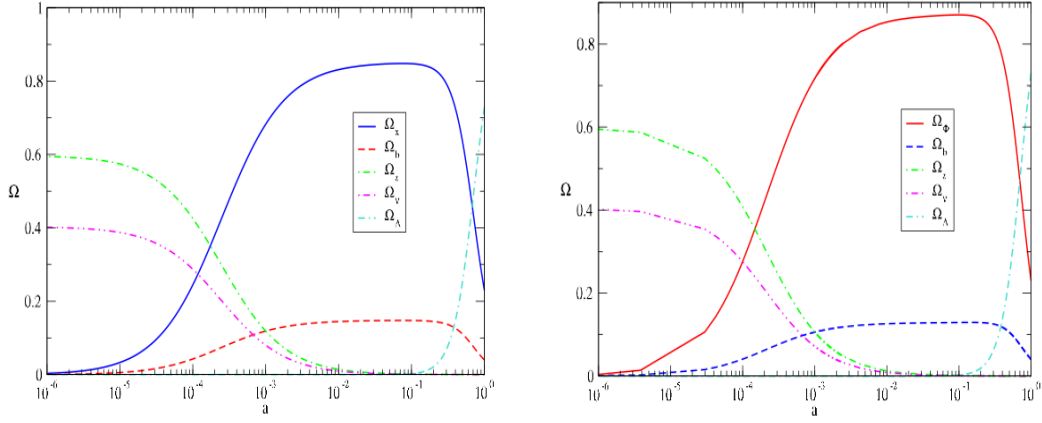


Figure 3.1: Left: Cosmological evolution of the density parameter Ω of all the components in CDM. Right: Cosmological evolution of Ω for all components but now the dark matter is a psyon (scalar field) with a mass $m = 1 \times 10^{-23} \text{eV}/c^2$.

that describes the expansion of the universe with a scalar field as the dark matter in a FRW universe is called the Einstein-Klein-Gordon (EKG) given by

$$H^2 = \frac{\kappa^2}{3}(\rho_\Phi + \rho_b + \rho_\gamma + \rho_\nu + \rho_\Lambda), \quad (3.22)$$

$$\ddot{\Phi} + 3H\dot{\Phi} + V_{,\Phi} = 0, \quad (3.23)$$

$$\dot{\rho}_b + 3H\rho_b = 0, \quad (3.24)$$

$$\dot{\rho}_\gamma + 4H\rho_\gamma = 0, \quad (3.25)$$

$$\dot{\rho}_\nu + 4H\rho_\nu = 0, \quad (3.26)$$

$$\dot{\rho}_\Lambda = 0. \quad (3.27)$$

3.2.1 Cosmological evolution of a scalar field with $V(\Phi) = m^2\Phi^2/2$

The above system of equations can be solved for a specific potential $V(\Phi)$. One of the potentials of much interest is

$$V(\Phi) = \frac{1}{2}m^2\Phi^2, \quad (3.28)$$

this potential specifies the mass of the scalar field $V_{,\Phi\Phi} = m^2$, we are concerned with BICS, in particular with psyons (very low mass bosons) whose mass is $\sim 10^{-22} \text{eV}$, henceforth we

will omit the subscript Φ for the SF quantities. Clearly the pressure and density will be

$$\rho = \frac{1}{2}\dot{\Phi}^2 + \frac{1}{2}m^2\Phi^2, \quad (3.29)$$

$$p = \frac{1}{2}\dot{\Phi}^2 - \frac{1}{2}m^2\Phi^2, \quad (3.30)$$

with

$$\omega = \frac{\frac{1}{2}\dot{\Phi}^2 - \frac{1}{2}m^2\Phi^2}{\frac{1}{2}\dot{\Phi}^2 + \frac{1}{2}m^2\Phi^2}. \quad (3.31)$$

A numerical solution of the EKG system was given in [Magaña et al.(2012)], in Figure (3.1) we show the background evolution of all the components for the potential $V(\phi) = m^2\Phi^2/2$ using a mass of $1 \times 10^{-23}\text{eV}$ from $a = 10^{-6}$ until today $a = 1$. For comparison we also show the evolution in the standard model (CDM) where the fluid is pressureless $p=0$.

We observe that results using a psyon with potential (3.28) are completely equivalent to those in CDM, this is a major success of the model. For the SFDM we have the early phase where photons and neutrinos(radiation) are dominant, later on as the universe keeps expanding the matter and radiation energy densities are equal at $a_{eq} \sim 1.6 \times 10^{-4}$ (using data from WMAP-7³), from this point the matter is the dominant component and small DM fluctuations can start growing as we will see below. The time in which the photon's energy is small enough that electron can start combining with protons to form atomic nuclei, the decoupling time, happens at $a \sim 10^{-3}$ ($z \sim 1000$) similar to CDM. We see that as expected, the cosmological constant will dominate the late time dynamics at $z_\Lambda \sim 0.7$. But what causes the SFDM to behave as a CDM cosmologically? The answers lies in the fact that despite the rapid oscillation of the field around the minimum of $V(\Phi)$, the time average of the pressure is $\langle p \rangle \approx 0$, this in turn makes $\langle \omega_\Phi \rangle \approx 0$, hence the equation of state for the psyons tends to zero and the field behaves effectively as a pressureless fluid (dust) implying $\rho \sim a^{-3}$ [Matos et al.(2009)] and hence mimics the CDM model.

Before jumping to the study of linear fluctuations, we will discuss the case where the two-body interactions of the SF are included in the potential.

³In this calculation $\Omega_{dm,0} = 0.226$, $\Omega_{b,0} = 0.0455$, $\Omega_{\gamma,0} = 4 \times 10^{-5}$, $\Omega_{\nu,0} = 2.7 \times 10^{-5}$, $\Omega_{b\Lambda,0} = 0.728$, $T_{CMB,0} = 2.702K$ and $h = 0.704$.

3.2.2 Cosmological evolution of a SF with self-interactions.

As this case is of particular importance in our future study of galaxies in the SFDM, we get back to physical units ($c \neq 1 \neq \hbar$) to make the discussion more clearly in the hope that the upcoming results are easily followed.

When self-interactions are included in a real scalar field the Lagrangian density for the field is

$$L_\Phi = -\frac{1}{2}g^{\mu\nu}\partial_\mu\Phi\partial_\nu\Phi - V(\Phi), \quad (3.32)$$

with

$$V(\Phi) = \frac{1}{2}\frac{m^2c^2}{\hbar^2}\Phi^2 + \frac{\hat{\lambda}}{4\hbar^2c^2}\Phi^4, \quad (3.33)$$

where the dimensionless self-interaction parameter is $\hat{\lambda}$. This same scalar field model has been studied considering it to be complex [Pitaevskii & Stringari(2003), Woo & Chihue(2009)] It is this latter case that will occupy our attention in this subsection, we will follow the approach of [Li et al.(2014)]. We write then the Lagrangian for the complex scalar field as

$$L_\Psi = -\frac{\hbar^2}{2m}g^{\mu\nu}\partial_\mu\Psi\partial_\nu\Psi - V(\Psi), \quad (3.34)$$

and

$$V(\Psi) = \frac{1}{2}m|\Psi|^2 + \frac{\lambda}{4}|\Psi|^4. \quad (3.35)$$

We choose to denote the complex scalar field by Ψ . We recall that any two Lagrangians that differ by a constant yield the same equations of motion, therefore if Φ is complex in (3.32) we can relate (3.33) and (3.35) by

$$L_\Phi \rightarrow \frac{1}{\hbar c}L_\Phi := L_\Psi \quad (3.36)$$

$$\Phi \rightarrow \left(\frac{\hbar^3c}{m}\right)^{1/2}\Psi \quad (3.37)$$

noting that $\lambda = \frac{\hat{\lambda}\hbar^3}{2m^2c}$. The units are then $[L_\Psi]=J/m^3$, $[\Psi]=m^{-3/2}$, $[\lambda]=Jm^3$, $[\Phi]=J$, $[\hat{\lambda}]=1$. For example, for the QCD axion with decay constant $f \simeq 10^{12}$ GeV we have a dimensionless coupling $\hat{\lambda} \approx 10^{-53}$ [Sikivie & Yang (2009)]. It is a good approximation to ignore higher order interactions when the bosonic gas is dilute, i.e. when the particle self-interaction range is much smaller than the mean inter particle distance, as the cosmological

expansion dilutes the field, it is sufficient to consider only two-body s-wave scatterings, then the coupling coefficient λ is a constant and related to the s-wave scattering length a_s as $\lambda = 4\pi\hbar^2 a_s/m$, which is the first Born approximation. An interesting property of the Lagrangian for a complex field is the global U(1) symmetry ($\Psi \rightarrow e^{i\theta\Psi}$), by Noether's theorem this leads to a conserved charge density Q in real space, or equivalently, the conservation of the comoving charge density Qa^3 , this conserved charge corresponds to the particle number and it should not be confused with the electrical charged of a particle, in our case the scalar field is not electrically charged. Moreover, the charge is defined as the total number of bosons and the total number of anti-bosons, in particular, the formation of a BEC the charge is essentially equal to the total number of bosons. The conservation of particle number is an inherent property of complex scalar fields minimally coupled to gravity and is not present for a real scalar field, as the latter does not possess a U(1) symmetry, in fact, we already mentioned that in this case the boson is its own anti-boson.

The cosmological evolution is determined by the Friedmann equation

$$H^2 = \left(\frac{da/dt}{a}\right)^2 = \frac{8\pi G}{3c^2}(\rho_\Phi + \rho_b + \rho_\gamma + \rho_\nu + \rho_\Lambda), \quad (3.38)$$

and the energy conservation equation

$$\frac{\partial\rho}{\partial t} + \frac{3da/dt}{a}(\rho + p) = 0. \quad (3.39)$$

Where now the density and pressure are

$$\rho = \frac{\hbar^2}{2mc^2}|\partial_t\Psi|^2 + \frac{1}{2}mc^2|\Psi|^2 + \frac{1}{2}\lambda|\Psi|^4 \quad (3.40)$$

$$p = \frac{\hbar^2}{2mc^2}|\partial_t\Psi|^2 - \frac{1}{2}mc^2|\Psi|^2 - \frac{1}{2}\lambda|\Psi|^4 \quad (3.41)$$

and (3.23) becomes

$$\frac{\hbar^2}{2mc^2}\partial_t^2\Psi + \frac{\hbar^2}{2mc^2}\frac{3da/dt}{a}\partial_t\Psi + \frac{1}{2}mc^2\Psi + \lambda|\Psi|^2\Psi = 0. \quad (3.42)$$

Due to the oscillations of the field over time, it is convenient to define the oscillation angular frequency as $\omega = \partial_t\theta$. This system of equations is solved numerically in [Li et al.(2014)].

There are certain limits in which the behavior of the field changes, we first get an expression for ω in the limit when the SF oscillates faster than the Hubble expansion ($\omega/H \gg 1$). By rewriting the complex function in terms of its amplitude and phase as $\Psi = |\Psi|e^{i\theta}$ and plugging it back into (3.42) we get

$$\frac{\hbar^2}{2mc^2}(\partial_t^2|\Psi| - |\Psi|(\partial_t\theta)^2) + \frac{\hbar^2}{2mc^2}\frac{3da/dt}{a}\partial_t|\Psi| + \frac{1}{2}mc^2|\Psi| + \lambda|\Psi|^3 = 0, \quad (3.43)$$

$$\frac{\hbar^2}{2mc^2}(2\partial_t|\Psi|\partial_t\theta + |\Psi|(\partial_t^2\theta) + \frac{\hbar^2}{2mc^2}\frac{3da/dt}{a}|\Psi|\partial_t\theta = 0. \quad (3.44)$$

It is the phase θ that carries the oscillation behavior of Ψ , the time dependence of the amplitude is smooth, hence it is safe to assume $\partial_t|\Psi|/|\Psi| \ll \partial_t\theta$. Assuming also that $\omega := \partial_t\theta \gg H = (da/dt)/a$, then we can neglect the terms $\partial_t|\Psi|$ and H in (3.43) and it results

$$-\frac{\hbar^2}{2mc^2}|\Psi|(\partial_t\theta)^2 + \frac{1}{2}mc^2|\Psi| + \lambda|\Psi|^3 = 0, \quad (3.45)$$

using $\omega := \partial_t\theta$ the above equation becomes

$$\omega = \frac{mc^2}{\hbar}\sqrt{1 + \frac{2\lambda}{mc^2}|\Psi|^2}, \quad (3.46)$$

valid only when $\omega \gg H$. In the free field case ($\lambda=0$) we get $\omega = mc^2/\hbar$, from here it is easy to see that small values of the mass translates into high oscillation frequencies.

Integrating (3.44) we get

$$\partial_t(a^3|\Psi|^2\partial_t\theta) = 0 \iff |\Psi|^2\partial_t\theta = \frac{const.}{a^3}. \quad (3.47)$$

where $a^3|\Psi|^2\partial_t\theta$ is the conserved charge, in fact it is the conservation of the comoving charge density Qa^3 .

Given the fast oscillation of the field we can follow the cosmological evolution of the time-average values of ρ and p , a similar situation is found for the non-interacting case, although in that case the equivalence of the exact and time-average evolution of the scalar field has been worked out[Magaña et al.(2012)].

If we now multiply (3.42) by Ψ^* and average over a time interval much longer than the field oscillation period ($\propto 1/\omega$) but shorter than the Hubble time results in[Woo & Chihue(2009), Dutta & Scherrer (2010)]

$$\frac{\hbar^2}{2mc^2}\langle|\Psi|^2\rangle = \frac{1}{2}mc^2\langle|\Psi|^2\rangle + \lambda\langle|\Psi|^4\rangle = 0. \quad (3.48)$$

Now it is possible to combine this equation with the expressions for ρ and p and obtain

$$\langle \rho \rangle = mc^2 \langle |\Psi|^2 \rangle + \frac{3}{2} \lambda \langle |\Psi|^4 \rangle \approx mc^2 \langle |\Psi|^2 \rangle + \frac{3}{2} \lambda \langle |\Psi|^2 \rangle^2, \quad (3.49)$$

$$\langle p \rangle = \frac{1}{2} \lambda \langle |\Psi|^4 \rangle \approx \frac{1}{2} \lambda \langle |\Psi|^2 \rangle^2 \quad (3.50)$$

with the equation of state

$$\langle p \rangle = \frac{m^2 c^4}{18\lambda} \left(\sqrt{1 + \frac{6\lambda \langle \rho \rangle}{m^2 c^4}} - 1 \right)^2 \quad (3.51)$$

or equivalently

$$\langle \omega \rangle = \frac{\langle p \rangle}{\langle \rho \rangle} = \frac{1}{3} \left[\frac{1}{1 + \frac{2mc^2}{3\lambda \langle |\Psi|^2 \rangle}} \right] \quad (3.52)$$

this equation is also found for a real scalar field [Steigman (2012)], this is interesting as the cosmological evolution for a real and complex field depends on ω that defines the equation of state, hence the complex and real give equivalent descriptions to the cosmological evolution.

We now have the EOS and can identify the phases:

1. Non-relativistic(CDM-like) phase: $\langle \omega \rangle = 0$.

Here the rest-mass energy density dominates the total SFDM energy density, this means that $\frac{3}{2} \lambda \langle |\Psi|^2 \rangle^2 \ll mc^2 \langle |\Psi|^2 \rangle$, and (3.51) reads

$$\langle p \rangle \approx \frac{\lambda}{2m^2 c^4} \langle \rho \rangle \approx 0, \quad (3.53)$$

the last equality is due to the scalar field behaving as dust (that is $p \ll \rho$) to mimic CDM. Therefore we get $\rho \sim a^{-3}$. This phase also occurs in the non-interacting case ($\lambda = 0$).

2. Relativistic(radiation-like) phase: $\langle \omega \rangle = 1/3$. At early times the SFDM will be so dense that the self-interaction term dominates, ($\frac{3}{2} \lambda \langle |\Psi|^2 \rangle^2 \gg mc^2 \langle |\Psi|^2 \rangle$), and (3.51) reduces to

$$\langle p \rangle \approx \frac{1}{3} \approx \frac{\lambda}{2} \langle |\Psi|^2 \rangle^2, \quad (3.54)$$

which is the EOS of radiation, thus in this limit the field behaves like radiation, and its energy density $\rho \sim a^{-4}$ and $a \sim t^{1/2}$. This extra phase is a notable difference with the $\lambda = 0$ case.

3. Stiff phase: $\langle \omega \rangle = 1$. Before the radiation-like phase, when the expansion rate of the universe is much greater than the oscillation frequency, $\omega \ll H$, the kinetic term dominates over the potential and $\frac{\hbar^2}{2mc^2} |\partial_t \Psi|^2 \propto H^2$. Then

$$p \approx \rho \approx \frac{\hbar^2}{2mc^2} |\partial_t \Psi|^2. \quad (3.55)$$

In this case $\rho \sim a^{-6}$ and $a \sim t^{1/3}$. This phase was expected from (3.20), in this case the field cannot complete even one oscillation, instead it rolls down the potential well.

From the CMB we know there was a time in which the universe is dominated by radiation, when the photons and elemental particles are in thermal equilibrium. As the universe expands and the temperature decreases some particles will no longer be produced and fall out of equilibrium, this time is called freeze-out, there is a time then when light elements can form leaving the primordial abundances, this epoch is the big bang nucleosynthesis(BBN), in the standard model this epoch extends from the beginning of the neutron-proton ratio freeze-out at $T_{n/p}=1.293$ MeV($a_{n/p} \sim 10^{-10}$)(the difference between the neutron and proton mass) to the epoch of nuclei production around $T_{nuc} \approx 0.085$ MeV[Durrer (2008)]. The observations of the primordial element's abundance are in good agreement with theoretical calculations in CDM, the stiff phase found above is an epoch when the SFDM dominates, in order to prevent conflicts with BBN the universe should be dominated by radiation at that epoch, this implies that the stiff phase should end at $a \sim 10^{-10}$ at the latest should the BBN remain unaffected by the SF. On the other hand, the radiation-like phase of the SF shall end at $z_{eq} \sim 3000$ so that it can become non-relativistic and behave as cold dark matter.

Solving numerically the cosmological evolution and taking into consideration the above constrains for the scalar field, the evolution of the energy density that results is shown in figure 3.2 obtained in [Li et al.(2014)]. They manage to place an upper bound on the parameters by demanding that the SFDM be fully non-relativistic at z_{eq} requiring that at this time $\omega = 0.001$ yielding

$$\frac{\lambda}{(mc^2)^2} \leq 4 \times 10^{-17} eV^{-1} cm^3, \quad (3.56)$$

while imposing that the SFDM changes from the stiff to the radiation-like phase by the end of BBN (a_{nuc}) and that the number of relativistic degrees of freedom N_{eff} during the BBN be all the time within 1σ of the measured value

$$N_{eff} = 3.71^{+0.47}_{-0.45} \quad (3.57)$$

taken from [Arbey et al.(2002)], results in

$$9.5 \times 10^{-19} eV^{-1} cm^3 \leq \lambda/(mc^2)^2 \leq 1.5 \times 10^{-16} eV^{-1} cm^3. \quad (3.58)$$

It is important to notice that (3.58) is rather arbitrary, in principle the radiation phase can also be reached before a_{nuc} and this bound will no longer hold. Instead, if we want the scalar field to be the dark matter that forms the large scale structure of the universe the radiation-CDM transition should take place before decoupling (z_{dec}) which makes (3.56) a strong bound for a large class of models whose particle candidate is BICS.

The stiff phase is also present in the free field case ($V(\Phi) = \frac{1}{2}m^2\Phi^2$), we expect a similar situation but the transition would be from the stiff to the non-relativistic phase, however, temperature corrections of the field, insofar neglected, could lead to the appearance of a relativistic phase, this interesting fact is of relevance mainly in the non-interacting case of the scalar field and we are currently studying.

It is also relevant to note that when self interactions are considered in the potential, the cosmological constraints are on $\frac{\lambda}{(mc^2)^2}$, hence we require independent tests to constraint the mass or the interaction given that they appear in the above combination and are degenerated.

§3.3 Density perturbations

In the study of perturbations we require to specify the coordinates. A choice of coordinates defines a *threading* of space-time into lines (corresponding to fixed \mathbf{x}) and a *slicing* into hypersurfaces (corresponding to fixed t). The lines of fixed \mathbf{x} are chosen to be timelike, so they are world lines of possible observers, and the slices are chosen to be spacelike. As a reminder to the reader, unless otherwise specified (like in the previous section), we keep using natural units.

Consider for instance the case of the unperturbed universe (in our case the FRW universe). In this case there are preferred coordinates. The threading corresponds to the motion of comoving observers, defined as those who see zero momentum density at their own position. The comoving observers are free-falling and the expansion defined by them is isotropic. The slicing is orthogonal to the threading, and on each slice, the universe is homogeneous. The time coordinate is chosen to correspond to proper time along each worldline. In the case that slices are flat (zero spatial curvature), the space coordinates can be chosen to be Cartesian. This array of properties makes this preferred coordinate so valuable that no others are considered. This is the slicing and threading that we have been using in all this work for the cosmological description.

When we deal with perturbations, it is impossible to find coordinates satisfying all these properties, and there is no uniquely preferred choice. The way people have dealt with this issue is by requiring that the coordinates must reduce to the standard ones in the limit where the perturbations vanish. A choice of coordinates satisfying this constraint is called a *gauge*, and there is no unique preferred gauge.

As we see, the only function of a gauge choice in cosmological perturbation theory is to define a slicing and threading of space-time. The slicing and threading in turn define the perturbations. For a perturbation $g(\mathbf{x}, t)$, the space-time coordinates can be regarded as those of unperturbed space-time because to include their perturbation would be a second order effect. Hence, the perturbations live in the unperturbed space-time.

As we will be concerned with scalar perturbations we will choose a suitable gauge to isolate them from the vector and tensor perturbations. Notice that a slicing is needed to specify perturbations in quantities such as the energy density, which have nonzero (and time-varying) values in the unperturbed universe. Take for instance the energy density, given a slicing, we write

$$\rho(\mathbf{x}, t) = \rho(t) + \delta\rho(\mathbf{x}, t). \quad (3.59)$$

The first term is the unperturbed part, the one we have been calling the background density in the FRW universe, and as mentioned, once $\delta\rho(\mathbf{x}, t)$ is defined the coordinates \mathbf{x} and t can be identified to the standard ones in the unperturbed space-time. The slicing that we will use to make use of the unperturbed (or background) space-time is the comoving

slicing, orthogonal to the worldlines of comoving observers. Also, it can be shown that the perturbation in a scalar quantity is independent of the threading, the only effect of a change in threading is to change the values of the space coordinates of each point, the measured scalar perturbation by one observer will differ only by an amount of order v^2 , with v the relative velocity of the other observer [Liddle & Lyth (2000)].

When the scalar field perturbations are small, we can study them with linear perturbation theory. We consider the real scalar field. We then write

$$g_{\mu\nu} = g_{\mu\nu}^0 + \delta g_{\mu\nu} \quad (3.60)$$

here $g_{\mu\nu}^0$ is the unperturbed FRW metric. In conformal time η the most general form of the linearly perturbed FRW metric is ([Malik(2001)])

$$ds^2 = a^2(\eta)[-(1 + 2\psi)d\eta^2 + 2B_{,i} d\eta dx^i + [(1 - 2\phi)\delta_{ij} + 2E_{,ij}]dx^i dx^j]. \quad (3.61)$$

where the perturbations are given in terms of four scalar functions: ψ the lapse function, ϕ gravitational potential, B the shift, and E the anisotropic potential. The perturbed component are

$$\delta g_{00} = -a^2(\eta)2\psi, \quad (3.62)$$

$$\delta g_{0i} = \delta g_{i0} = a^2(\eta)B_{,i} \quad (3.63)$$

$$\delta g_{ij} = -2a^2(\eta)(\phi\delta_{ij} - E_{,ij}). \quad (3.64)$$

Additionally, $\Phi(\eta, \mathbf{x}) = \Phi_0(\eta) + \delta\Phi(\eta, \mathbf{x})$, in the linear regime $\delta\Phi \ll \Phi_0$ so we can approximate $V(\Phi) \approx V(\Phi_0)$. We define the density contrast by

$$\delta := \frac{\delta\rho}{\rho_0}, \quad (3.65)$$

the density contrast δ gives information about the amplitude of the perturbations as they evolve in the expanding homogeneous background, according the CMB observations this are $\delta \sim 10^{-5}$. We can use the freedom in the gauge choice to set two of the four scalar metric perturbations to zero, we choose the Newtonian gauge where $B = 0 = E$ leaving only the Bardeen potentials, the metric reads

$$ds^2 = a^2(\eta)[-(1 + 2\psi)d\eta^2 + [(1 - 2\phi)\delta_{ij}dx^i dx^j]. \quad (3.66)$$

In this gauge, the physics appears rather simple since the hypersurfaces of constant time are orthogonal to the worldlines of observers at rest in the coordinates (since $B = 0$) and the induced geometry of the constant-time hypersurfaces is isotropic (since $E = 0$). In the absence of anisotropic stress the metric is diagonal and $\psi = \phi$. Note the similarity of the metric to the usual weak-field limit of general relativity about Minkowski space; then ϕ can be identified with the gravitational potential. The Newtonian gauge is our preferred gauge for studying the formation of large-scale structures.

For the perturbed energy momentum tensor we have

$$T = T_0 + \delta T, \quad (3.67)$$

with $T_0 = T_0(t)$ and $\delta T = \delta T(x^\mu)$ with $x^\mu = (t, \mathbf{x})$. Explicitly the perturbed density $\delta\rho$ and the perturbed pressure δp in comoving time t ($d/d\eta = a(d/dt)$) are defined in terms of the perturbed energy momentum tensor as

$$\begin{aligned} \delta T_0^0 &= -\delta\rho = -(\dot{\Phi}_0\delta\dot{\Phi} - \dot{\Phi}_0^2\psi + V_{,\Phi}\delta\Phi), \\ \delta T_i^0 &= -\frac{1}{a}(\dot{\Phi}_0\delta\Phi_{,i}), \\ \delta T_j^i &= \delta p = (\dot{\Phi}_0\delta\dot{\Phi} - \dot{\Phi}_0^2\psi - V_{,\Phi}\delta\Phi)\delta_j^i. \end{aligned} \quad (3.68)$$

$\delta\rho$ is the perturbed energy density of the scalar field, δp is the perturbed pressure and $\delta\Phi$ the scalar field fluctuation.

The perturbed EKG system in the Newtonian gauge $\delta G_j^i = \kappa^2\delta T_j^i$ is

$$\begin{aligned} -8\pi G\delta\rho &= 6H(\dot{\phi} + H\phi) - \frac{2}{a^2}\nabla^2\phi, \\ 8\pi G\dot{\Phi}_0\delta\Phi_{,i} &= 2(\dot{\phi} + H\phi)_{,i}, \\ 8\pi G\delta p &= 2[\ddot{\phi} + 4H\dot{\phi} + (2\dot{H} + 3H^2)\phi] \end{aligned} \quad (3.69)$$

with $\dot{} = \partial/\partial t$ and $H = d(\ln a)/dt$.

The above system of equations describe the evolution of the scalar perturbations (Malik(2001), Ma & Bertschinger(1995)). Summing the first and third equations in (3.69) and from (3.68) we get $\delta p - \delta\rho = -2V_{,\Phi}$ and we get an equation for the gravitational potential

$$\delta\ddot{\phi} + 7H\delta\dot{\phi} - \frac{1}{a^2}\nabla^2\delta\phi + 2(\dot{H} + 3H^2)\phi + 8\pi GV_{,\Phi}\Phi = 0. \quad (3.70)$$

To study the evolution of the SF perturbations we use the perturbed Klein-Gordon equation

$$\delta\ddot{\Phi} + 3H\delta\dot{\Phi} - \frac{1}{a^2}\nabla^2\delta\Phi + V_{,\Phi\Phi}\delta\Phi + 2V_{,\Phi}\phi - 4\dot{\Phi}_0\dot{\phi} = 0. \quad (3.71)$$

Equation (3.71) can be rewritten as:

$$\square\delta\Phi + \left.\frac{d^2V}{d\Phi^2}\right|_{\Phi_0}\delta\Phi + 2\left.\frac{dV}{d\Phi}\right|_{\Phi_0}\phi - 4\dot{\Phi}_0\dot{\phi} = 0, \quad (3.72)$$

where the D'Alambertian operator is defined as

$$\square := \frac{\partial^2}{\partial t^2} + 3H\frac{\partial}{\partial t} - \frac{1}{a^2}\nabla^2. \quad (3.73)$$

The equations can be studied in the Fourier space, this approach is usually convenient because in the linear regime each Fourier mode evolves independently. The Fourier transform at first order is readily obtain

$$\delta\Phi(t, \mathbf{x}) = \int d^3k\delta\Phi(t, \mathbf{k})\exp(i\mathbf{k}\cdot\mathbf{x}) = \int d^3k\delta\Phi_k\exp(i\mathbf{k}\cdot\mathbf{x}) \quad (3.74)$$

k is the wave number defined by $k = 2\pi/\lambda_k$, where λ_k denotes the size of the scalar field perturbation. The perturbed EKG system can be transform to its Fourier equivalent by changing $\delta\Phi \rightarrow \delta\Phi_k$, $\nabla^2 \rightarrow -k^2$ with $k^2 = k_i k^i$ and $\partial_i \rightarrow -ik_i$. The system transforms to

$$\begin{aligned} 8\pi G(3H\dot{\Phi}_0\delta\Phi_k) + \frac{2k^2}{a^2}\phi_k &= -8\pi G(\dot{\Phi}_0\delta\dot{\Phi} - \dot{\Phi}_0^2\phi_k + V_{,\Phi}\delta\Phi), \\ 2(\dot{\phi}_k + H\phi_k) &= 8\pi G\dot{\Phi}_0\delta\Phi_k, \\ 2[\ddot{\phi}_k + 4H\dot{\phi}_k + (2\dot{H} + 3H^2)\phi_k] &= 8\pi G(\dot{\Phi}_0\delta\dot{\Phi} - \dot{\Phi}_0^2\phi_k - V_{,\Phi}\delta\Phi) \end{aligned} \quad (3.75)$$

and

$$\delta\ddot{\phi}_k + 7H\delta\dot{\phi}_k + \left(\frac{k^2}{a^2} + 2\dot{H} + 6H^2\right)\phi_k + 8\pi GV_{,\Phi}\Phi_k = 0. \quad (3.76)$$

$$\delta\ddot{\Phi}_k + 3H\delta\dot{\Phi}_k + \left(\frac{k^2}{a^2} + V_{,\Phi\Phi}\right)\delta\Phi_k + 2\phi_k V_{,\Phi} - 4\dot{\Phi}_0\dot{\phi}_k = 0. \quad (3.77)$$

The system (3.75), (3.76) and (3.77) describe the cosmological evolution in the linear regime for a scalar field perturbation with wave number k . Essentially, equation (3.77) represents a harmonic oscillator with a damping $3H\delta\dot{\Phi}_k$ and an extra force $-2\phi_k V_{,\Phi}$. The damping term in (3.76) goes as $6H\dot{\phi}_k$, the term $2\dot{H} < 0$ and the gravitational fluctuations can grow provided $(\frac{k^2}{a^2} + 2\dot{H} + 6H^2) < 0$. Equation (3.77) has oscillatory solutions if $(V_{,\Phi\Phi} +$

$\frac{k^2}{a^2}) < 0$. This equation contains growing solutions if this term is negative, that is, if $V_{,\Phi\Phi} < 0$ and $\frac{k^2}{a^2}$ is small enough. From here we see an important feature. These perturbations grow only if V has a maximum, even if it is a local one. Here, the potential is unstable and during the time when the scalar field remains in the maximum, the scalar field fluctuations grow until they reach a new stable point where the gravitational structures can keep growing until they collapse and form the dark matter halos. Therefore, the term $(V_{,\Phi\Phi} + \frac{k^2}{a^2})$ defines a wave number below which the fluctuations don't grow and keep oscillating, this is equivalent to the Jeans length in CDM,

$$k_{efJ} := \sqrt{a^2 V_{,\Phi\Phi}}. \quad (3.78)$$

Only fluctuations with $k < k_{efJ}$ can grow. We can define an associated Jeans length [Ma et al. (1999), Hwang& Noh (2001)]

$$\lambda_{efJ} = \frac{2\pi}{a\sqrt{V_{,\Phi\Phi}}} = 2\pi/ma. \quad (3.79)$$

From this relation we see that the mass of the boson ($V_{,\Phi\Phi} = m^2$) determines a minimum scale for the growing modes, thus fixing the mass naturally implies a cut-off in the mass power spectrum, this particular feature is of extreme importance because it implies a supresion of dark matter substructure below a certain scale k_{efJ} , which helps to reduce the satellite overabundance and serve to solve the missing satellite problem present in CDM [Hu, Barkana & Gruzinov(2000), Matos & Ureña(2001), Marsh & Silk(2014)]. For instance, if $m \sim 10^{-23}$ eV we have $\lambda_{efJ} \sim 4$ kpc at the epoch of recombination $a \sim 10^{-3}$.

§3.4 Linear growth of scalar field perturbations

Although it is possible to obtain the complete evolution of the psyon perturbations by solving the perturbed EKG system [Magaña et al.(2012)], it is nevertheless useful to have an equation for the linear evolution of the density contrast δ . The equation follows after doing a lengthy but otherwise straightforward algebra in complete analogy to the calculation for CDM perturbations [Suárez & Matos (2011), Suárez & Chavanis (2015)].

For the cold dark matter model the equation for the evolution of the density contrast is given by

$$\frac{d^2\delta}{dt^2} + 2H\frac{d\delta}{dt} + \left(c_s^2\frac{k^2}{a^2} - 4\pi G\rho_0\right)\delta = 0, \quad (3.80)$$

where c_s is defined as the sound velocity. For cold and pressureless dark matter the equation of state $\omega = 0$ and the sound speed $c_s = \delta p / \delta \rho = 0$, then at $a \geq a_{eq}$ the interesting fluctuation modes (galactic-size) are well within the horizon, we have $a \sim t^{2/3}$ and $\rho \sim a^{-3}$, thus

$$\frac{d^2\delta}{dt^2} + \frac{4}{3t} \frac{d\delta}{dt} - \frac{2}{3t^2} \delta = 0, \quad (3.81)$$

The solutions to this equation are of the form

$$t \rightarrow t^{2/3} C_1 + \frac{C_2}{t} \quad (3.82)$$

where C_1 and C_2 are integration constants, from this solution we can see that we have modes that will disappear as time goes by, and modes that grow proportionally to the expansion of the Universe $\delta \sim a$. The matter fluctuations that enter the horizon in the radiation era ($a < a_{eq}$) have a logarithmic growth $\delta \sim \ln(a)$, had there been no logarithmic growth these fluctuations would have experience no growth from horizon entry until the epoch of equality, their amplitude relative to large scale modes (small k) would be suppressed. A more detailed analysis will not be treated here, but can be found in [Dodelson (2003)].

Now, in the case of a free scalar field $V(\Psi) = m^2\Phi^2/2$, the relevant scale is the Hubble scale, H . The (time average) equation of state (EOS) transitions from $\omega = -1$ to $\omega = 0$ when the psyon mass overcomes the Hubble friction in the Klein-Gordon equation, also the structure is suppressed on scales of order the horizon when $H \sim m$ [Marsh & Silk(2014), Hu, Barkana & Gruzinov(2000), Marsh & Ferreira(2010)]. When the field is oscillating about the potential minimum at times $t > t_{osc}$, where $H(t_{osc}) \sim m$, the EOS and sound speed in the effective fluid description averaged over periods $t > 1/m$ are given by ([Hu, Barkana & Gruzinov(2000), Park et al. (2012)])

$$\omega = 0, \quad (3.83)$$

$$c_s^2 = \frac{v_q^2}{1 + v_q^2}. \quad (3.84)$$

where we define

$$v_q^2 := \frac{k^2}{4m^2 a^2}. \quad (3.85)$$

Notice that c_s is now scale-dependent, the term v_q^2 comes from the oscillation frequency of the field. The equation for the density contrast takes the form

$$\frac{d^2\delta}{dt^2} + 2H\frac{d\delta}{dt} + (c_s^2\frac{k^2}{a^2} - 4\pi G\rho_0)\delta = 0, \quad (3.86)$$

or in conformal time

$$\frac{d^2\delta}{d\eta^2} + 2H(\eta)\frac{d\delta}{d\eta} + (c_s^2k^2 - 4\pi G\rho_0a^2)\delta = 0, \quad (3.87)$$

where $H(\eta) = aH(t)$ is the conformal Hubble rate as usual.

For the large scale perturbations with $k^2 \ll a^2m^2$ we have $c_s^2 \approx v_q^2 \ll 1$ and the sound speed goes to zero, here we recover the scale-independent linear growth with $\delta \sim a$ on large scales. For large k , or $k^2 \gg a^2m^2$, the sound speed $c_s^2 \approx 1$ and the overdensity oscillates rather than grows. This is consistent with the discussion in the last section, the transition between growth and oscillation occurs at the Jeans scale

$$k_J = a(16\pi G\rho_0)^{1/4}m^{1/2}. \quad (3.88)$$

For $k > k_J$ there is no growth of structure. There is scale-dependent growth as k decreases from k_J , continuously interpolating to the standard scale-independent linear growth on the largest scales, $k \ll k_J$.

When self-interactions are included as in (3.33), (3.86) turns

$$\frac{d^2\delta}{dt^2} + 2H\frac{d\delta}{dt} + ((c_s^2 + \omega_\lambda\rho_0)\frac{k^2}{a^2} - 4\pi G\rho_0)\delta = 0, \quad (3.89)$$

with $\omega_\lambda = 9\lambda/2m^2$ [Suárez & Matos (2011)]. Therefore $\lambda \neq 0$ changes the Jeans scale in the free-field case.

The evolution of the linear growth of psyon perturbations when $c_s^2 \approx v_q^2$ was obtained in (Suarez & Matos 2011), as shown in figure (3.4) linear growth after $a_{eq} \sim 10^{-4}$ proceeds just like CDM ($\delta \sim a$), the case self-interacting field however, shows an earlier amplitude growth. These results can impact the large scale structure, a faster growth implies that the structures can become non-linear faster and the dark matter potential wells that will host galaxies are formed before CDM, after decoupling the gas will follow the potential wells and can condense earlier forming stars and hence galaxies at high redshift, this can

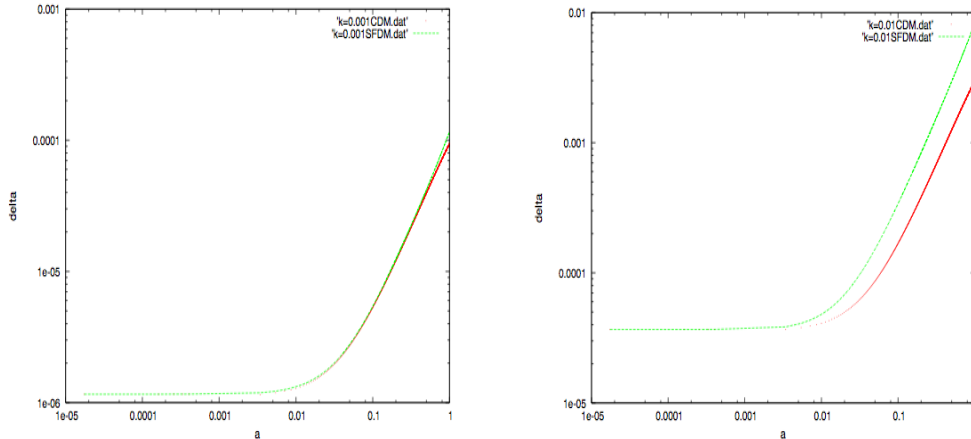


Figure 3.3: Left: Evolution of the perturbations for the CDM model (dots) and SFDM model with $\lambda = 0$ (lines) for $k = 1 \times 10^3 h \text{ Mpc}^{-1}$. After the epoch of equality ($a_{eq} \sim 10^{-4}$) the evolution of both perturbations is nearly identical, normalized to $a(z = 0) = 1$. Right: Evolution of the perturbations for the CDM model (dots) and SFDM model (lines) for $k = 1 \times 10^{-2} h \text{ Mpc}^{-1}$ and $\lambda \neq 0$ and negative. In this case we see that the SFDM fluctuations grow earlier than in the CDM model.

be tested by the abundance of galaxies at high redshift placing better constraints as more observations become available.

§3.5 Halo Mass function and Power Spectrum

Early on, of the modes (short, medium and large-wavelength modes) are outside the horizon ($k\eta \ll 1$) and the gravitational potential ϕ is constant. At intermediate times, the wavelengths fall within the horizon and the universe evolves from radiation domination ($a \ll a_{eq}$) to matter domination ($a \gg a_{eq}$). Large scale modes enter $k \sim 0.001 h \text{ Mpc}^{-1}$ the horizon well after a_{eq} , evolves much differently than the small-scale ($k = 2 h \text{ Mpc}^{-1}$) modes which enter the horizon before equality. At late times the evolve identically again, it is in this late stage that we can observe the distribution of matter. In order to relate the potential during these times to the primordial set up during inflation, we write schematically

$$\phi(\mathbf{k}, a) = \phi_p(\mathbf{k}) \times [TransferFunction(k)] \times [GrowthFunction(a)]. \quad (3.90)$$

where ϕ_p is the primordial value of the potential, set during inflation. The transfer function describes the evolution of perturbations through the epochs of horizon crossing and radiation/matter transition, while the growth factor describes the wavelength-independent growth at late times. There are two conventions, one is to set the transfer function equal to on large scales, therefore the transfer function is defined as

$$T(k) := \frac{\phi(k, a_{late})}{\phi_{Large-scale}(k, a_{late})} \quad (3.91)$$

where a_{late} denotes an epoch well after the transfer function regime and the *Large-scale* solution is the primordial ϕ decreased by a small amount, in CDM this factor is equal to (9/10) neglecting anisotropic stresses [Dodelson (2003)]. The second convention concerns the growth function. The ratio of the potential to its value right after the transfer function regime is defined to be

$$\frac{\phi(a)}{\phi(a_{late})} := \frac{D(a)}{a} \quad (a > a_{late}) \quad (3.92)$$

where D is called the growth function. When the potential is constant $D(a) = a$. With these conventions we have

$$\phi(\mathbf{k}, a) = \frac{9}{10} \phi_p(\mathbf{k}) T(k) \frac{D(a)}{a} \quad (a > a_{late}) \quad (3.93)$$

From the above section we saw that when the potential is constant and all the modes are within the horizon, the overdensity grows as $\delta \sim a$, D describes the growth of the matter perturbations at late times, for this reason D is called the growth function despite the potential remains constant. This picture is consistent with the intuitive idea that as time evolves, overdense regions attract more matter, thereby becoming more overdense.

Let us first the case of the standard model. The simplest way to relate the matter overdensity to the potential at late times is to use Poisson's equation in Fourier space (for the large- k and no-radiation limit)

$$\phi = \frac{4\pi G \rho_m a^2 \delta}{k^2} \quad (3.94)$$

where the background density of matter $\rho_m = \Omega_m \rho_{crit}/a^3$, and $4\pi G \rho_{crit} = (3/2)H_0^2$, so

$$\delta(\mathbf{k}, a) = \frac{k^2 \phi(\mathbf{k}, a) a}{(3/2)\Omega_m H_0^2} \quad (a > a_{late}), \quad (3.95)$$

substituting the expression for $\phi(\mathbf{k}, \mathbf{a})$ allow us to relate the overdensity today to the primordial potential

$$\delta(\mathbf{k}, a) = \frac{3}{5} \frac{k^2}{\Omega_m H_0^2} \phi_p(\mathbf{k}) T(k) D(a) \quad (a > a_{late}), \quad (3.96)$$

this equation holds regardless of how the initial perturbation ϕ_p was generated. In the context of inflation $\phi_p(\mathbf{k})$ is drawn from a Gaussian distribution with mean zero and variance

$$P_\phi = \frac{50\pi^2}{9k^3} \left(\frac{k}{H_0}\right)^{n-1} \delta_H^2 \left(\frac{\Omega_m}{D(a=1)}\right)^2 \quad (3.97)$$

so the power spectrum of matter at late times is

$$P(k, a) = 2\pi^2 \delta_H^2 \frac{k^n}{H_0^{n+3}} T^2(k) \left(\frac{D(a)}{D(a=1)}\right)^2 \quad (a > a_{late}). \quad (3.98)$$

The power spectrum has dimensions of (length)³, to convert it into a dimensionless quantity one often associates $dk^3 P(k)/(2\pi)^3$ with the excess power in a bin of width k centered at k , after integrating over all orientations of \mathbf{k} this becomes $(dk/k)\Delta^2(k)$, with

$$\Delta^2(k) := \frac{k^3 P(k)}{2\pi^2} \quad (3.99)$$

Small Δ then corresponds to small inhomogeneities, while a large value indicates nonlinear perturbations. With the conventions used, for a Harrison-Zel'dovich-Peebles spectrum ($n = 1$) today we have $\Delta^2 = \delta_H^2$ on a horizon-sized scale ($k = H_0$).

On large scales the transfer function is unity and $P \propto k$ corresponding to the simplest inflationary model, wherein $n = 1$. There is a turn over over in the power spectrum at a scale corresponding to the one which enters the horizon at matter/radiation equality. We can see why this happens with an example. A small-scale mode with $k = 2h\text{Mpc}^{-1}$ enters the horizon well before matter/radiation equality, during the radiation era the potential decays, so $T(k)$ is much smaller than unity. The effect on matter perturbations will be to retard the growth of δ after the mode has entered the horizon until the universe is matter dominated. Modes that enter the horizon earlier undergo more suppression, thus the power spectrum is a decreasing function of k on small scales. This turnover is important as it can restricts the number of small scale modes that remain at $z=0$. One scale that is also important is in which nonlinearities cannot be ignored, this is set by $\Delta(k_{nl} \simeq 1)$, corresponding in CDM usually to $k_{nl} \simeq 0.2h\text{Mpc}^{-1}$.

Now, in a cosmology where the pions are the dark matter, or in general a fraction of it $f_p = \Omega_p/\Omega_d$, the suppression scale occurs for modes that enter the horizon when the sound speed was large, we will neglect self-interactions. The suppression is centered around k_m , which depends on the mass, and the fraction Ω_p .

In [Marsh & Silk(2014)], they compute the transfer function and matter power spectrum in cosmologies containing CDM plus SFDM using a modified version of the code `CAMB`. They define the transfer function of the SFDM

$$T_{sfdm}(k) = \left(\frac{P_{sfdm}}{P_{\Lambda CDM}} \right)^{1/2}. \quad (3.100)$$

A well defined characteristic scale to assign to any such step-like transfer function is the 'half mode'

$$T(k_m) = 0.5(1 - T(k \rightarrow \infty)), \quad (3.101)$$

where $T(k \rightarrow \infty) \geq 0$ is the constant value of the transfer function on small scales. For comparison we include the warm dark matter(WDM) model transfer function [Bode et al.(2001)]

$$T_{WDM}(k) = (1 + (\alpha k)^{2\mu})^{-5/\mu}, \quad (3.102)$$

where $\mu = 1.12$ and $\alpha \approx 0.065h^{-1}\text{Mpc}$ chosen to give the same k_m than in SFDM. This selection of k_m in SFDM is not the Jeans scale where all structure is suppressed, but it is useful when comparing different dark matter models because it is well-defined. Taking a typical mass of the psyon $m \sim 10^{-22}\text{eV}$, it is found $k_m(10^{-22}) = 6.7h\text{Mpc}^{-2}$.

One popular way to characterize power on a particular scale is to compute the expected root-mean-squared overdensity in a sphere of radius R ,

$$\sigma_R^2 := \langle \delta_R^2(x) \rangle \quad (3.103)$$

Here

$$\delta_R(\mathbf{x}) := \int d^3x' \delta(\mathbf{x}) W_R(\mathbf{x} - \mathbf{x}') \quad (3.104)$$

where $W_R(x)$ is the *top-hat* window function, equal to 1 for $x < R$ and 0 otherwise; the angular brackets denote the average over all space. The variance of the power spectrum, can be rewritten as

$$\sigma_R^2 := \int_0^\infty \frac{dk}{k} \Delta^2(k) \tilde{W}_R^2(k) \quad (3.105)$$

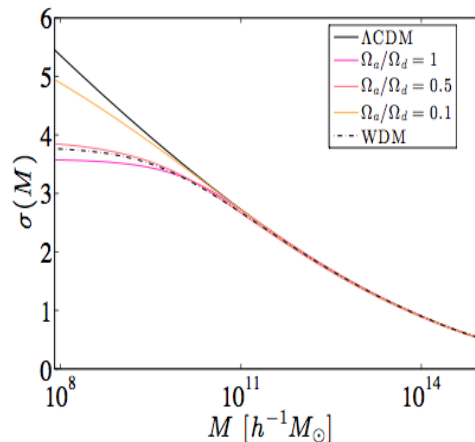


Figure 3.4: Variance $\sigma(M)$ for Λ CDM, and SFDM with various $\Omega_p h^2$ at a fixed total $\Omega_p h^2 = 0.112$ and psyon mass $m = 10^{-22} \text{eV}$ [Marsh & Silk(2014)].

where $\tilde{W} = \frac{3}{(kR)^3}(\sin(kR) - kR\cos(kR))$ is the Fourier transform of $W_R(x)$, $\Delta^2 = d\sigma^2/d\ln(k)$ is the contribution to the variance per $\ln(k)$.

The variance computed for the Λ CDM, WDM, and the SFDM model for different fractions of psyon to cold dark matter are shown in figure 3.5. When the psyons comprise the total DM $\Omega_p/\Omega_d = 1$ the reduce in power is the highest.

This send us back to the Missing-Satellite problem, the discrepancy with observations in the expected number of satellite galaxies in the Local Group. In the absence of simulations, to quantify the problem it is possible to adopt the Press-Schechter approach (Press & Schechter (1974)) to compute the abundance of halos of a given mass; this is called the *halo mass function* (HMF). In the usual formalism this reads

$$\frac{dn}{d\ln M} = -\frac{1}{2} \frac{\rho_0}{M} f(\nu) \frac{d \ln \sigma^2}{d \ln M} \quad (3.106)$$

where $\nu := \delta_c/\sigma$, $dn = n(M)dM$ is the abundance of halos within a mass interval dM . The function $f(\nu)$ can be obtained form the model of [Sheth & Tormen (1999)]:

$$f(\nu) = A \sqrt{\frac{2}{\pi}} \sqrt{q} \nu (1 + (\sqrt{q} \nu)^{-2p}) \exp \left[-\frac{q \nu^2}{2} \right] \quad (3.107)$$

with parameters $A = 0.3222$, $p = 0.3$, $q = 0.707$. This approach was followed in Marsh & Silk(2014), in the HMF one can use the variance of the matter power spectrum, computed at redshift $z=0$ if the barrier for collapse, δ_c , is given by the Einstein-de Sitter value at

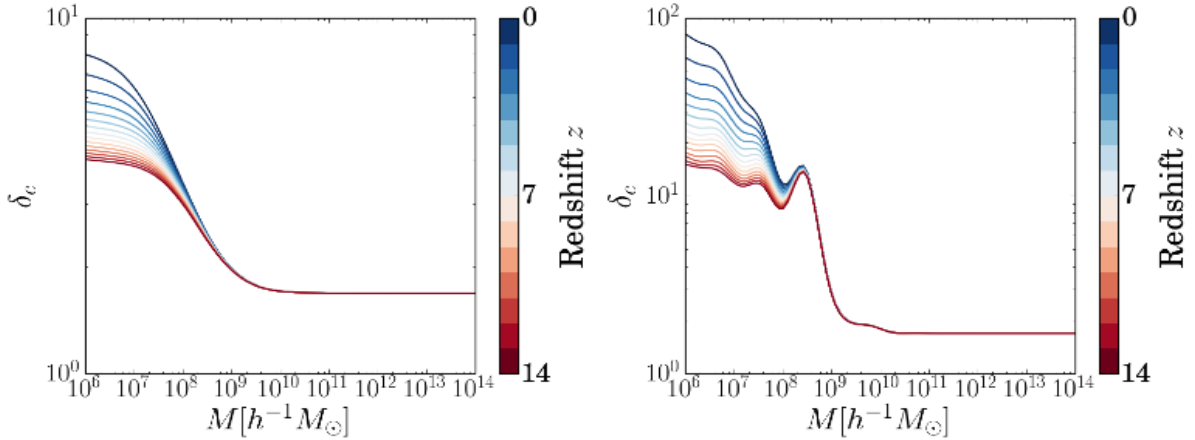


Figure 3.5: The mass dependent critical overdensity for two benchmark models in which some or all of the dark matter is in the form of SFDM, shown for each redshift in the range $0 \leq z \leq 14$. Left Panel: $m = 10^{-22}$ eV, $\Omega_p/\Omega_c = 0.5$. Right Panel: $m = 10^{-22}$ eV, $\Omega_p/\Omega_c = 1$.

$z = 0$, $\delta_{c,EdS} \approx 1.686$, scaled by the linear growth: $\delta_c(z) = \delta_{c,EdS}/D(z)$. Marsh & Silk (2013) proposed that one could account for scale-dependent growth by simply replacing $D(z) \rightarrow D(k, z)$ and then using the enclosed mean mass to define a halo-mass dependent barrier for collapse, $\delta_c(M, z)$.

In figure 3.5 is plotted $\delta(M, z)$ computed in the above manner for two SFDM cosmologies. They each take $m = 10^{-22}$ eV while varying the fractional energy density in psyons, $\Omega_p = \rho_p/\rho_{crit}$, and CDM, Ω_c , and holding the total DM density, $\Omega_d = \Omega_p + \Omega_c$, fixed. The first model takes $\Omega_p/\Omega_c = 0.5$, so that half of the DM is in SFDM, and the second takes $\Omega_p/\Omega_c = 1$. As may be seen in the figure, the barrier for collapse becomes large for low mass objects due to the vanishing growth on scales below the Jeans scale.

The mass-dependent barrier for collapse can simply be substituted into the Sheth-Tormen mass function along with the correct variance to find $dn/d\ln M$, the number-density of halos per logarithmic mass bin. The HMFs for the two cosmologies of Fig. 3.5 are shown in Fig. 3.5. The rising value of $\delta_c(M)$ for low M is seen to suppress the HMF relative to CDM in both cosmologies, particularly at high- z . The existence of this sharp suppression due to scale-dependent growth is a key prediction of SFDM. At high redshift we should expect many fewer objects to have formed when the DM contains a ultra light

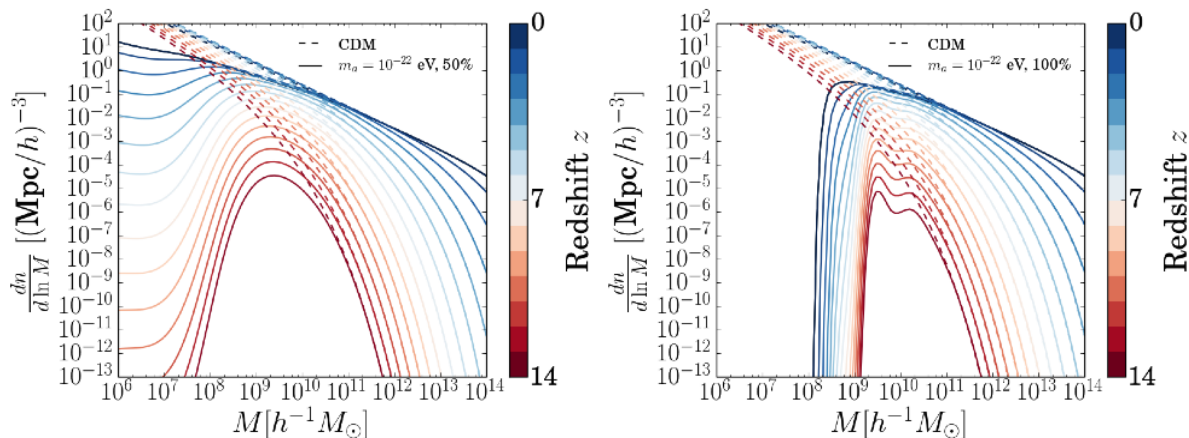


Figure 3.6: Sheth-Tormen mass function for SFDM including scale-dependent growth, shown for each redshift in the range $0 \leq z \leq 14$ [Bozek et al.(2015)]. The result for CDM is shown for reference. Left Panel: $m = 10^{-22}$ eV, $\Omega_p/\Omega_c = 0.5$. Right Panel: $m = 10^{-22}$ eV, $\Omega_p/\Omega_c = 1$.

boson compared to a pure CDM universe, even when these bosons are only a fractional component of the DM.

The cut off in the HMF at $z = 13$ in Fig 3.5 (Right Panel) occurs at $M \approx 10^9 h^{-1} M_\odot$, and the HMF peaks near this value. This cut off is what causes the reduction in the MSP, in fact, the number of halos decreases sharply not by tidal stripping or by astrophysical mechanisms, but by the smallness of the mass of the psyon. This solution to the MSP seems to be preferable to invoking unknown stellar feedback and poorly understood baryonic physics, especially as a high suppression due to stellar feedback may be in conflict with the observations of local dwarfs as we discussed in chapter 2.

Quite recently, the first high-resolution simulations of the formation of structure in a universe dominated by psyon DM with $m = 8.1 \times 10^{-23}$ eV and no self-interactions carried out by [Schive et al.(2014)], found that the large scale structure is remarkably similar to CDM, as desired, but differs radically inside galaxies where quantum interference forms solitonic cores surrounded by extended halos of fluctuating density granules, denser more massive solitons are predicted for Milky Way sized galaxies, providing a substantial seed to help explain early spheroid formation. They report a first object of mass $M = 10^9 M_\odot$ at $z = 13$. This is consistent with the above semi-analytic model, so far the full HMF from their

simulations has not been reported which makes difficult addressing more quantitatively either the Too-Big-To-Fail or the satellite problem.

Although the self interactions do change the linear structure, it is uncertain how different the cosmological nonlinear evolution will be from the free field case, mainly due to the small coupling parameter for a $m \sim 10^{-22}$ eV and the fact that after a_{dec} the equation of state for the field $p \approx 0$ cosmologically just as in the CDM model, this would be an interesting study for the future.

§3.6 Spontaneous symmetry break

We have exploited the smallness of the psyon mass to show that the large scale structure is well reproduced in the SFDM model. So far we have considered a scalar field to be at zero temperature and use the classical description, as we mentioned the BICS candidates have a large fraction of bosons in the ground state which may lead to BEC condensation, this implies that a large number of bosons are in single state justifying the classical approach. But how do we include the effects of a non zero temperature?

Given the similarity with a flat FRW space-time, let us first remember the situation in flat four-dimensional Minkowski's space.

The equation of motion for a real scalar field Φ of mass m is the Klein-Gordon equation

$$(\square + m^2)\Phi := \ddot{\Phi} - \nabla^2\Phi + m^2\Phi = 0. \quad (3.108)$$

where the dot denotes differentiation with respect to time. The general solution of this equation is expressible as a superposition of plane waves, corresponding to the propagation of particles of mass m and momentum k [Bogolyubov & Shirkov (1980)]

$$\begin{aligned} \Phi(x) &= (2\pi)^{-3/2} \int d^4k \delta(k^2 - m^2) [e^{ikx} \Phi^+(k) + e^{-ikx} \Phi^-(k)] \\ &= (2\pi)^{-3/2} \int \frac{d^3k}{\sqrt{2k_0}} [e^{ikx} a^+(\mathbf{k}) + e^{-ikx} a^-(\mathbf{k})], \end{aligned} \quad (3.109)$$

where $a^\pm(\mathbf{k}) = \frac{1}{\sqrt{2k_0}} \Phi^\pm(k)$, $k_0 = \sqrt{\mathbf{k}^2 + m^2}$, $kx = k_0t - \mathbf{k} \cdot \mathbf{x}$. According to (??), the field will oscillate about the point $\Phi = 0$, the reason being that the minimum of the potential energy density for the field occurs at this value. The functions $a^\pm(\mathbf{k})$ can be put in correspondence

with the creation and annihilation operators a_k^\pm for particles with momentum k . The commutation relations take the form[Bogolyubov & Shirkov (1980)]

$$\frac{1}{2k_0}[\Phi_k^-, \Phi_k^+] := [a_k^-, a_k^+] = \delta(\mathbf{k} - \mathbf{q}), \quad (3.110)$$

where the operator a_k^- acting on the vacuum gives zero:

$$a_k^-|0\rangle = 0; \langle 0|a_k^+ = 0. \quad (3.111)$$

The operator a_k^+ creates a particle with momentum k and a_k^- annihilates it,

$$a_k^+|\Phi\rangle = |\Phi, \mathbf{k}\rangle \quad (3.112)$$

$$a_k^-|\Phi, \mathbf{k}\rangle = |\Phi\rangle. \quad (3.113)$$

The Green's function for the scalar field

$$G(x) = \langle 0|T[\Phi(x)\Phi(0)]|0\rangle = \frac{1}{(2\pi)^4} \int \frac{e^{-ikx}}{m^2 - k^2 - i\epsilon} d^4k. \quad (3.114)$$

Here T denotes the time-ordering operator, and ϵ shows how to perform the integration near the singularity at $k^2=m^2$. Calculating $G(0)$ one obtains (after transforming to Euclidean space by a Wick rotation $k_0 \rightarrow -ik_4$)

$$G(0) = \langle 0|\Phi^2|0\rangle = \frac{1}{(2\pi)^4} \int \frac{d^4k}{k^2 + m^2} = \frac{1}{(2\pi)^3} \int \frac{d^3k}{2\sqrt{k^2 + m^2}} \quad (3.115)$$

or if the average is carried out over a state containing particles other than the conventional vacuum state, representing $\langle \Phi^2 \rangle := \langle 0|\Phi^2|0\rangle$ we get

$$\langle \Phi^2 \rangle = \frac{1}{(2\pi)^3} \int \frac{d^3k}{\sqrt{k^2 + m^2}} \left(\frac{1}{2} + n_k \right) \quad (3.116)$$

where $n_k = \langle a_k^+ a_k^- \rangle$ is the number density of particles with momentum k . For a Bose gas at nonzero temperature

$$n_k = \frac{1}{\exp\left(\frac{\sqrt{k^2+m^2}}{T}\right) - 1}. \quad (3.117)$$

An important case is the Bose Einstein condensate Φ_0 of non-interacting particles of the field Φ , with mass m and vanishing momentum (\mathbf{k}) for which

$$n_k = (2\pi)^3 \Phi_0^2 m \delta(\mathbf{k}), \quad (3.118)$$

or a coherent wave of particles of momentum \mathbf{p} :

$$n_k = (2\pi)^3 \Phi_p^2 \sqrt{\mathbf{p} + m^2} \delta(\mathbf{k} - \mathbf{p}). \quad (3.119)$$

in both cases, $n_k \gg 1$ at some value \mathbf{k} , this means that the fact that the operators a_k^\pm do not commute can be ignored in (3.116) and the field can be treated as classical.

Let us now consider the following Lagrangian

$$L = \frac{1}{2}(\partial_\mu \Phi)^2 + \frac{\mu}{2}\Phi^2 - \frac{\lambda}{4}\Phi^4. \quad (3.120)$$

with potential

$$V(\Phi) = -\frac{\mu}{2}\Phi^2 + \frac{\lambda}{4}\Phi^4 \quad (3.121)$$

Instead of oscillations about $\Phi = 0$, the solution corresponding to (3.109) gives modes that grow exponentially near $\Phi = 0$ when $\mathbf{k} < \mu^2$:

$$\delta\Phi(\mathbf{k}) \sim \mathbf{exp}(\pm\sqrt{\mu^2 - \mathbf{k}^2}\mathbf{t}) \cdot \mathbf{exp}(\pm i\mathbf{k} \cdot \mathbf{x}). \quad (3.122)$$

This means that the minimum of the potential will now occur at $\Phi_c = \pm\mu/\sqrt{\lambda}$. Thus even if the field is zero initially, it soon undergoes a transition (after a time of order μ^{-1}) to a stable state with the classical field $\Phi_c = \pm\mu/\sqrt{\lambda}$, this phenomenon is known as *spontaneous symmetry breaking*(SB).

After spontaneous SB, excitations of the field Φ near Φ_c can also be described by a solution like (3.109), we require a change of variables to do it

$$\Phi \rightarrow \Phi + \Phi_0 \quad (3.123)$$

Then (3.120) takes the form

$$\begin{aligned} L(\Phi + \Phi_0) &= \frac{1}{2}(\partial_\mu(\Phi + \Phi_0))^2 + \frac{\mu}{2}(\Phi + \Phi_0)^2 - \frac{\lambda}{4}(\Phi + \Phi_0)^4, \\ &= \frac{1}{2}(\partial_\mu\Phi)^2 - \frac{3\lambda\Phi_0 - \mu^2}{2}\Phi^2 - \lambda\Phi_0\Phi^3 - \frac{\lambda}{4}\Phi^4 \\ &\quad + \frac{\mu^2}{2}\Phi_0^2 - \frac{\lambda}{4}\Phi_0^4 - \Phi(\lambda\Phi_0^2 - \mu)\Phi_0. \end{aligned} \quad (3.124)$$

from here we see that when $\Phi \neq 0$, the effective mass squared of the field ϕ is not $-\mu^2$, but becomes

$$m^2 = 3\lambda\Phi_0^2 - \mu^2, \quad (3.125)$$

and when $\Phi_0 = \pm\mu/\sqrt{\lambda}$, at the minimum of the potential $V(\Phi)$ we have

$$m^2 = 2\lambda\Phi_0^2 = 2\mu^2 > 0; \quad (3.126)$$

this is the mass of the field. Reverting to the original variables, we can write the solution for Φ in the form

$$\Phi(x) = \Phi_0 + (2\pi)^{-3/2} \int \frac{d^3k}{\sqrt{2k_0}} [e^{ikx} a^+(\mathbf{k}) + e^{-ikx} a^-(\mathbf{k})]. \quad (3.127)$$

the integral in (3.127) corresponds to particles (quanta) of the field Φ with mass given by (3.126), propagating against the background of the constant classical field Φ_0 . The presence of Φ_0 over all space will not give rise to any preferred reference frame associated with that field: the Lagrangian (3.124) is covariant, irrespective of the magnitude of Φ_0 .

3.6.1 Quantum and thermal corrections in Minkowski space-time

Quantum corrections to the classical expression for the potential are given by a set of all one-particle irreducible vacuum diagrams (diagrams that do not dissociate into two when a single line is cut) in a theory with the Lagrangian $L(\Phi + \Phi_0)$ without the terms linear in Φ [Coleman & Weinberg(1973), Jackiw (1973)]. In the case of (3.121) expansion in the number of loops corresponds to expansion in the small coupling constant λ . In the one-loop approximation

$$V(\Phi) = -\frac{\mu}{2}\Phi^2 + \frac{\lambda}{4}\Phi^4 + \frac{1}{2(2\pi)^4} \int d^4k \ln[k^2 + m^2(\Phi)]. \quad (3.128)$$

Here $k^2 = k_4^2 + \mathbf{k}^2$ (resulting after a Wick rotation $k_0 \rightarrow -ik_4$ and integrating over Euclidean momentum space), and the effective mass of the field $m = 3\lambda\Phi^2 - \mu^2$ (we omit the subscript 0 from the classical field Φ). The integral in (3.128) diverges at large k . To supplement the definition counter terms must be added in order to renormalize the wave function, mass, coupling constant, and vacuum energy [Slavnov & Faddeev (1980), Taylor(1976), 't Hooft(1971)]. The counter terms for $L(\Phi + \Phi_0)$ in (3.120) are $C_1\partial_\mu(\Phi + \Phi_0)\partial^\mu(\Phi + \Phi_0)$, $C_2(\Phi + \Phi_0)^2$, $C_3(\Phi + \Phi_0)^4$ and C_4 . Integrating (3.128) over k_4 , the result (up to an infinite constant that is eliminated by renormalization of the vacuum energy, i.e. by the addition of C_4 to $L(\Phi + \Phi_0)$) is

$$V(\Phi) = -\frac{\mu}{2}\Phi^2 + \frac{\lambda}{4}\Phi^4 + \frac{1}{(2\pi)^3} \int d^3k \sqrt{k^2 + m^2(\Phi)}. \quad (3.129)$$

thus in the one-loop approximation the effective potential $V(\Phi)$ is given by the sum of the classical expression for the potential energy of the field Φ and a Φ -dependent vacuum energy shift due to quantum fluctuations of the field. To determine the quantities C_i , we require to impose normalization conditions on the potential, these can be chosen [Linde (1976)]

$$\begin{aligned}\frac{dV}{d\Phi}\Big|_{\Phi=\mu/\sqrt{\lambda}} &= 0, \\ \frac{d^2V}{d\Phi^2}\Big|_{\Phi=\mu/\sqrt{\lambda}} &= 2\mu^2.\end{aligned}\tag{3.130}$$

These conditions ensure that the location of the minimum of $V(\Phi)$ for $\Phi = \mu/\sqrt{\lambda}$ and the curvature of $V(\Phi)$ at the minimum (which is the same to lowest order in λ as the mass squared of the scalar field Φ) remain the same as in the classical theory. This conditions are suitable to study theories that have spontaneous symmetry breaking. Applying this conditions, the potential takes the form

$$V(\Phi) = -\frac{\mu}{2}\Phi^2 + \frac{\lambda}{4}\Phi^4 + \frac{(3\lambda\Phi^2 - \mu^2)^2}{64\pi^2} \ln\left(\frac{3\lambda\Phi^2 - \mu^2}{2\mu^2}\right) + \frac{21\lambda\mu^2}{64\pi^2}\Phi^2 - \frac{27\lambda^2}{128\pi^2}\Phi^4.\tag{3.131}$$

For $\lambda \ll 1$, quantum corrections only become important for asymptotically large Φ (when $\lambda \ln(\Phi/\mu) \gg 1$, where higher order corrections need to be taken into account, however, for $\lambda > 0$, it becomes extremely difficult to sum all higher-order corrections to the expression for $V(\Phi)$ at large Φ . Based on this calculation, given that in the SFDM we have $\lambda \ll 1$, to first approximation the quantum corrections can then be neglected.

Having discussed the basic features of spontaneous SB, we can now turn to a consideration of symmetry behavior in systems of particles in thermodynamic equilibrium. For scalar particles Φ with Lagrangian (3.120), they carry no charge, nor their number is a conserved quantity, the chemical potential therefore vanishes for such particles and their density in momentum space is

$$n_k = \frac{1}{\exp(k_0/T) - 1}\tag{3.132}$$

where $k_0 = \sqrt{\mathbf{k}^2 + \mathbf{m}^2}$ is the energy of a particle with momentum \mathbf{k} and mass m . In this case, at finite temperatures, the symmetry breaking parameter is the classical scalar field and depends on the temperature. A theory of phase transitions involving the disappearance of the classical field Φ is discussed in [Linde (1979)]. The idea is that the equilibrium

value of the field at fixed temperature $T \neq 0$ is governed not by the location of the minimum of the potential energy density $V(\Phi)$, but by the location of the minimum of the free energy density $F(\Phi, T) := V(\Phi, T)$, which equals $V(\Phi)$ at $T=0$. The temperature dependent contribution to the free energy F from ultra relativistic scalar particles of mass m at temperature $T \gg m$ was given in [Landau & Lifshitz (1968)], see also[Linde (1990)]. We briefly summarize the process. To calculate $V(\Phi, T)$, it suffices to recall that at $T \neq 0$, quantum statistics is equivalent to Euclidean quantum field theory in a space which is periodic, with period $1/T$ along the “imaginary time” axis[Weinberg (1974), Dolan & Jackiw (1974)]. To go from $V(\Phi, 0)$ to $V(\Phi, T)$ one should replace all boson momenta k_4 in the Euclidean integrals by $2\pi nT$ for bosons and $(2n + 1)\pi T$ for fermions, and sum over n instead of integrating over k_4 :

$$\int d^4k \rightarrow 2\pi T \sum_{n=-\infty}^{\infty}$$

. For example, at $T \neq 0$, equation (3.128) for $V(\Phi)$ in the theory (3.120) transforms into

$$V(\Phi, T) = -\frac{\mu^2}{2}\Phi^2 + \frac{\lambda}{4}\Phi^4 + \frac{T}{2(2\pi)^3} \sum_{n=-\infty}^{\infty} \int d^3k \ln[(2\pi nT)^2 + k^2 + m^2(\Phi)], \quad (3.133)$$

where $m^2(\Phi) = 3\lambda\Phi^2 - \mu^2$. This expression can be normalized using the same counter terms as for $T=0$. The potential for $T \gg m$ then reads

$$V(\Phi, T) = -\frac{\mu^2}{2}\Phi^2 + \frac{\lambda}{4}\Phi^4 + \frac{\lambda T^2}{8}\Phi^2 - \frac{\pi^2}{90}T^4 + \dots, \quad (3.134)$$

where the other terms do not depend on Φ and are of lower order in (m/T) , in fact as derived in [Landau & Lifshitz (1968)] the temperature-dependent contribution in this limit is

$$\Delta F = \Delta V(\Phi, T) = -\frac{\pi^2}{90}T^4 + \frac{m^2}{24}T^2 \left(1 + O\left(\frac{m}{T}\right)\right). \quad (3.135)$$

with $m^2(\Phi) = 3\lambda\Phi^2 - \mu^2$. The equation that determines the minimum $dV/d\Phi = 0$ is

$$\Phi(T)[\lambda\Phi^2(T) - \mu^2 + \frac{\lambda}{4}T^2] = 0, \quad (3.136)$$

at sufficiently low temperature, this equation has two solutions,

$$\Phi_0(T) = 0 \quad (3.137)$$

$$\Phi_0(T) = \sqrt{\frac{\mu}{\lambda} - \frac{T^2}{4}}. \quad (3.138)$$

The second of these vanishes above a critical temperature T_c

$$T_c = \frac{2\mu}{\sqrt{\lambda}}. \quad (3.139)$$

The excitation spectrum (perturbations of the background) can be computed carrying out the shift $\Phi \rightarrow \Phi + \delta\Phi$. We determine the mass of the scalar field with $d^2V/d\Phi^2$, when $\Phi = 0$ the mass is

$$m^2 = -\mu^2 + \frac{\lambda}{4}T^2 \quad (3.140)$$

which is positive when $T > T_c$. For the second solution (3.138) $\Phi_c := \sqrt{\frac{\mu}{\lambda} - \frac{T^2}{4}}$, the mass, corresponding to the normalization conditions (3.130) that we will use for the potential, takes the value

$$m^2(\Phi) = 3\lambda\Phi^2 - \mu^2 + \frac{\lambda}{4}T^2 = 2\lambda\Phi_c^2(T). \quad (3.141)$$

This solution is stable $T < T_c$, and vanishes for $T > T_c$ at the instant when the solution $\Phi = 0$ becomes stable. This means that a phase transition with restoration of symmetry takes place at a temperature $T = T_c$ [Kirzhnits (1972), Kirzhnits & Linde (1972)]. From (3.133) it follows that as T rises, the equilibrium value of Φ at the minimum of $V(\Phi, T)$ decreases continuously to zero with increasing temperature, above T_c the only minimum is the one at $\Phi = 0$ and symmetry is restored, the restoration of symmetry corresponds to a second-order phase transition. Finally it is interesting to note that when $\lambda \ll 1$ and $T \gg m$ ($\Phi \leq \Phi_c$) the high-temperature expansion of $V(\Phi, T)$ in powers of m/T is justified.

3.6.2 Thermal corrections in FRW universe

Here we return to our notation where Φ_0 denotes the background cosmological scalar field. We will use the results of the previous subsection in the spirit that the potential energy density of a scalar field is (up to quantum corrections that we will neglect) takes the form of its classical description.

Additionally, in the flat FRW universe, the preferred slicing that we are using and the Newtonian gauge make the surfaces of constant time spatially flat, in fact the FRW metric in conformal time is (see (1.13)) conformally flat (to Minkowski's metric). This semi-classical approach seems to be reasonable when the system we are dealing is composed of a large number of bosons because we are interested in the collective behavior of all of the

particles, as an order of magnitude estimate if we assume that psions comprise all the dark matter today, then $\rho_{dm,0} \approx 23\% \rho_{crit}$, where $\rho_{crit} \approx 4.19 \times 10^{-11} \text{eV}^4$, thus the number of bosons will be $n \approx (\rho_{dm}/m) \approx 10^{12} \text{eV}^3$, moreover, for a mass of $m \sim 10^{-23} \text{eV}$ this estimate implies according to (3.1) a critical temperature of condensation of $T_{BEC} \approx 1.7 \times 10^{17} \text{eV} \sim 10^{21} \text{K}$, suggesting that cosmologically mostly all bosons would be in the form of a BEC, the study of BE condensation in a relativistic boson gas was given in [Ureña-López (2009)]. We now consider the potential energy density with thermal correction given by

$$V(\Phi) = -\frac{\mu^2}{2}\Phi^2 + \frac{\lambda}{4}\Phi^4 + \frac{\lambda T^2}{8}\Phi^2 - \frac{\pi^2}{90}T^4. \quad (3.142)$$

notice that in the FRW universe the d’Alambertian operator is given by (3.73). If we plug this potential in (3.71) we obtain

$$\square\delta\Phi + \frac{\lambda}{4}[(T^2 - T_C^2) + 12\Phi_0^2]\delta\Phi - 4\dot{\Phi}_0\dot{\phi} + \frac{\lambda}{2}[(T^2 - T_C^2) + 4\Phi_0^2]\Phi_0\phi = 0. \quad (3.143)$$

The numerical evolution of this equation has been solved in [Magaña et al.(2012)]. They have analyzed with some detail the evolution of a perturbation with wavelength 2 Mpc and density contrast $\delta = 1 \times 10^{-7}$ after the SB, they took as initial condition $a=10^{-6}$ and evolve it until $a=10^{-3}$. They also analyzed the case $T \sim T_c$ and show that as the temperature decreases and goes below T_c , Φ_0 converges rapidly to a new minimum where it remains oscillating with small amplitudes, whereas the SF fluctuation grows quickly as Φ_0 approaches the new minimum.

It is always desirable and useful to obtain analytical solutions when possible as they are frequently easier to handle. In order to get such solution we have to restrict ourselves to a simple limit which is given in the following section.

3.6.3 Analytical solution for SFDM halos

We are concerned with DM halos after their formation, thus, we constrain ourselves to solve the weak field limit of equation (3.143) when Φ is near the minimum of the SF potential and after the SB, where we expect it to be stable as suggested by the numerical result showing small amplitude oscillations around the minimum. In this limit, the gravitational potential may be locally homogeneous in the beginning of its collapse, thus, $\dot{\phi} \approx 0$. For clarity, we stop using units in which $c=1$.

Assuming the SF is at the minimum of the potential ($V'(\Phi)|_{\Phi_0} = 0$), i.e., when $\Phi_0^2 = \Phi_{\min}^2 = k_B^2(T_c^2 - T_\Phi^2)/4$ and $T_\Phi < T_c$ (neglecting the expansion $H = 0$), eq. (3.143) reads

$$\ddot{\delta\Phi} - \nabla^2 \delta\Phi + \frac{\lambda k_B^2}{2\hbar^2} (T_c^2 - T_\Phi^2) \delta\Phi = 0. \quad (3.144)$$

Equation (3.144) describes a SF fluctuation which formed in the regime where the symmetry is broken. We mentioned that after the SB, the perturbations can grow until they reach their new minimum, thus, each perturbation has a temperature at which it forms and separates from the background field following its own evolution, we denote this temperature of formation by T_Φ . We can regard equation (3.144) as a first approximation to DM halos of early isolated galaxies or those not heavily influenced by their neighbors, for instance, systems that were born in low density regions.

Taking the ansatz

$$\delta\Phi = \delta\Phi_0 \frac{\sin(kr)}{kr} \cos(\omega t) \quad (3.145)$$

we found that it is an exact solution to equation (3.144) provided

$$\omega^2 = k^2 c^2 + \frac{\lambda k_B^2}{2\hbar^2} (T_c^2 - T_\Phi^2). \quad (3.146)$$

Here $\delta\Phi_0$ is the amplitude of the fluctuation. It is convenient to write the latter equation using the standard definition of number density $n(x, t) = \kappa(\delta\Phi)^2$, where κ is a constant that gives us the necessary units so that we can interpret $n(x, t)$ as the number density of DM particles, as in our treatment Φ has units of energy. With this in mind, we can define an effective mass density of the SF fluctuation by $\rho = mn$ and a central density by $\rho_0 = m\kappa(\delta\Phi_0)^2$. The value of ρ_0 is a more familiar quantity and can be obtained fitting rotation curves.

For the static solution of a SFDM halo the analytical approximation has the following mass density profile [Robles & Matos (2013)]

$$\rho(r) = \rho_0 \frac{\sin^2(kr)}{(kr)^2}, \quad (3.147)$$

provided $\Phi_0^2 = \Phi_{\min}^2$, here k and $\rho_0 = \rho_0$ are parameters to be constrained by observations.

Equation (3.147) results in a mass and rotation curve profiles given by

$$M(r) = \frac{4\pi G \rho_0 r}{k^2} \left(1 - \frac{\sin(2kr)}{2kr} \right), \quad (3.148)$$

$$V^2(r) = \frac{4\pi G \rho_0}{2k^2} \left(1 - \frac{\sin(2kr)}{2kr} \right). \quad (3.149)$$

respectively. Considering the SFDM distribution to be localized in a given spherical region of space of radius R , we get a cut-off radius set by the condition $\rho(R) = 0$. This in turn results in the appearance of excited states (identified by the number of nodes, n , in their density profile), as solutions of equation (3.144), in fact, they provide the relation

$$k_j R = j\pi, \quad j = 1, 2, 3, \dots \quad (3.150)$$

where $j := 1+n$ serves to index the state of the halo, usually being the minimum state to fit a galaxy RC up to the last measured point. In general, there can be halos in combination of excited states in which the total density ρ_{tot} is the sum of the densities in the different states, given by

$$\rho_{\text{tot}} = \sum_j \rho_0^j \frac{\sin^2(j\pi r/R)}{(j\pi r/R)^2}, \quad (3.151)$$

with ρ_0^j the central density of the state j . The number of states that compose one DM halo depends of each halo and can vary, on the other hand, it would be reasonable to expect that the smallest structures are those that are in the ground state, although there might be some contribution from other states, we will explore this issues in the next chapter.

An additional feature of equation (3.147) is the presence of “wiggles,” these oscillations characteristic of SF configurations in excited states were also seen in [Sin (1994)]. Also, if we define the distance where the first peak (maximum) in the RC is reached as r_{max}^1 , this determines the first local maximum of the RC velocity, which can be obtained from equation (3.152)

$$\frac{\cos(2\pi jy)}{2(\pi j)^2 y} \left[\frac{\tan(2\pi jy)}{2\pi jy} - 1 \right] = 0, \quad (3.152)$$

where we used equation (3.150) and $y := (r_{\text{max}}^1/R)$.

As galaxies are thought to form inside DM halos, we can get a rough estimate for j , taken as the minimum excited state necessary to agree with the data up to the outermost regions, for some galaxies where the rotation curves(RCs) allow to resolve the first maximum in the profile, we can identify the last measured point in a RC as R and the innermost visible peak in the RC as r_{max}^1 , then, we look for the closest value of j associated with this y in Figure 3.6.3 (the values of Figure 3.6.3 are determined by equation (3.152)). This provides us roughly with the dominant state in the center of the galaxy and at the same time with the minimum state required to fit current observations. This estimate is in fact a lower

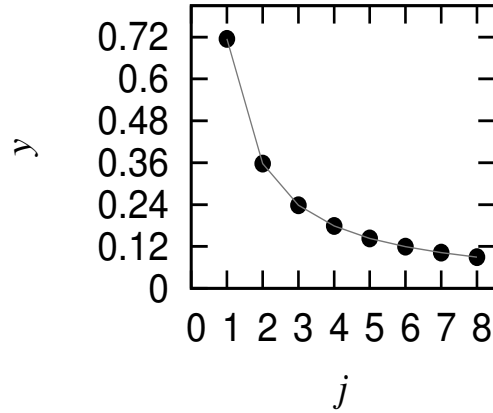


Figure 3.7: We plot the relation between y and j obtained by solving equation (3.152). Notice that for halos with large excited states (large j), the first maximum is attained at a smaller y for a fixed radius. A more compact structure would imply a higher excited state.[Robles & Matos (2013)]

bound because upcoming observations in the outskirts of galaxies might increase R , in such case y will decrease implying larger values of j , although we should point out that our analytical approximation is not intended to give a detailed fit of all galaxies, if this is desired the full numerical solutions would be more accurate.

As we will see in the next chapter this solution represents a good approximation to galaxies, and despite the limitations the qualitative properties inferred using this profile are consistent with previous works that have used numerical solutions [Ureña-López & Bernal(2010), Ureña-López ,Valdez-Alvarado, & Becerril(2012), Arbey et al.(2003), Bernal et al.(2010), Kaup (1968), Balakrishna, Seidel, & Suen(1998), Ji & Sin (1994), Glesier (1988), Friedbeg (1987), Ruffini & Bonazzola (1969)] keeping this in mind we may proceed with the comparison our model and observations in galaxies.

CONSEQUENCES OF SFDM IN GALAXIES

In this chapter we will apply the results that have been widely discussed in the literature regarding equilibrium configurations of self gravitating scalar field dark matter in the weak field limit, including our approximate solution given in the previous chapter. It is not my aim to redo all the calculations, but for the sake of completeness i provide a brief background on the Schrödinger-Poisson analysis including references for the interested reader.

§4.1 SFDM halos in equilibrium

There has been considerable work to find numerical solutions to the non-interacting SFDM in the non-relativistic regime to model spherically symmetric halos [Guzmán & Matos(2000), Guzmán & Ureña-López(2004), Ureña-López & Bernal(2010), Bernal et al.(2010), Bray(2012), Ruffini & Bonazzola (1969), Kaup (1968), Seidel & Suen(1991), Lee & Koh(1996), Lee & Lim(2010)] and also for the self-interacting SFDM [Böhmer & Harko(2007), Robles & Matos(2012), Colpi,Shapiro,& Wasserman(1986), Rindler-Daller & Shapiro(2012), Balakrishna, Seidel, & Suen(1998), Goodman (2000), Rindler-Daller & Shapiro(2014)], the equation that describes a dilute gas of bosons in the non relativistic limit with two-body point-like interactions of the form $V(\vec{r}' - \vec{r}) = g\delta(\vec{r}' - \vec{r})$ is the non-linear equation

$$i\hbar\frac{\partial}{\partial t}\psi(\vec{r},t) = \left(-\frac{\hbar^2}{2m}\nabla^2 + m\phi + g|\psi(\vec{r},t)|^2\right)\psi(\vec{r},t). \quad (4.1)$$

Where $g|\psi(\vec{r},t)|^2$ is the interaction term. The scattering cross-section of indistinguishable bosons becomes constant in the low-energy limit, $\sigma_s = 8\pi a_s^2$, with the s-wave scattering

length being a_s . The coupling constant of the effective interaction is then simply proportional to a_s

$$g = \frac{4\pi\hbar^2 a_s}{m}, \quad (4.2)$$

which is the (first) Born approximation. As before ϕ is the gravitational potential that satisfies the Poisson equation

$$\nabla^2\phi = 4\pi G\rho, \quad (4.3)$$

and $\rho = m|\psi|^2$. In spherical symmetry (in units $\hbar=1$, $c=1$) the SF solutions index by the number of nodes Φ_n , satisfying the Einstein-Klein-Gordon system are related to the Schrödinger-Poisson (SP) wavefunctions through

$$\sqrt{8\pi G}\Phi_n(\mathbf{x}, t) = e^{-imt}\psi_n(\mathbf{x}, t) \quad (4.4)$$

with m the mass of the SF. It is worth noting that in the absence of interactions, as mentioned in [Guzmán & Ureña-López(2004)], in the weak field limit the Einstein-Klein-Gordon system, for a complex and a real scalar field reduces to solving the Schrödinger-Poisson equations[Arbey et al.(2003)].

From current bounds reported in [Li et al.(2014)] obtained by imposing that the SF behaves cosmologically as pressureless matter(dust) we obtained that the interacting parameter would be extremely small for the typical mass of $\sim 10^{-22}\text{eV}/c^2$ (see eq. (3.56)), therefore solutions to the SP system without interactions would behave qualitatively similar to those when self-interactions are included, this assumption is supported by the similarity in the solutions for a small self-coupling found in other works[Balakrishna, Seidel, & Suen(1998), Colpi,Shapiro,& Wasserman(1986), Briscese(2011)], nevertheless, including interactions can increase the maximum mass of stability[Colpi,Shapiro,& Wasserman(1986)] and modify the configuration radius, for instance, without the self interactions (SIs) $\lambda\Phi^4$, the mass of a self-bound zero node configuration is

$$M = 0.633m_{pl}^2/m$$

where m_{pl} is the Planck mass, while including a repulsive SI term [Balakrishna, Seidel, & Suen(1998)] the mass becomes

$$M \sim 0.06\sqrt{\lambda}\frac{m_{pl}^3}{m^2},$$

which for $m = 1\text{GeV}$ it is larger than the former by $\sim \sqrt{\lambda} \frac{m_{pl}}{m} \sim 10^{19} \lambda$.

In principle both terms, the mass and self interaction, are contributing to the profile of the self gravitating object, solving different limits can give us an idea of the behavior of the solutions, in fact a complete numerical treatment of these two regimes can be found in [Chavanis (2011), Chavanis & Delfini (2011), Chavanis & Harko (2012)]. In the case where the SI are neglected the equation is

$$i\hbar \frac{\partial}{\partial t} \psi(\vec{r}, t) = \left(-\frac{\hbar^2}{2m} \nabla^2 + m\phi \right) \psi(\vec{r}, t), \quad (4.5)$$

in the other regime called the Thomas-Fermi limit the self interacting term dominates over the kinetic term (also called the *quantum term*).

Given the similarities in the solutions, such as the density profiles, the existence of a stable and unstable branch and stationary solutions with a characteristic oscillation frequency [Ureña-López & Bernal(2010), Chavanis & Harko (2012), Balakrishna, Seidel, & Suen(1998), Seidel & Suen(1990)] we may explore the non-interacting case and take it as representative of the SFDM predictions.

The SP system has been solved to look for equilibrium configurations that could be compared with some of the nearby galaxies, assuming they are in equilibrium. One characteristic feature of stationary solutions of the form $\psi(\mathbf{x}, t) = e^{-iE_n t} \varphi(r)$ for the SP system is the appearance of nodes in the spatial function $\varphi(r)$, these nodes are associated to different energy states of the SF, the zero node solution corresponds to the ground state, one node to the first excited state, and so on. These excited states solutions fit rotation curves(RCs) of large galaxies up to the outermost measured data and can even reproduce the wiggles seen at large radii in high-resolution observations [Sin (1994), Colpi, Shapiro, & Wasserman(1986), Robles & Matos(2013)]. Halos that are purely in a single excited state seem to be unstable when the number of particles is not conserved(finite perturbations) and decay to the ground state with different decay rates [Guzmán & Ureña-López(2004), Balakrishna, Seidel, & Suen(1998)], though they appear to be stable when the number of particles is conserved(infinitesimal perturbations). The ground state solution is stable under finite perturbations and infinitesimal perturbations [Bernal et al.(2010), Seidel & Suen(1990)], but has difficulties to correctly fit the rotation curves in large galaxies because its associated RC has a fast keplerian behavior

shortly after reaching its maximum value unable to remain flat enough at large radii, recently [Guzman et al.(2014)] have included rotation and find that the RCs can flatten at large radii for certain values of angular momentum, although it remains unclear if the same scheme works for galaxies of all sizes.

Another approach to get better fits in the RCs for both, large and small radii, was to consider that bosons are not in one state but instead coexist in different states within the halo, given the intention to describe dark matter halos I will refer to such configurations as multistate halos(MSHs), albeit they were first study in the context of boson stars[Ureña-López & Bernal(2010), Matos & Ureña-López(2007), Robles & Matos(2013), Robles & Matos(2013b)]. The size of the MSH is determined by the most excited state that accurately fits the RC for large radii, bosons in excited states are distributed to larger radii than the ground state, and in contrast to the halo with a single state there are MSHs that are stable under finite perturbations provided the ground state in the final halo configuration has enough mass to stabilize the coexisting state[Ureña-López & Bernal(2010), Bernal et al.(2010)]. In other words, when the ground state becomes the dominant state(in terms of boson number density) in a MSH, it will provide enough support to prevent the halo to collapse to a single state only, we may think of this as a quantum pressure produced due to the degeneracy of the state.

In [Bernal et al.(2010)] it was shown that MSHs can be studied in the classical approach as a collection of classical scalar fields coupled through gravity, one field ψ_i for each state, this would modify the SP system such that its source of energy density would be the sum of densities in each state[Ureña-López & Bernal(2010)], which corresponds to the non linear case of eq (3.151), each state satisfies its respective Schrödinger equation while remaining coupled through the Newtonian gravitational potential ϕ .

For stationary solutions we can assume wavefunctions of the form $\psi_n(\mathbf{x}, t) = e^{-iE_n t}\varphi(r)$, then the SP system effectively reads

$$\begin{aligned}\nabla^2\varphi_n &= 2(\phi - E_n)\varphi_n \\ \nabla^2\phi &= \sum_n |\varphi_n|^2\end{aligned}\tag{4.6}$$

with ∇^2 the Laplacian operator, and E_n the energy eigenstates.

Solving the equation for a simple MSH configuration using numerical methods [Ureña-López & Bernal(2010)] has shown an interesting feature during its evolution towards stability.

One interesting feature of multistates is a "population inversion¹" for initially unstable halos. This was seen in the simple cases of taking a MSH in a superposition of the lowest two energy states. For a MSH with only the ground and first excited states, [Ureña-López & Bernal(2010), Bernal et al.(2010)] studied the critical value for its stability under small perturbations. If the ground state has $N^{(1)}$ particles and there are $N^{(2)}$ in the excited state, the authors found that MSH would be stable under small perturbations provided its ratio satisfies

$$\eta := \frac{N^{(2)}}{N^{(1)}} \leq 1.2 = \eta_{max}. \quad (4.7)$$

In all the configurations studied in which η is larger than the maximum for stability η_{max} , the induced instability causes the configuration to lose a few particles and a remarkable effect takes place, the excited state does a fast transition to the ground state and vice versa, that is, the populations of the states are inverted such that the final η complies with the stability condition (4.7), after the inversion the MSH approaches a stable configuration where the particle number remains constant for each state, after the transition the particles that were initially in the excited state are now in the ground state where they are redistributed and become more compact than in their original distribution, providing pressure support in the central region, in Figure 4.1 ([Bernal et al.(2010)]) we can see the inversion early on and the convergence to the new states in time by looking at the frequencies ($\propto N^i$) of each state. The time to settle down into a stable configuration, increases as the fraction gets closer to η_{max} . This population inversion(PI) is a characteristic feature of MSHs and as we will see below such effect fits qualitatively good in our proposed halo formation scenario in the SFDM model. In fact, we will explore its consequences in the gas distribution during the period of galaxy formation. Additionally, given the cut-off in the

¹The name might be more familiar from the phenomenon laser, in which the population inversion occurs an emits photons. However, even though we have borrowed the name inspired in the laser phenomenon, in the case of dark matter there is not photon emission, as we are considering the field to be effectively decoupled from the rest of the particles, including the electromagnetic interaction.

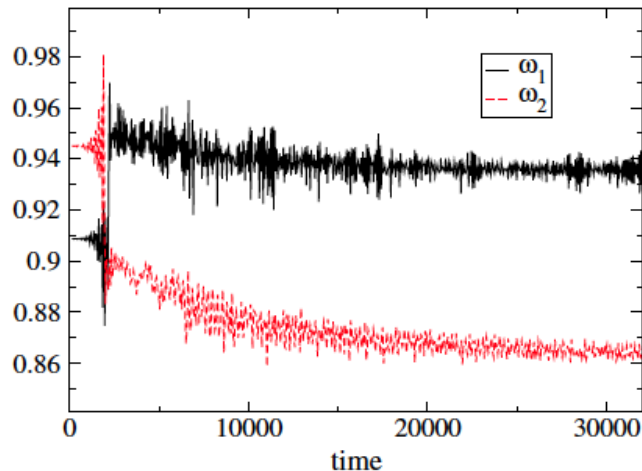


Figure 4.1: Plotted are the eigenfrequencies of each state during the transition of states in a multistate configuration formed by a superposition of the ground and the first excited state, characterized by their respective frequencies ω_1 and ω_2 (Bernal et al. 2010). The transition inverts the eigenfrequencies and happens early due to the instability being triggered due to the initial fraction of psyons in the excited states being larger than the critical value for stability.

mass power spectrum for small mass halos (due to the small mass of the psyon) we expect a delay in the formation of the first gravitational structures compared to the those found in CDM[Matos & Ureña(2001), Marsh & Silk(2014), Bozek et al.(2015)], this was observed with cosmological simulations for a mass of $8 \times 10^{-23} eV$ [Schive et al.(2014)](although the halo mass function was not reported by the authors), therefore, this intrinsic change of states within MSHs at high redshift might have observable consequences in the gas and stellar properties of the galaxies in the early stages of their formation, at those times the gas would be tracing the potential wells and likely substantial changes in the halo will impact the gas distribution too.

§4.2 LSB and dwarf galaxies

Among the vast number of galaxies that are currently observed, there are a large number of them with stellar masses of $M_* \sim 10^{10} - 10^{11} M_\odot$, comparable to our Milky Way galaxy, the masses of these structures make their detection easy with current space telescopes, the detection becomes harder for smaller objects as their baryonic content decreases, despite

the limitations we know there are galaxies with $M_* \sim 10^4 - 10^7 M_\odot$ that remain bounded even in our own galaxy, these dwarf galaxies required large mass-to-light ratios ($\sim 10 - 100$ [Walter & Peñarrubia(2011)]) which is usually interpreted as being in massive dark matter halos that contribute largely to their mass budget, this interpretation becomes more probable when the estimated mass-to-light ratios expected from stellar population models lie below the inferred ratio obtained from the movements of the stars in the galaxy. Dwarf spheroidal galaxies (dSphs) orbiting the MW are effectively devoid of gas and although they have a variety of star formation histories most of them have old stellar populations[Madau et al.(2014), Weisz et al.(2014a), Weisz et al.(2014b), Weisz et al.(2014c), Weisz et al.(2015)]. In addition to nearby dwarfs there are extragalactic low surface brightness galaxies whose dark matter content is also thought to be high [Kuzio de Naray et al.(2010), Kuzio de Naray & Spekkens(2011), Kuzio de Naray & Kaufmann(2011)] but these are usually more extended with observed radii larger than $\sim 1kpc$ as is frequently the case for dwarfs. These systems are particularly interesting candidates to test dark matter models as their baryonic matter may be neglected as a first approximation, on the other hand some of them lack enough resolution that frequently hinders the comparison in the inner parts.

Assuming that the stellar systems of the dSphs are pressure supported and in dynamic equilibrium², we follow the procedure of [Walker et al.(2009)] to find the relationship between the mass distribution of a SFDM halo and the stellar distribution, this is given by the Jeans equation

$$\frac{1}{\nu} \frac{d}{dr}(\nu \langle v_r^2 \rangle) + 2 \frac{\beta \langle v_r^2 \rangle}{r} = - \frac{GM(r)}{r^2}, \quad (4.8)$$

where $\nu(r)$, $\langle v_r^2 \rangle$, and $\beta(r)$ describe the 3-dimensional density, radial velocity dispersion, and orbital anisotropy, respectively, of the stellar component. The parameter β quantifies the degree of radial stellar anisotropy and there is no preference for either radially, $\beta > 0$, or tangentially, $\beta < 0$, biased systems. For circular orbits $\beta = -\infty$, $\langle v_r^2 \rangle = 0$; if $\langle v_r^2 \rangle =$

²The assumption of dynamical equilibrium is not necessarily true for all galaxies, the environment can affect such condition and even play a significant role in the halo and stellar distributions making the conclusions from the dynamical equilibrium hypothesis dubious and could possibly be the cause of discrepancies between the fits and observations. Although it is uncertain if galaxies are in true dynamical equilibrium, assuming the latter is often a good first approximation in dwarf spheroidals.

$\langle v_\theta^2 \rangle = \langle v_\phi^2 \rangle$, $\beta = 0$ (isotropic orbits); and for radial orbits $\beta = 1$, $\langle v_\phi^2 \rangle = \langle v_\theta^2 \rangle = 0$. Although β can take all these values, we restrict the anisotropy to be in the range $-0.6 \leq \beta \leq 0.3$ for the most realistic scenarios [Walker et al.(2009)], and consistent with other estimates using also the dSphs [Lokas(2009)].

In the simplest case the orbital anisotropy is independent of r ($\beta = const$), the solution of the Jeans equation relates the projection of the velocity dispersion along the line-of-sight, $\sigma_{los}^2(R)$, and the mass profile $M(r)$, to the stellar density $I(R)$ [Binney & Tremaine (2008)] through

$$\sigma_{los}^2 = \frac{2G}{I(R)} \int_R^\infty dr \nu(r) M(r) (r)^{2\beta-2} F(\beta, R, r), \quad (4.9)$$

with

$$F(\beta, R, r) \equiv \int_R^r dr \left(1 - \beta \frac{R^2}{r^2} \right) \frac{r^{-2\beta+1}}{\sqrt{r^2 - R^2}}, \quad (4.10)$$

and R the projected radius.

We adopt an analytic profile for the projected stellar density $I(R)$. As in [Walker et al.(2010), Salucci et al.(2011)], we consider a Plummer profile for the stellar density with the projected half-light radius, r_{half} , as the only shape parameter,

$$I(R) = \frac{L}{\pi r_{half}^2} \frac{1}{[1 + (R/r_{half})^2]^2}, \quad (4.11)$$

where L is the total luminosity. With the projected stellar density known, one can recover the 3-dimensional stellar density [Binney & Tremaine (2008)]

$$\nu(r) = -\frac{1}{\pi} \int_r^\infty \frac{dI}{dR} \frac{dR}{\sqrt{R^2 - r^2}}. \quad (4.12)$$

substituting eq. (4.11) in eq. (4.12) for the Plummer profile we have

$$\nu(r) = \frac{3L}{4\pi r_{half}^3} \frac{1}{[1 + (r/r_{half})^2]^{5/2}}. \quad (4.13)$$

Using eqs. (4.9) and (4.10) we can find the halo parameters that best reproduce the velocity dispersion data. We have three free parameters per galaxy: the scale radius $\sim 1/k_j$, the density, and the orbital anisotropy β . For the stellar component we use r_{half} from [Walker et al.(2009)].

One advantage of the analytical approximation we derived in the last chapter is that in the core region where the density will be dominated by the ground state once the halo

has reach stability the analytical approximation resembles the numerical solution with high accuracy, this is not surprising as the inner distributions is given by the quantum pressure which is just Heisenberg's uncertainty principle acting on such scales. In fact, from the simulations in [Schive et al.(2014)] the inner kiloparsec of the density profiles of different SFDM halos displays an ubiquitous core, in the supplementary information of [Schive et al.(2014)] the authors provided an empirical fit to the inner profile (where the solitonic core is present) for the dwarf galaxy Fornax given by

$$\rho(r) \approx \frac{1.9(m/10^{-23}eV)^{-2}(r_c/kpc)^{-4}}{[1 + 9.1 \times 10^{-2}(r/r_c)^2]^8} M_\odot pc^{-3}. \quad (4.14)$$

where core radius r_c is defined as the radius in which the density has dropped to one-half its peak value, for appropriate normalization values our analytical profile is in good agreement with the latter numerically motivated. We will comment on the reason of these similarities and the interpretation below when we give our halo formation scenario, for the moment we will assume (3.147) to model the dwarf galaxies.

We first model the dSphs assuming the ground state is enough, this means setting $j=1$ and thus eq.(3.147) has no oscillations, we obtained good fits restricting to realistic values of the orbital anisotropy, $-0.6 \leq \beta \leq 0.3$, in previous studies where the Thomas-Fermi(TF) approximation is taken at zero temperature [Robles & Matos(2012), Böhmer & Harko(2007), Lora & Magaña(2014), Diez-Tejedor et al.(2014)] only the pure condensate was physically allowed, for reference we include the solution under the TF approximation [Robles & Matos(2012), Böhmer & Harko(2007)]

$$\rho(r) = \rho_0^0 \frac{\sin(\pi r/r_{max}^0)}{(\pi r/r_{max}^0)}, \quad (4.15)$$

where ρ_0^0 is the central density of the condensate, $r_{max}^0 = \sqrt{\pi^2 \Lambda / 2} (\hbar / mc)$ is considered as a configuration radius where $\rho(r_{max}^0) = 0$ and therefore $\rho(r) = 0$ for $r \geq r_{max}^0$, m is the mass of the scalar field, $\Lambda = \lambda m_{Planck}^2 / 4\pi m^2$, and λ is the dimensionless parameter that determines the two-body interactions of the field.

Using only the ground state for our analytical profile produces dispersion velocity fits in dSphs that are almost indistinguishable to those using eq. (4.15) within $\sim 500pc$, the region where the condensed state best fits the data. The latter implies that within this

radius the dSphs are also well reproduced using our profile

$$\rho_j(r) = \rho_0^j \frac{\sin^2(k_j r)}{(k_j r)^2},$$

with only the condensed state ($j = 1$). There are several values of β that produce a fit consistent within the error bars of σ_{los} , with the upcoming surveys MaNGA, Gaia it will be possible to have much better precision of the velocities of nearby stars, allowing possibly to improve to distinguish subtle differences such as the existence of more than the ground state bosons conforming the halos.

If we now include the first excited state in the analysis we see in Figure 4.2 that there is a difference mostly in the outer regions, associated to a wider distribution of excited-state psyns in the halo[Martinez-Medina, Robles, & Matos(2015)]. The relevance of adding excited states is mostly seen in larger galaxies as they play an important role to flatten the rotation curves and reach agreement with HI observations.

We see that dSphs of similar sizes and properties are described with a single state, in fact this is shown in Fig. 4.2 for the dSphs within $500pc$, notice that the corrections due to the first excited state are small but not zero, we must take into consideration that the larger the galaxy is, the more relevant are the contributions of other states. In Table 1 we give the values of the best fit parameters used for the modeled galaxies. Indeed, if we model extended galaxies where the rotation curves remain flat for more than 10 kpc the need of more excited states becomes clear, Figure 4.3 illustrates this feature, here we fitted three LSB galaxies assuming multistate halos and we obtained good fits to all radii, in fact the wiggles in the data are also nicely reproduced. In this figure we have also compared with the typical Einasto profile that is used to model CDM halos[Navarro et al.(2010), Merrit et al.(2006), Graham et al.(2006)],

$$V_E^2 = 4\pi G \rho_{-2} \frac{r_{-2}^3}{r} \left[\frac{e^{2/\alpha}}{\alpha} \left(\frac{\alpha}{2} \right)^{(3/\alpha)} \gamma\left(\frac{3}{\alpha}, x'\right) \right], \quad (4.16)$$

with γ the incomplete gamma function given by

$$\gamma\left(\frac{3}{\alpha}, x'\right) = \int_0^{x'} e^{-\tau} \tau^{(3/\alpha)-1} d\tau$$

with $x' := \frac{2}{\alpha} \left(\frac{r}{r_{-2}} \right)^\alpha$, r_{-2} is the radius in which the logarithmic slope of the density is -2 , ρ_{-2} is the density at the radius r_{-2} , and α is a parameter that describes the degree of curvature of the profile[Merrit et al.(2006), Graham et al.(2006)].

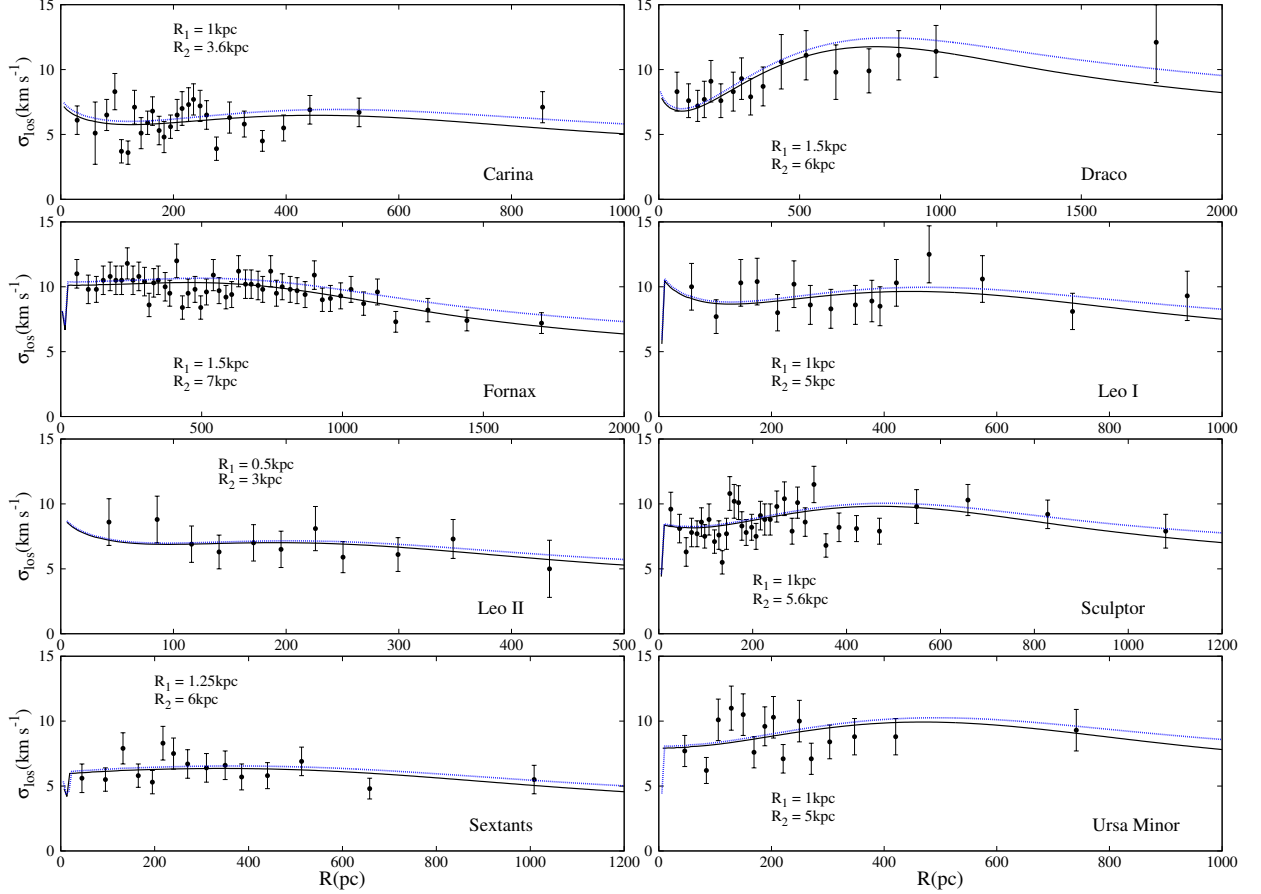


Figure 4.2: Projected velocity dispersion profiles for the eight brightest dwarf spheroidal satellites of the Milky Way [Walker et al.(2009)]. The solid (black) lines correspond to the profiles calculated with the anisotropy parameter that best fits the data using the BEC model(eq.4.15), and the dotted (blue) lines show the multistate halo profile (eq.3.147) that includes the sum of the first excited state and the ground state. The effects of the first state are more pronounced for the galaxies with measurements in $r > 1$ kpc, these states have $R_2 > R_1$ implying that dwarf dark matter halos extend to at least $R_2 \approx 5$ kpc, however the dominant component of the mixed state within 500 pc remains to be the ground state, this region is also where the BEC profile provides a good description.

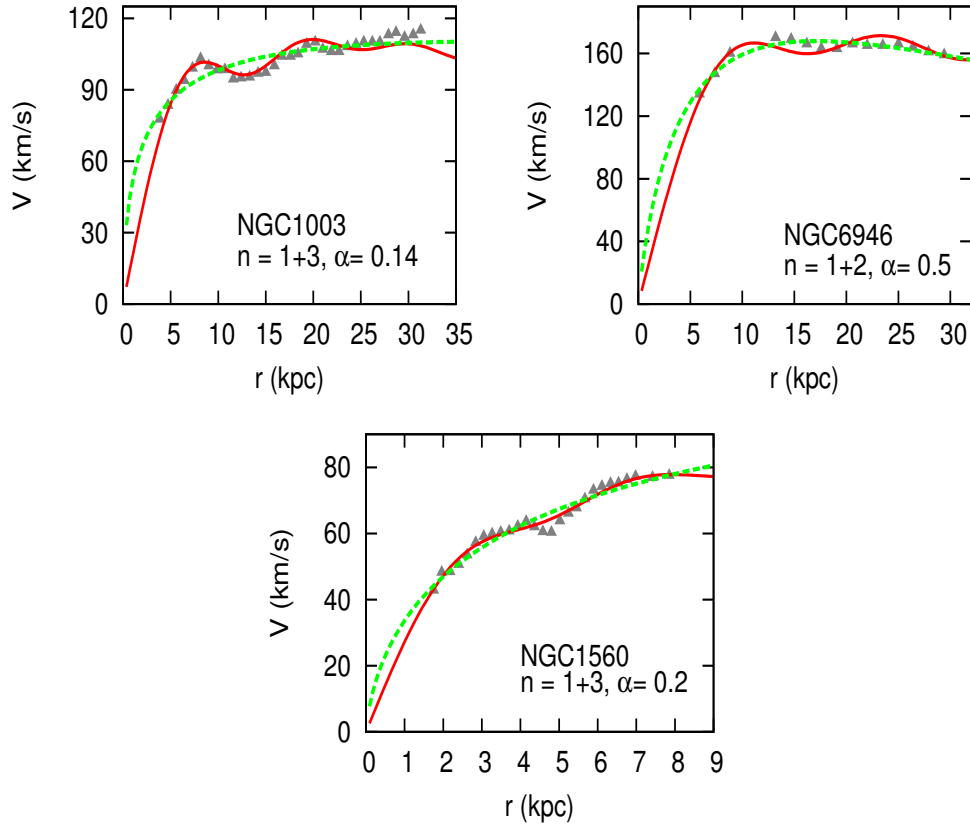


Figure 4.3: Rotation curve fits to three LSB galaxies. *top left panel*: NGC 1003, *top right panel*: NGC 6946, *bottom panel*: NGC 1560. Solid lines are the fits using the SFDM model, here n represents the states used for the fit, dashed line represents Einasto's fits, and triangles are the observational data. In NGC 1560 we see that the dip at $r \approx 5$ kpc is reproduced more accurately in the SFDM profile. Einasto fits show different values of α in each galaxy, suggesting a non-universality in the DM halos, the same is concluded in the SFDM model due to the different states involved in the fits.

Table 4.1: Parameters for the condensate state and the first excited state that together form the potential well for each dSph (blue lines in Fig 4.2.)

dSph	ρ_0^{BEC} ($10^{-2}M_{\odot}pc^{-3}$)	R_1 (kpc)	$\rho_0^{1st-state}$ ($10^{-2}M_{\odot}pc^{-3}$)	R_2 (kpc)	β
Carina	6.60	1	0.45	3.6	0.3
Draco	10.6	1.5	0.51	6	0.3
Fornax	5.09	1.5	0.16	7	0
Leo I	14.5	1	0.37	5	0.3
Leo II	28.5	0.5	0.46	3	0.3
Sculptor	13.5	1	0.24	5.6	0.1
Sextants	2.42	1.25	0.07	6	-0.1
Ursa Minor	13.1	1	0.34	5	0

The agreement with dark matter dominated systems is one remarkable success of the SFDM, moreover, looking at the functional form of the density profile we can observe that this models produces a flat density profile in the center, this translates into a a linear increase in the rotation curve ($v \sim r$ for small r), although this is notably a difference to the usual cusp in CDM simulations currently it remains challenging to observationally disprove either model based only on the inner slope of their profiles, one particular reason is because some CDM simulations have shown that through stellar feedback the dark matter slopes can yield a "shallow cusp" resembling a slightly steeper core profile($\rho \sim r^{-0.5}$), it is nevertheless reassuring that the model is able to provide an explanation without contrived hypotheses or relying on unknown parameters for the stellar feedback that in dark matter dominated systems are not expected to play a major role anyway. In this sense the SFDM is a viable model. Looking back at Figure 4.3 we notice that the number of excited states that live in a SFDM halo is in fact not known a priori, it is until we do the fitting of the data that can have information about the composition of the halos. It would be desirable to look for possible correlations in galaxy mass, size and the required combination of states j in a large sample of galaxies that allow to get better statistics and find the trends, if any.

§4.3 Tidal Stripping in SFDM halos

A particular feature of a SFDM halo is to possess a flat density profile, although this property may not be totally true when baryons can not be neglected in the center of the halos, it seems to be common in satellite halos where the baryons are not dominating the mass content, as shown in the previous section³. It is true however, that we observe galaxies and not dark halos⁴, additionally MW galaxies⁵ rapidly assemble most of their mass (in CDM simulations tends to be at redshift ~ 2) and don't undergo major changes later on, unless a major merger occurs, for this reason it is often assumed that the MW is a static halo and thus, simplify the study of tidal effects in small satellites that are being accreted on a MW host.

Previous studies have shown, using empirical core-like density profiles for DM halos, that tidal disruption can be more important in core-like DM halos than in halos with NFW profiles, especially if they pass close to the galactic disk (see Klimentowski et al. (2009) and Peñarrubia et al. (2010) for collisionless simulations). However, until now there has not been studies addressing whether the tidal effects are strong enough to remove completely the stars in classical and ultra faint dwarf galaxies hosted by BEC halos. We investigated [Robles et al.(2014)] this issue through a series of simulations of a stellar component described by a Plummer profile when it is embedded in a SFDM subhalo subject to the influence of a MW SFDM host halo with a disk component. The Plummer profile reads

$$\rho(r) = \frac{3M_*}{4\pi r_p^3} \left(1 + \frac{r}{r_p}\right)^{-5/2}, \quad (4.17)$$

³In fact, as galaxies become more luminous by increasing their baryonic content within a dark halo, the adiabatic contraction can increase the central density resulting in larger logarithmic slopes in the inner kpc, as seen in some dwarf galaxies that favor a more cuspy density distribution, it would be interesting to verify whether this effect is enough in the SFDM model to be in agreement with these observations.

⁴Given the large number of expected dark mini halos with halo masses $M_h < 10^8 M_\odot$ in CDM simulations, mainly around massive galaxies including those of Milky Way-like masses ($M_h \sim 1 \times 10^{12}$) there have been proposals to detect them using techniques like weak lensing, this research is still ongoing and so far there are not signatures of their existence.

⁵We use the standard jargon where a Milky Way-like galaxy refers to a galaxy with a comparable mass to our real Milky Way, frequently this mean galaxies with comparable halo masses and morphology.

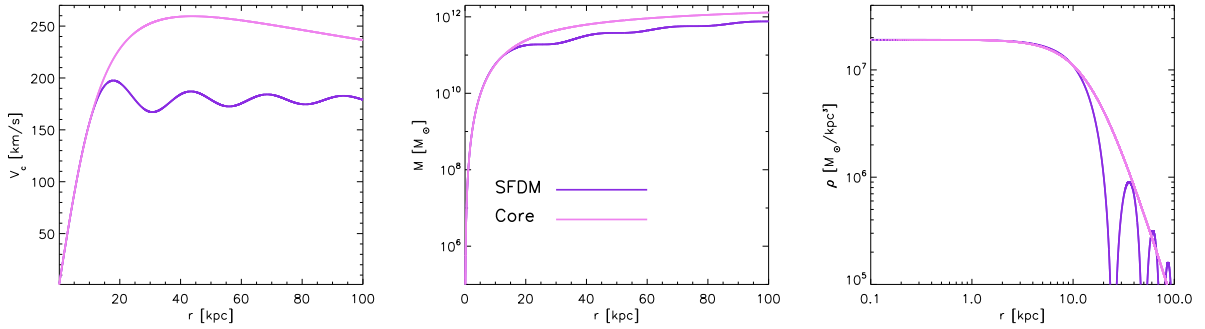


Figure 4.4: From left to right are the circular velocity, mass, and density profiles used for: the MW’s SFDM halo model (purple lines), and the cored DM halo (pink lines).

where M_* is the mass of the stellar component, and r_p is the Plummer radius, One should note that r_p can be related to the half-mass radius r_h through $r_h = 1.3r_p$. In our simulations[Robles et al.(2014)], we have set a half-mass radius of 200 pc, and a stellar mass of $M_* \simeq 7.3 \times 10^5 M_\odot$, motivated by the typical values for Draco, which is one of the classical dSph galaxies and also one of the least luminous satellites (e.g., see [Martin et al.(2008)] and [Odenkirchen et al.(2001)], for Draco). For the MW disk we adopted the Miyamoto-Nagai potential[Miyamoto & Nagai(1975)]

$$\Phi_d(R, z) = -\frac{GM_d}{\sqrt{R^2 + (a + \sqrt{z^2 + b^2})^2}}. \quad (4.18)$$

In the latter equation, M_d stands for the mass of the disc, and a and b stand for the horizontal and vertical scale-lengths, respectively. We have set the mass of the disk $M_d = 7.7 \times 10^{10} M_\odot$, and the scale length $a = 6$ kpc, and $b = 0.3$ kpc.

We used similar parameters that reproduce current MW data for our SFDM MW host. We found that using $\rho_{0,4} = 0.0191 M_\odot \text{pc}^{-3}$, $j = 4$, and $R_h = 100$ kpc (see purple lines in Figure (4.4)) in Equation (3.147) gives a good representation to the MW DM in the SFDM model. We compared with an empirical cored profile [Peñarrubia et al.(2010)]

$$\rho(r) = \frac{\rho_0}{(1 + (r/R_s)^2)^{3/2}}. \quad (4.19)$$

For the MW’s cored DM profile (Equation 4.19), we set $R_s = 15$ kpc. The corresponding circular velocity, mass and density of the cored DM halo, are shown with pink lines in

Figure (4.4). It has to be noted that, for both (SFDM and cored) MW halos, the core radius is ~ 11.5 kpc, and that the mass estimations within 100 kpc are comparable. Therefore, the DM profiles are not identical but the total mass enclosed at the halo radius is the same. The wiggles found in the halo and shown in Figure 4.4 are also a particular difference of this SFDM profile with respect to other core models.

For the mass models in our satellite subhalos, the mass of the dark halo enclosed at $R_h = 2$ kpc lies in the range 10^8 - $10^9 M_\odot$ and we use only $j = 1$ for simplicity, as we showed before the excited state will not contribute strongly to the inner dynamics as it is the ground states that dominates in this region. The resulting mass-to-light ratios represent DM dominated dSphs. For instance, the mass-to-light ratios of dSphs ($[M/L]_{half}$) in the MW range from $\sim 7 M_\odot/L_\odot$ (Leo I, Fornax) to $\sim (10^3) M_\odot/L_\odot$ (UMa II, Seg, UMaI) [Collins et al.(2014)]. In particular, Draco has a very low luminosity but a high estimated total mass within the tidal radius of $M(r_t) = 2.2 - 3.5 \times 10^7 M_\odot$ [Odenkirchen et al.(2001)], this leads to a high mass-to-light ratio of $(M/L)_i \simeq 92 - 146$. For the dwarf central density of the dwarf, we select two different values that encompass the range of masses found in dwarfs, $0.16 M_\odot \text{ pc}^{-3}$ (model A) and a less massive one with $0.031 M_\odot \text{ pc}^{-3}$ (model B). In Figure (4.5), the dashed lines show the circular velocity, mass, and density associated with the SFDM halos of models A and B. The corresponding SFDM dwarf core radius (defined as the radius at which the central density drops a factor of two) is ~ 750 pc for both A and B models and its presence is distinctive prediction of the model. For the orbit of the dwarf galaxy, we assume an apocenter distance from the MW, $r_a = 70$ kpc and two different pericenter distances ($r_p = 14$ and 35 kpc). We conducted simulations with and without adding the presence of a Miyamoto-Nagai disk in the MW potential to assess the effects on the dwarfs due to the close encounter with the disk component. Our main interest is the stellar component evolution that is located deep inside the subhalo. [Peñarrubia et al.(2010)] show that the major effect of tidal disruption of a DM subhalo occurs in the outermost radius, while inner regions ($\lesssim 1$ kpc) are less affected by tides and the central density profiles are only shifted to a slightly lower value maintaining the same inner shape during the evolution. Table 2 summarizes our simulations.

Figure (4.6) shows the dwarf galaxy stellar mass profile at $t = 0$ and $t = 10$ Gyr in all our simulations. From the upper-left panel in Figure (4.5) we see that all *A* models lose some

Table 4.2: Parameters used in our simulations. Column 1 identifies the simulation, column 2 specifies r_p/r_a for the orbit, column 3 shows the plane of the orbit, next two columns give the central density for the dwarf and the MW DM halos in each simulation, respectively, column 6 determines if a disk is present in the Milky Way halo, and column 7 gives the DM model used in the simulation.

Simulation	$\frac{r_p}{r_a}$	Dwarf orbit plane	Dwarf ρ_0 ($10^7 M_\odot (\text{kpc})^{-3}$)	MW ρ_0 ($10^7 M_\odot (\text{kpc})^{-3}$)	MW disk	DM model
A1	1/2	x-y	16	1.91	–	SFDM
B1	1/2	x-y	3.1	1.91	–	SFDM
A2	1	x-y	16	1.91	✓	SFDM
B2	1	x-y	3.1	1.91	✓	SFDM
A3	1/2	x-y	16	1.91	✓	SFDM
A3 _{core}	1/2	x-y	16	1.91	✓	Core
B3, B6	1/2	x-y	3.1	1.91	✓	SFDM
B3 _{core} , B6 _{core}	1/2	x-y	3.1	1.91	✓	Core
A4, A6	1/5	x-y	16	1.91	✓	SFDM
A4 _{core} , A6 _{core}	1/5	x-y	16	1.91	✓	Core
B4	1/5	x-y	3.1	1.91	✓	SFDM
B4 _{core}	1/5	x-y	3.1	1.91	✓	Core
A5	1/5	45°	16	1.91	✓	SFDM
B5	1/5	45°	3.1	1.91	✓	SFDM

- Simulations B6(B6_{core}) use the same parameters of B3(B3_{core}) but with a satellite stellar mass $M_* = 1 \times 10^4 M_\odot$
- Simulations A6 (A6_{core}) use the same parameters of A4(A4_{core}) but with a satellite stellar mass $M_* = 1 \times 10^4 M_\odot$

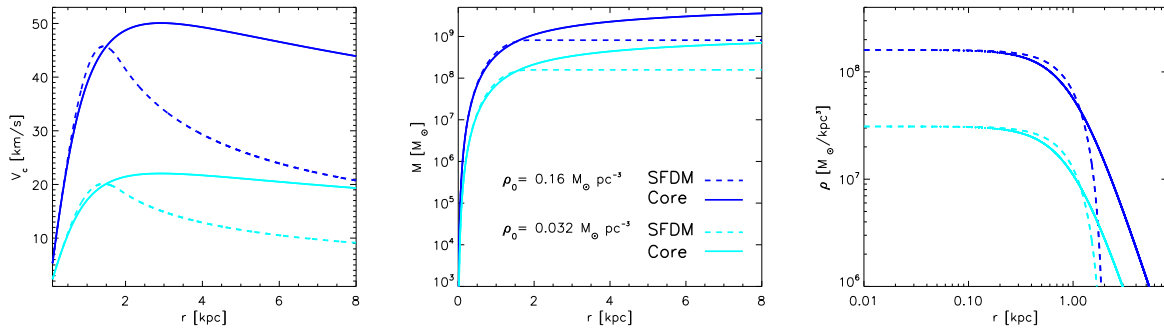


Figure 4.5: The circular velocity(left), mass(center), and density profile(right) associated to the two SFDM halos of the dwarf galaxy (dashed black line (blue in the online version) is model A: $0.16 M_\odot \text{pc}^{-3}$, and dashed gray line (cyan in the online version) is model B: $0.031 M_\odot \text{pc}^{-3}$). The corresponding core DM models are shown with solid lines with their respective colors for comparison.

particles, but the loss is not substantial and the galaxies survive with essentially the same initial mass after 10 Gyr. These simulations suggest that the density is high enough to strongly bound the stars and prevent the disruption of the satellite. A similar behavior is seen when a cuspy-like profile is used [Klimentowski et al.(2009), Łokas et al.(2012)], making tidal disruption an inefficient process in both core and cusp-like subhalos to reduce their stellar mass within 1kpc and therefore making it not the relevant mechanism that decreases the abundance of massive dwarf satellites around MW type galaxies, even for orbits with close pericenters of 14 kpc.

The *B* models for the SFDM halo show a slightly larger particle loss than the *A* models (upper-right panel in Figure 4.6) except for model *B4* which shows a more pronounced particle loss. The small central density of the SFDM dwarf subhalo, plays a crucial role in its survival. The final mass (at $t = 10$ Gyr) for *B* models is smaller than the high *A* density case in all cases. This shows that even if the orbit is far from the MW disk, whenever the DM subhalos have low densities the stars in the center are susceptible to spread out more than in denser halos as seen by comparing the two upper panels in Figure (4.6) within 500 pc.

The considerable disruption in both *B4* simulations indicates the need to include the disruption of the halo. In our simulations, the satellites still remain due to the assumption

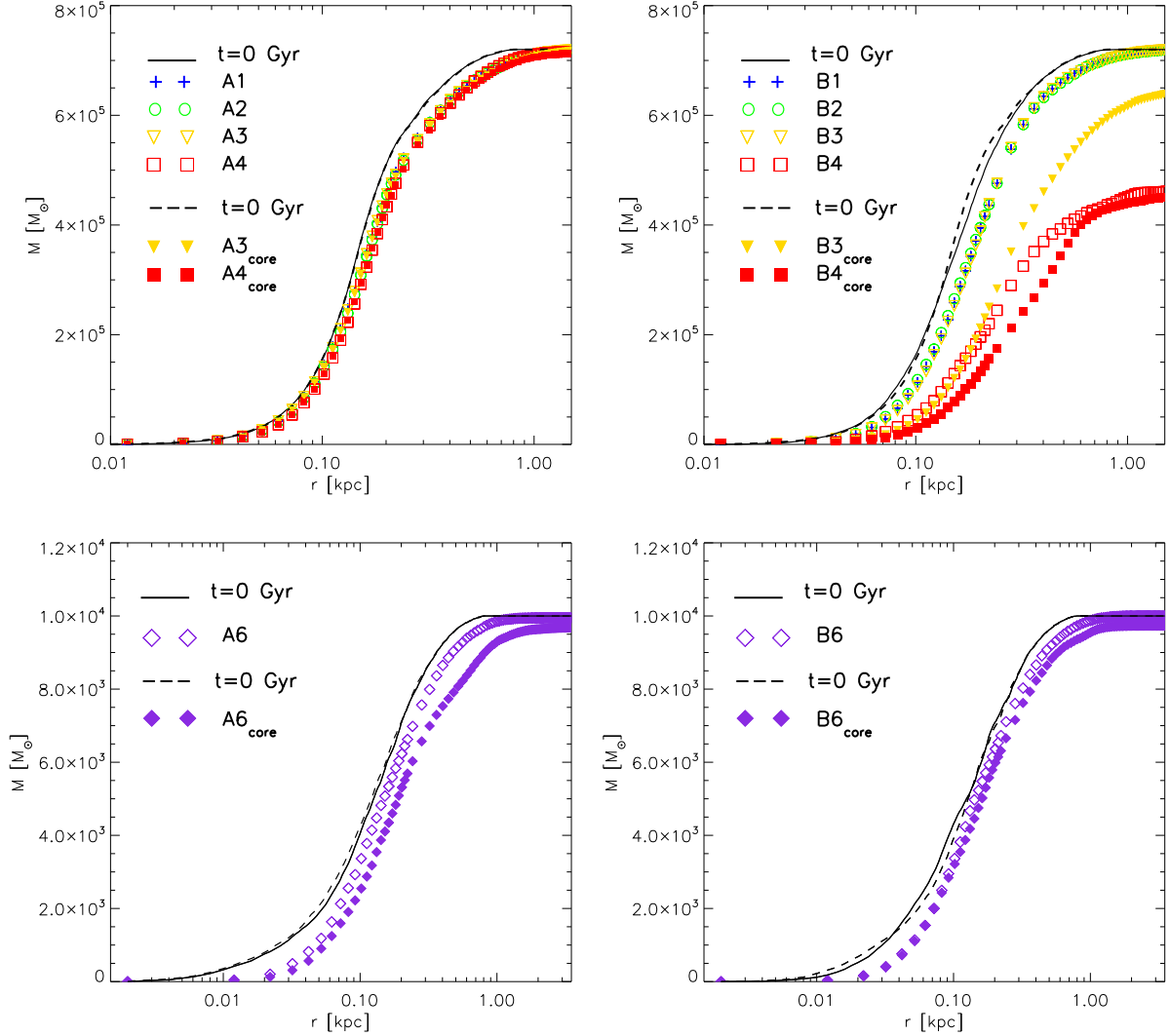


Figure 4.6: Upper panel: Dwarf stellar mass for models A(left) and B(right) at $t = 0$ and $t = 10$ Gyr. The upper left panel would represent a classical dwarf and the upper right would be an ultra faint-like galaxy. The different symbols in the panel represent the dark matter model used in that simulation according to Table 1. Bottom panels show small mass satellites with $M_* = 1 \times 10^4$ (models A6, A6_{core}, B6, and B6_{core}) at $t = 0$ and $t = 10$ Gyr, different symbols correspond to different simulations. In all A models of the SFDM the galaxy survives at the end of the simulation independent of the stellar mass and the orbits we considered, even the presence of a disk in the MW scalar field halo cannot destroy the satellite. In B models where the subhalo is less dense, the satellite losses more mass than in A cases but will still survive inside the subhalo, except when the pericenter becomes comparable to the disc’s scale length where we expect the scalar field subhalo to be disrupted too.

of fixed subhalo, but we expect the dwarf halos to fully disrupt and that their stars get dispersed around the MW halo. This one of the restrictions of the simulation, given that the dark halos are fixed, we can track the evolution of the stars and used them as tracers of the strength of the tidal interactions. As stars in the center become strongly affected, shown by the decrease in the stellar densities, it is also a likely that the halo will suffer some disruption too, this effect is not substantial for most of our simulations but it appears for B4 due to its proximity to the MW disk and the small subhalo central density.

We also conducted a couple of simulations (*A5* and *B5*) where we set the dwarf galaxy embedded in the MW SFDM halo potential, with a $r_p/r_a = 1/5$ including the baryonic MW disk component and similar to *A4* and *B4* models, but now we place the dwarf galaxy in an orbit inclined 45° from the $x - y$ plane. In this case we observe that the dwarf galaxy gets destroyed within ~ 1.5 Gyr. This suggests that orbits with close pericenter distances and inclination effects are important factors to the survival of low density SFDM dwarf satellites. In *A6* and *A6_{core}*, the parameters are identical to *A4* and *A4_{core}* respectively, but the stellar mass of the satellite is smaller $M_* = 1 \times 10^4 M_\odot$. These parameters correspond to the closest orbit where the tidal effects should be the largest. The other pair, *B6* and *B6_{core}*, uses $M_* = 1 \times 10^4 M_\odot$ and the parameters of *B3* and *B3_{core}* respectively. Despite their low mass the satellites can remain with most of their initial mass after 10 Gyr. Here we show that if the satellites are in scalar field subhalos with central densities comparable to classical dSphs, some of their stars are stripped but the galaxies can survive with smaller masses and hence contribute to the number of dwarf satellites around a MW host. It must be noted that, in the SFDM model, the substructure is smaller due to the wave properties causing the cut-off in the power spectrum, as confirmed in [Schive et al.(2014)].

For the lower density dwarfs (comparable to ultra faint dwarfs), we obtained that they could survive but only if their orbits do not get well inside the disk of their host. On the other hand, low density halos with close pericenter orbits can be fully stripped of stars if evolved for a long time even with a fixed subhalo potential, but as we expect them to be destroyed once the fixed halo hypothesis is relaxed. Therefore, we do not get DM halos that are tiny and dark, contrary to the CDM predictions where the cusp prevents total disruption.

Therefore, our results point to an alternative solution to the satellite overabundance prob-

lem and the cusp-core issue by means of the quantum DM properties of the scalar field, and without relying strongly on the messy astrophysical processes. Here, small mass subhalos with core profiles ($\rho(r) \sim r^0$) and with orbits not crossing the host's disk are able to survive for a long time, otherwise the close encounters with the disk could completely destroy them. On the other hand, more massive dwarfs can get closer or farther from the host's disk and still survive with core profiles. To determine the final fate of these galaxies and make a fair comparison with current CDM simulations it is necessary to invoke the astrophysics but so far we have found that this model seems to offer a good description to the nearby galaxies, although this is not meant to be a compelling reason to prefer this model over CDM. In fact, the results might vary if we relax the fixed halo hypothesis for the satellite, and include gas that is self gravitating⁶, both conditions could show results that differ from the ones we found, particularly because the self-gravity of the gas will make it less difficult to be stripped of stars as the gravitational potential is now deeper, on the other hand, the subhalo will also feel the tidal interaction, in this case we expect the the mass loss to be similar to that in [Peñarrubia et al.(2010)], however it is not clear what effect the oscillations of the MW halo have on the subhalo when both are not fixed, and how they compare when smooth DM distributions are considered, the limitations of our approach cannot assess this question but it is undoubtedly something that requires further exploration.

§4.4 Rings and shells in early type galaxies

An interesting feature of the intrinsic nature of psyons is to allow for some bosons in excited states. This property has been pointed out before in the context of multistates in a SFDM halo, we mentioned the possibility of a population inversion in the states that can turn an initially unstable *multistate halo* (MSH) into a stable one according to the ratio of the particle numbers in each state. This MSHs present ripples in the density profile that are a consequence of the quantum nature of the psyons, in [Robles, Medina & Matos (2015)] we have modeled these properties using an analytical model that captures the effect of the transition and explore how the transition affects the gas embedded in a MSH halo.

⁶When gas is self gravitating the mass of the gas also contributes to the gravitational potential in addition to the dark matter.

We consider a multistate halo with only the first and ground state coexisting, this is because we know the stability threshold for this multistate configuration. In [Bernal et al.(2010)] it was seen that the larger the η above the critical value, the faster it settles to its final stable configuration, to be sure that the MSH is initially in the unstable regime we pick an intermediate value $\eta=1.6$. We explore the evolution of the gas distribution that follows a disk of gas with a Miyamoto-Nagai profile[Miyamoto & Nagai(1975)] with gas mass of $M_g = 3.9 \times 10^9 M_\odot$, and for the horizontal and vertical scale-lengths we use $a = 6.5$ kpc and $b = 0.5$ kpc respectively, we modified the code ZEUS-MP[Hayes et al.(2006)] to evolve the gaseous component embedded in the MSH, the gas is not self gravitating and is treated as a tracer of the potential only.

We use a semi-analytical model that let us control the rate of the transition to a stable state, this type of isolated and simplified simulations help to identify the main effects of the transition in the gas and aid the interpretation of the results. However, It remains unclear when the transition is set for a given halo or its duration, this requires a better sampling of the problem, first by considering a larger representative sample of halos, and second, how the properties vary with the transition time. It is in these semi-analytical simulations that an analytical form of the density profile becomes handy, keeping in mind the limitation of this profile, we use the form (3.147) to model our MSH, the main idea is to start from an unstable MSH halo and invert the masses of the states neglecting any particle loss in the total halo, during the population inversion in the numerical solution both states lose a few percentage of their initial masses($<10\%$ [Ureña-López & Bernal(2010), Bernal et al.(2010)]), but this loss would not substantially affect the final halo profile, for this reason we may neglect the mass loss in our analytical study.

After the inversion the total initial mass of the ground state $M_1^i(R_1^i)$ becomes the final mass of the excited state $M_2^f(R_2^f)$ and vice versa, and the nodes in the wavefunctions will also have changed, that is

$$M_1^i(R_1^i) \longrightarrow M_2^f(R_2^f), \quad M_2^i(R_2^i) \longrightarrow M_1^f(R_1^f) \quad (4.20)$$

$$j : 1, 2 \longrightarrow 2, 1 = j'. \quad (4.21)$$

where the mass profiles for each state j are now flipped, R_j is taken as a truncation radius of the corresponding state, that is, for radii greater than R_j the number of particles in the

Table 4.3: Initial and final parameters defining the MSH.

	Initial		Final	
	j		j'	
	1	2	1	2
M	1.844	2.953	2.953	1.844
R	10	20	10	20

state j is neglected, i.e we take $\rho_j(r)=0$ for all $r > R_j$ whereas for $r \leq R_j$ the density profile of the state j is given by (3.147). The total density of the MHS would be described by $\rho(r)=\rho_1(r)+\rho_2(r)$.

The function that models the time evolution of the transition to the stable configuration, is based on the numerical solution, for unstable halos the transition happens really fast, during this period the central density varies until it settles down in the new stable value, the inversion also modifies the radius of each state which is related to its central density $\rho_{c,j}$ by the mass profile

$$M_j(R_j) = \left(\frac{2}{\pi}\right) \frac{\rho_{c,j} R_j^3}{j^2}. \quad (4.22)$$

A smooth function that captures the population inversion(PI) of the numerical evolution and allows an interpolation between an initial and final R_j is

$$R_{j'}^f(t) = R_j^i + \frac{\epsilon_{j',j}}{2} \left(1 + \tanh[\alpha(t - t_{inv})]\right), \quad (4.23)$$

where α determines the transfer rate from the initially unstable to the final stable MSH, $\epsilon_{j',j} = R_{j'}^f - R_j^i$ is a parameter that relates the initial radius to the one after the inversion, and t_{inv} is the time where the PI is halfway to reach its final stage with j' confined in $R_{j'}^f$, we use the same functional dependence to invert j to j' .

With implemented this analytical model in ZEUS and follow a gaseous disk used as a tracer of the gravitational potential, setting the initial condition such that the gas velocities are those of the background dark matter halo. We explore an early and late transition specified by $t_{inv}=1$ and 3 Gyrs respectively, and we also evolve these cases when $\alpha = 1, 1/4$ corresponding to an fast and slow inversion, we denote by $A_\alpha^{t_{inv}}$ a realization that had a PI with parameters t_{inv} and α .

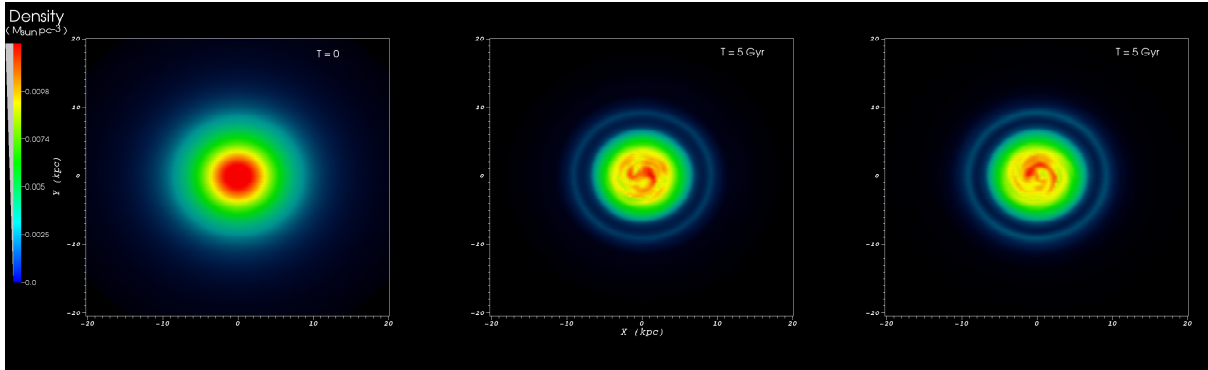


Figure 4.7: Comparison of initial gas distribution(left) and its final stage. The central panel corresponds to a halo that had an early transition to its stable configuration at $t_{inv}=1$ Gyr(A_1^1) and on the last panel(right) the transition was at a later epoch $t_{inv}=3$ Gyrs(A_1^3). A ring appears in both simulations at the corresponding density peak at 9 kpc.

In Figure 4.7 we show the initial and final gas distributions of a halo with the parameters in table 4.3 where the mass is in units $1 \times 10^{10} M_\odot$ and R is in kpc . In Figure (4.7) we see a surprising agglomeration of gas at 9 kpc that reaches up to $\sim 20\%$ of the mean central density ($\approx 0.45 M_\odot pc^{-3}$), the fact that it remains well after the transition is an important issue as this could be a key signature of the model that is not found in CDM or other alternatives, this suggest a potential mechanism to form substructure around some of the isolated early galaxies, in fact, the ring of gas orbiting around the denser central concentration is reminiscent of those found in certain elliptical galaxies. The ring keeps its location until the end of the simulations in our isolated galaxy because its origin lies in the shape of the background SFDM halo, moreover, the stability of the halo under small perturbations, such as accretion of small galaxies, mildly change the inner DM potential but may alter the ring structure in a similar way that the population inversion modified the initial gas profile, however, after the merging process has concluded the gas will start redistributing and, according to our results, had enough gas remain on the outskirts a ring-like structure would appear again. The final amplitude of the ring's density will depend more strongly on the details of the merging process but its location should be similar

to the non perturbed halo provided the DM halo potential was not severely modified as expected for minor mergers in the past or those relatively more recent, thus, tidal features are not exclusive of galaxy mergers when the dark matter is an ultra light scalar field.

In these results we have seen that the presence of the symmetric ring is due to the spherical symmetry hypothesis in the SFDM halo, deviations from this symmetry could result in incomplete rings and shells although a certain degree of symmetry should remain, which may be a feature to distinguish the SFDM halo debris from remnants that come from recent galaxy mergers that depend on the path of the accreted satellites and do not necessarily leave tidal debris of a particular symmetry, our results suggest that outer regions of dark halos may not be totally smooth. Exploring in more detail the regions where shells and rings form could also help to put constraints on their origin, their formation, and serve to test galaxy and halo formation scenarios such as the quantum dark matter(QDM) paradigm.

§4.5 Galaxy formation scenario in SFDM haloes

Initial fluctuations that grow due to the cosmological expansion of the universe eventually separate from it and start collapsing due to its own gravity, at this time (known as turnaround) the halo has a number of psyons that can be in different states, their values would be determined before the collapse of the configuration, and have some dependence on the its local environment. Depending on the number density of bosons populating the excited states we can have different fates and for the halos.

Based on the results exposed in this chapter and the ones reported in the literature, it is clear that the QDM paradigm deserves some further attention, it is convenient to describe how the known features would relate, at least qualitatively, with the observed galaxy populations, for this reason we propose the following galaxy formation scenario in SFDM halos.

The smallest and less dense systems, such as dwarf galaxies, would reside in SFDM halos with most bosons in the ground state except possibly for just a few excited particles as seen in [Martinez-Medina, Robles, & Matos(2015)], this is because the potential wells of these haloes, being the lowest density systems, would be just massive enough to collapse and

allow the existence of the minimum energy state that would form a bound configuration. Larger configurations that had initially a larger number of bosons in excited states than in the ground state can undergo a population inversion and reach a stable state, collapse to a dense ground state or become a black hole depending on how large the fraction of particles in excited states is after turnaround, given the different possible outcomes for this case we expect that most galaxies are formed this way, for instance, ellipticals can form when halos transition to a stable configuration that quickly increases the ground state and deepens the gravitational potential resulting in a dense and compact structure where the bulge can form. High surface brightness galaxies usually have RCs that fall slowly after its maximum speed, they would likely correspond to SFDM halos whose final stable configuration has a comparable number of bosons in the excited and ground states as both states would contribute evenly in the central region increasing the gravitational potential well where more star formation can take place, and for distances larger than a given radius (likely the first maximum peak in the RC) the ground state would be a small contribution to the density, thus in the outer regions the baryonic RC would remain below its maximum. Another possible outcome for extended halos is when the fraction of excited particles is below its stability threshold, in these cases gravity will slowly redistribute DM bosons in the stable MSH but mostly keeping the particle number constant, considering that psyons in the excited states are subdominant and more widely distributed than the ones in the ground state of a MSH, the DM gravitational potential in the center would be less dense than in the high surface brightness case so that gas accretion would also proceed more slowly resulting in rotation curves for the baryonic matter that slowly increase to large radii or with almost flat profiles, this case is quite similar to what is found in low surface brightness galaxies[Kuzio de Naray et al.(2010), Kuzio de Naray & Spekkens(2011), Kuzio de Naray & Kaufmann(2011)].

Overall, this galaxy formation scenario broadly describes different galaxy types showing that only due to the dark matter properties in the context of SFDM it is possible to agree with the general features of several galaxies. However, we do not expect this scenario to represent all galaxies, in fact, to get a better description of individual galaxies we require taking into account other fundamental parameters that affect their evolution, such as the environment, angular momentum, galaxy mergers etc., we will leave a more in-depth

exploration of the model and comparison to this scenario including the full astrophysical processes for the years to come, for now the SFDM model looks a promising alternative.

SELF INTERACTING DARK MATTER

In the last chapter we have explored the SFDM model, here we will consider another alternative idea proposed in [Spergel & Steinhardt (2000)], it assumes that cold dark matter has weak interactions with baryons but strong self-interactions, this model received the name of self-interacting dark matter (SIDM). The required scattering cross-section is roughly $(m/g)^{-1} \text{ cm}^2$ where m in this chapter denotes the particle mass of the dark matter possessing this type of interaction, a value of $1 \text{ cm}^2/g \approx 2 \text{ barn GeV}^{-1}$ is approximately a nuclear-scale cross section. In this case, frequent elastic scattering in the dense central regions of halos can redistribute energy and angular momentum among particles, creating an isothermal, round core of approximately constant density [Burkert(2000)].

For the SIDM model to be an attractive alternative to the Cold Dark Matter paradigm, it should be able to address the issues that CDM faces today, for instance substantially reduce the central densities of dwarf-size halos.

Early studies suggested that this idea was ruled out by studies of gravitational lensing [Miralda-Escude(2000)] or by catastrophic gravitational core collapse found in a simulation of an isolated halo [Kochanek & White(2002)], but recent numerical studies show that these concerns are not borne out in fully cosmological simulations. SIDM simulations show that there is a viable window of mass and cross-section where self-interacting dark matter (SIDM) can produce cored dark matter profiles and remain consistent with observational constraints [Rocha et al.(2013), Peter et al.(2013)] Elastic scattering in the central regions, where an average particle experiences a few collisions per Hubble time, flattens the density cusp and reduces triaxiality, leading to halo shapes being more spherical in the inner regions. The scattering mechanism would operate across a wide range of halo masses, from Milky Way-like galaxies to dwarf satellites. Because of their shallower potential,

SIDM subhalos are more easily subject to tidal disruption than CDM subhalos. However, cosmological simulations suggest only small suppression of the low-mass subhalo count for allowed cross sections except in the innermost region of the host halo [Rocha et al.(2013), Vogelsberger et al.(2012)], this has questioned the preference of this alternative to the standard model.

§5.1 Satellites in SIDM halos

In the past few years there have been several simulations focusing on reproducing the properties of the dwarf galaxies around MW-like host, motivated in part by the increasing resolution in observations of local group dwarfs and more detailed observations in their star formation histories [Weisz et al.(2014a), Weisz et al.(2014b)].

Assuming velocity-independent cross sections in the range $0.1 - 0.5 \text{ cm}^2/g$ create cores that are approximately the right size for Milky Way dwarf galaxies [Markevitch et al.(2004)], spiral galaxies, and galaxy clusters [Newman et al.(2013a), Newman et al.(2013b)], although the core sizes in dwarf galaxies are still a matter of debate, the sizes can be modified if baryons are included in the simulations [Rocha et al.(2013), Kaplinghat et al.(2014)] or by lacking enough numerical resolution to study the inner kpc [Bastidas Fry et al.(2015), Vogelsberger et al.(2014)], which is essential in dwarfs. The same range for the cross sections above are also consistent with observations of merging galaxy clusters [Clowe et al.(2006), Randall et al.(2008), Dawson et al.(2012)]

Although there is not a particular particle candidate for the model, there have been some theoretical models that aim to produce SIDM particle candidates [Ackerman et al.(2009), Buckley & Fox (2010), Feng et al. (2010), Tulin et al. (2013a), Tulin et al. (2013b)], however in these models the strong self-interactions may only be present in a narrow range of halo mass, leaving halos on other scales effectively collisionless and indistinguishable from CDM expectations.

In [Zavala et al.(2013)] they use high resolution cosmological simulations of a Milky-Way size halo to assess whether a constant cross section per unit mass of $\sigma/m \sim 0.1 \text{ cm}^2/g$ is sufficient to account for the low mass densities in dwarf spheroidal galaxies, they found that such cross section produces a population of massive subhalos that is inconsistent with the kinematics of the classical dwarf spheroidals, in particular with the inferred

slopes of the mass profiles of Fornax and Sculptor. In their simulation the problem is solved if $\sigma/m \sim 0.1 \text{ cm}^2/g$ at the dwarf spheroidal scales. On the other hand this value may be in some tension with the constraints obtained from the offset of gas and mass distribution observed in collisions of galaxy clusters. Using the Chandra and Hubble Space Telescopes there are 72 observed collisions, including both major and minor mergers. [Harvey et al.(2015)] combined these measurements statistically, and detect the existence of dark mass at 7.6σ significance. The position of the dark mass has remained closely aligned within 5.8 ± 8.2 kpc of associated stars, they report that the self-interaction cross-section satisfies $\sigma_{DM}/m < 0.47 \text{ cm}^2/g$ at a 95% confidence level. Their results would disfavor some proposed extensions to the standard model [Foot (2014), Boddy et al.(2014), Cline et al.(2014), Tulin et al. (2013a)].

It is known from CDM that including the baryonic component in simulations can affect the results inferred from dark matter only simulations, in [Kaplinghat et al.(2014)] they estimated analytically the DM equilibrium configuration that results from a stellar distribution added to the centre of a SIDM halo, they studied the regime where the stellar component dominates the gravitational potential and found that the DM core sizes (densities) are smaller (higher) than observed in DM-only SIDM simulations, it is therefore expected that current SIDM constraints could change as more simulations in this regime are available.

One of the recent studies that includes baryons and self-interactions is given in Bastidas Fry et al.(2015), adopting a large constant cross section of $2 \text{ cm}^2/g$, they found that SIDM fails to significantly lower the central dark matter density at halo peak velocities $V_{max} < 30 \text{ km/s}$, they associate the cause to low central velocity dispersion and densities that translate in time scales for SIDM collisions greater than a Hubble time, as well as the weak supernova feedback found in such low mass galaxies. A direct consequence of their results is that both CDM and SIDM halos at these low masses have cuspy dark matter density profiles. In field dwarf galaxies with halo masses larger than $\sim 10^{10} M_{\odot}$, the baryonic processes create dark matter cores and central DM plus baryon distributions that are effectively indistinguishable between CDM and SIDM.

Another independent study was given in [Vogelsberger et al.(2014)], they explore the regime of dwarf galaxies where DM dominates the gravitational potential even in the

innermost regions. They include baryonic physics using the implementation described in [Vogelsberger et al.(2013)] employing the moving mesh code AREPO [Springel (2010)]. Their simulated dwarf has a halo mass $\sim 1.1 \times 10^{10} M_{\odot}$. They apply different models to this initial condition, including two cases with a constant cross section $\sigma/m = 1 \text{ cm}^2/g$ (SIDM1) and $\sigma/m = 10 \text{ cm}^2/g$ (SIDM10), and two cases with a velocity-dependent cross section motivated by the particle physics model presented in [Feng et al.(2009), Loeb & Weiner(2011)], and also studied in [Zavala et al.(2013)], vdSIDMa assumes $\sigma/m = 3.5 \text{ cm}^2/g$ and $V_{max} = 30 \text{ km/s}$, and vdSIDMb assumes $\sigma/m = 35 \text{ cm}^2/g$ and $V_{max} = 10 \text{ km/s}$.

For one of the dwarfs (shown in Fig5.1), they used DM particle mass resolution $m_{dm} = 7.75 \times 10^{10} M_{\odot}$, a cell mass $m_b = 1.48 \times 10^{10} M_{\odot}$, the Plummer-equivalent maximum physical softening length $\epsilon = 68pc$, and the number of DM particles in the high resolution region $N_p=15,353,772$. Their values were tested for convergence with a CDM only simulation with ~ 10 times more DM particles which allows to accurately resolve the inner 200pc of the galaxy, that is, for larger radius the two-body relaxation time is larger than a Hubble time, having good convergence ensures the lack of unphysical shallower slopes that are not formed due to the self interactions. One detailed comprehensive study for the convergence of mass profiles is given in [Power et al.(2003)], there are several considerations and numerical parameters that affect the structure of simulated N-body dark halo, choices of the gravitational softening, time-step, force accuracy, initial redshift, and particle number. In their tests, the authors found that for suitably chosen softenings that render particle discreteness effects negligible, convergence in the circular velocity is obtained at radii where the following conditions are satisfied: (i) the time-step is much shorter than the local orbital time-scale; (ii) accelerations do not exceed a characteristic acceleration imprinted by the gravitational softening; and (iii) enough particles are enclosed so that the collisional relaxation time-scale is longer than the age of the Universe. Convergence also requires sufficiently high initial redshift and accurate force computations. Poor spatial, time, or force resolution leads generally to systems with artificially low central density, but may also result in the formation of artificially dense central cusps. When dealing with self interactions and the cusp-core problem, where the relevant scale is of order 1kpc, it is required to chose the softening to resolve the innermost radii to avoid misinterpreting the

results.

[Garrison-Kimmel et al.(2013)] found that for a dwarf halo in CDM simulations with the Plummer-equivalent softening length to secure convergence at 250pc for a halo of $5 \times 10^9 M_\odot$ is of $\sim 70pc$, using three million particles, however a softening length of $\epsilon = 10pc$ is required to assure the convergence and study regions larger than 100 pc from the center of the halo, at this distance the forces are Newtonian and the code Gadget-2 safely tracks the acceleration of each particle. One of the latest SIDM simulations of a cosmological and isolated dwarf galaxy (in the field) was given in [Elbert et al.(2014)], they see that the SIDM has better convergence than CDM for the same number of particles, most likely the self-interactions are the dominant mechanism rather than being dominated by binary interactions. In the latter simulation the dark matter self-interactions were calculated using an SIDM smoothing length equal 0.25ϵ with a particle mass $1.5 \times 10^3 M_\odot$ and a Plummer-equivalent force softening $\epsilon = 28pc$, their halos are of $1 \times 10^{10} M_\odot$ with $V_{max} = 37km/s$ and use 4.6×10^6 particles, this softening allows the author to safely resolve regions as close as 200 pc.

In [Kauffmann (2014)] they suggested that galaxies with $M_* \sim 10^8 M_\odot$ suffer ongoing bursts of star formation with a typical duration (Δt_{burst}) of the order of the characteristic dynamical time of the galaxy (Δt_{dyn}). Although this might suggest that the gas outflows from these bursts could change the DM distribution, it is not clear how efficient this would be since the highly efficient regime occurs only once ($\Delta t_{burst} \ll \Delta t_{dyn}$). In [Vogelsberger et al.(2014)] the star formation rates of their two simulated dwarfs (one shown in Fig. 5.3) show that the rate of dA is fluctuating around a moderately non-evolving mean. Most importantly, none of our dwarfs have an exponentially declining star formation history.

They conclude that baryons have only a minor effect on the evolution and size of the cores in the SIDM halos, as expected the large $\sigma/m = 10 cm^2/g$ presents the largest difference, where the shallow DM profile allows supernovae feedback to expand the core a bit more compared to the DM-only case. They also found that the size of the stellar core is closely related to the size of the DM core as seen in Figure 5.1.

Additionally, they pointed out that in the constant σ/m case the density within the stellar core is reduced, in SIDM1 the reduction is by a factor of $\sim 2-3$ compared to the CDM case.

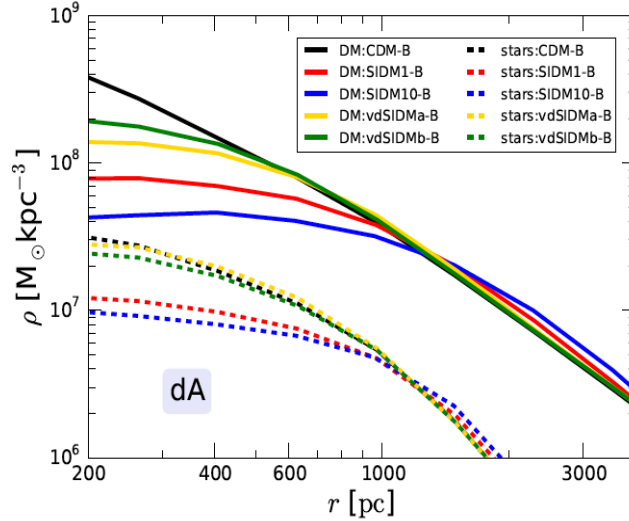


Figure 5.1: Density profile for DM (solid) and stars (dashed) within the inner 4 kpc for the different DM models of one dwarf halo from [Vogelsberger et al.(2014)] . The stars trace the evolution of DM and also form a core. The size of the stellar core is closely related to the size of the DM core. This can be seen most prominently for the SIDM1 and SIDM10 models.

The stellar mass in the sub-kpc region is reduced $\approx 30\%$ as a byproduct of the reduced DM gravitational potential due to self-scattering, and a reduced central stellar metallicity is found by 10% at $z = 0$ compared to the CDM case.

In the velocity dependent case, although a sizable DM core is also formed (400 pc), the effect in the stellar distribution at all scales is minimal relative to CDM. These features in the stellar distribution could give clues to distinguish among the SIDM models, although to pursue the comparison, the most important limitation lies in the lack of a significant number of simulated galaxies with baryons and dark matter self interactions. Because SIDM aims to be more than just an alternative model, the current goal is to find unambiguous observations to either rule out or find evidence for SIDM cross sections $\sigma/m > 0.1 \text{ cm}^2/g$, for smaller cross-sections the halo phenomenology is likely to be indistinguishable from CDM, in particular the abundance of satellites around Milky-Way-like halos[Vogelsberger et al.(2012), Zavala et al.(2013)].

§5.2 Too-Big-to-Fail in SIDM

Thanks to the continually increasing numerical resolution in simulations, we can carry a more quantitative comparison of the numerical results and our Local Group. One concern that is always present in simulations where baryonic processes are included, is the difficulty to disentangle the relevance of each effect in the evolution of a galaxy.

As a way to get a better insight of how a given baryonic process, e.g. supernovae(SNe) feedback, cosmic rays, stellar winds, photoionization, etc., impacts the evolution of a galaxy, it is useful to conduct controlled simulations where only one process is acting.

In [Garrison-Kimmel et al.(2013)] they followed this approach in the context of CDM, they aim to study whether supernova feedback alone can solve the “Too Big to Fail” problem for Milky Way subhalos. They initialize a dark matter halo with $V_{max} = 35$ km/s at 2.2 kpc using a Hernquist (1990) sphere, which roughly follows the expected $\rho \propto r^{-1}$ dependence at small radius, these parameters are motivated by the predictions of cosmological abundance matching models, where galaxies with $L_V \sim 10^5 L_\odot$ form in dark matter halos with $V_{max} \sim 35$ km/s [Guo et al(2010)] and also from simulations of Milky Way-size halos where the Too-Big-To-Fail(TBTF) subhalos typically have $V_{max} > 35$ km/s [Boylan-Kolchin et al.(2012)]. They run convergence tests and find that in order to resolve up to 100pc the high resolution parameters are required, corresponding to 3×10^6 particles with particle mass of $760M_\odot$, halo mass $5 \times 10^9 M_\odot$ and $\epsilon = 10pc$, where the numerical effects due to lack of convergence (some of these described in [Power et al.(2003)]) may manifest up to $\sim 4\epsilon$, that is still smaller than 100pc (Fig 5.2).

Using the high resolution parameters in idealized numerical simulations, they model the dynamical effects of supernovae feedback through the use of a time-varying spherically-symmetric gravitational potential placed at the center of the halo, they did this by adding an externally tunable Hernquist potential to the N-body code Gadget2 [Springel(2005)] such that each particle has an additional acceleration given

$$\vec{a} = \frac{-GM_{gal}(t)\vec{r}}{[r - b(t)]^2 r}, \quad (5.1)$$

with M_{gal} the total mass in the potential at a time t and $b = r_{1/2}(\sqrt{2} - 1)$, $r_{1/2}$ is the half-mass radius of the potential. They fix $r_{1/2}$ and vary M_{gal} , they focus in the typical

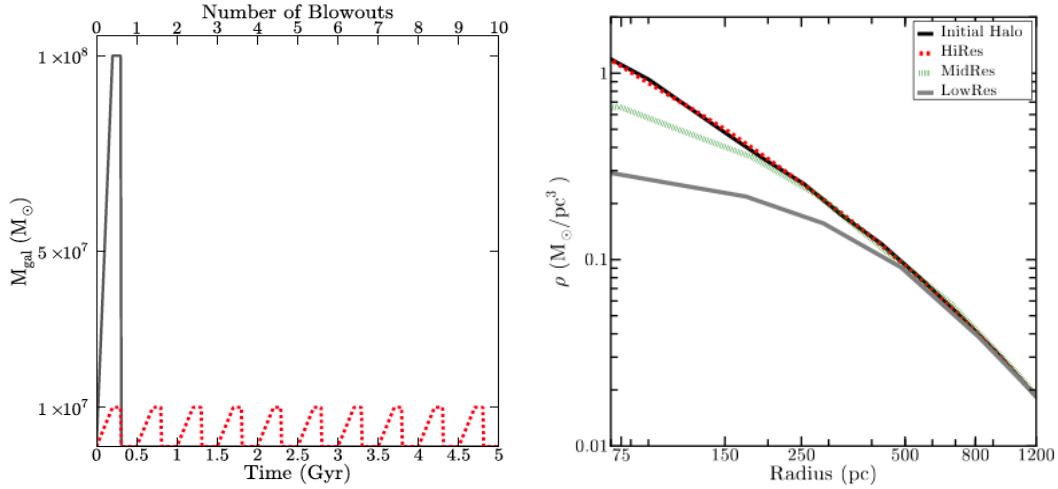


Figure 5.2: Plotted left: is the mass in the central potential as a function of time for the blowout scheme. The gray line shows how the mass varies for a single blowout with $M_{max} = 10^8 M_{\odot}$; the red dotted line shows the same for repeated blowouts with $M_{max} = 10^7 M_{\odot}$. A single cycle takes 500 Myr. These two cases result in the same cumulative total of mass displaced. Right: density profile for a CDM halo of $5 \times 10^9 M_{\odot}$ for different resolutions, unresolving the inner regions creates artificial cores[Garrison-Kimmel et al.(2013)].

value among the bright Milky Way dSphs of $r_{1/2} = 500 pc$. In order to mimic a blowout they vary M_{gal} in time according to the following cycle: first M_{gal} varies linearly from zero to its maximum value in 200 Myr (we can think of this as gas slowly accumulating in the center), it remains there for 100 Myr and then instantaneously returns to zero for another 200 Myr, the last step is what mimics the feedback from SNe (see figure 5.2).

They find that for a fixed amount of mass expelled from the galaxy (but not necessarily from the halo and hence it may be recycled) cyclic blowouts preferentially remove DM mass from the centers of halos, being most dramatic if $r_{1/2} = 100 pc$ for a fixed expelled mass. Despite the central density is reduced to a mild cusp $\rho \propto r^{-\alpha}$, with $\alpha \geq 0.5$, it is still above those observed in dSphs by [Walter & Peñarrubia(2011), Amorisco & Evans (2012)], they also found unlikely that SNe blowouts can affect the total mass within the stellar extent at the level required to resolve the TBTF problem without fine tuning, mainly because the required energy injected into the dark matter by explosive feedback exceeds, in six of the nine MW satellite galaxies of concern, the total available energy budget for all of the type

II supernova that have occurred in the galaxies assuming a typical initial mass function [Kroupa (2002)], where one expects approximately one SNII explosion per 100 M_{\odot} formed, these results consider that the energy is injected directly into the dark matter with 100% coupling. For instance, assuming a stellar-mass-to-light ratio M_*/L_V for Ursa Minor, the energy equivalent of more than 40,000 supernovae must be delivered with 100% efficiency directly to the dark matter in order to have the dwarf simulations agree with the mass of this galaxy.

The latter results suggest that in the CDM model solving simultaneously the cusp-core and TBFT requires more than just accounting for blowouts from SNe feedback. It is reasonable to question how the situation changes if self-interactions and blowout feedback from SNe are now working together.

To answer the question we use the same feedback model of [Garrison-Kimmel et al.(2013)] and consider two scenarios[Robles et al.(2015)], one in which each massive blowout cycle expels $10^8 M_{\odot}$ (A) and one less massive where $10^7 M_{\odot}$ (B) are driven out from the center of the halo. In order to maximize the differences between CDM and SIDM when baryons are included, we study the most efficient feedback model found in Garrison-Kimmel et al.(2013), thus, we use $r_{1/2} = 100$ pc. Following [Garrison-Kimmel et al.(2013)], we generated the initial condition(IC) with the publicly available code spherIC¹ and use the same parameters for the halo, the dark matter self-interactions were calculated using an SIDM smoothing length equal to 0.25ϵ , as described in [Rocha et al.(2013)].

From the last section σ/m seem to lie in the range $0.1 \text{ cm}^2\text{g}^{-1} < \sigma/m < 1 \text{ cm}^2\text{g}^{-1}$, [Miralda-Escude(2000), Yoshida et al.(2000), Davé et al.(2001), Peter et al.(2013)], taken $\sigma/m \approx 1 \text{ cm}^2\text{g}^{-1}$ is more consistent with dSphs and their observed core sizes as seen in [Rocha et al.(2013), Zavala et al.(2013)].

In [Peter et al.(2013)] they argue that $\sigma/m = 1 \text{ cm}^2\text{g}^{-1}$ may be in conflict with halo shapes in clusters, but taken into account the uncertainties in the halo shape analysis, and the preference of dSphs for such value, we decide to use $\sigma/m = 1 \text{ cm}^2\text{g}^{-1}$ in our analysis. All our simulations are high-resolution, that is, we use 3×10^6 particles, force softening of 10 pc and particle mass of $760 M_{\odot}$, these values guarantee that the radii of interest ($r < 1\text{kpc}$) is well resolved and the core, when formed, is due to self-interactions and not due to lack

¹The code and documentation can be downloaded from <https://bitbucket.org/migroch/spheric>.

of numerical resolution.

To compare with the standard model we do the simulations for CDM and SIDM for blowout (A) ten consecutive times, both are initialized with the same cusp profile (A_{cdm}, A_{sidm}), we run five blowouts type (B) for CDM and SIDM for the same IC ($B_{5,cdm}, B_{5,sidm}^{cusp}$), we also run the SIDM case but starting with a core profile ($B_{5,sidm}^{core}$), The initial condition with the core is taken from the isolated SIDM halo (no feedback) left to evolve for 10 Gyr, at this time the system has develop a core-like density profile and has become isothermal due to the self-interactions. To explore the effect of initializing the simulations with a cusp or core in a SIDM halo, we simulate only one blowout type (B) and let the system relax until 5 Gyrs ($B_{1,sidm}^{cusp}, B_{1,sidm}^{core}$), and compare them with one blowout type (B) in CDM ($B_{1,cdm}$). Finally inspired by the fact that some dwarf galaxies show more than one stellar population [Kirby et al.(2013), Weisz et al.(2014a), Willman & Strader(2012)], possibly indicating a starburst in the distant past and maybe another starburst some time later, we explore the case where a galaxy produces two major blowouts but they are sufficiently spaced (~ 3 Gyrs) so that the self-interactions have enough time to regrow the core after each event, for this two-blowout case, or type (C), we run two simulations, both start with the core-like IC and are subject to a blowout of $10^8 M_\odot$, then after 3 Gyrs we impart a second blowout ejecting $10^8 M_\odot$ in one of the runs (C_8) and ejecting $10^7 M_\odot$ (C_7) for the other run, after the blowout we let the system relax until 5 Gyrs.

We find that low mass ejections of $10^7 M_\odot$ are not effective enough to preclude the core from forming whereas massive blowouts not only conflict with the core formation but also erase any previous core if already present. We found a higher resistance of SIDM halos to be disrupted by feedback in the central regions, more events of massive blowout are needed in a SIDM simulation compared to its CDM counterpart to reach typical central densities of near dSphs [Wolf et al.(2010), Walker et al.(2009), Simon & Geha(2007), Muñoz et al.(2005), Koch et al.(2007), Mateo et al.(2008)]. This result is kept whether we start with a cuspy or a core density profile in the SIDM simulations. If we impart one more massive blowout to C_7 and C_8 we could bring the SIDM haloes to a better agreement with dSphs, however this would imply some star formation in the last few Gyrs which differs from the general trend of old stellar populations and the absence of current star formation found in dSphs.

In Figure 5.3 we see that SNe blowouts are more effective to reduce the central density if particles are collisionless, i.e. SIDM halos are less responsive to feedback. We can understand this as follows: when the SIDM halo is in isolation the collisions tend to make the velocity distribution isotropic, this is achieved by the displacement of DM particles with higher velocity dispersions in the outer regions toward the center where cold (lower velocity) particles reside, the particle displacement generates an inward heat flux that increases the collisions near the center. If SNe feedback is included, the particles receive an extra acceleration that decreases for large radii and changes their velocities such that fast moving particles are now located near the center, where the blowout is more effective, consequently there is a temporary inversion in the direction of heat transfer, particles move to the outside producing an outward heat flux, this effect is shown in the right panel of Figure 5.3. In the dynamical feedback scheme under consideration, when no feedback is acting $\vec{a} = \vec{0}$, called “*before infall*”, the inward flux is dominant and the interactions try to thermalize the halo, once the external potential reaches its maximum value and just before it returns to zero, we call this stage “*after infall*”, the outward flux is now dominant and the velocity dispersion changes drastically, the latter flux increases the number of collisions in various regions due to particles trying to escape and particles that were previously heading to the center, these regions act like “barriers” that preclude the escape of particles in the center and therefore make the effect of SN feedback less efficient to reduce the central density.

In Figure 5.4 we show the central densities at a distance of 250 pc for all of our simulations, the grey line represents the density of the isolated SIDM halo after 10 Gyrs and serves to compare the efficiency of SN feedback to reduce the central density in CDM and SIDM haloes. The simulations with values above that line started in a cuspy distribution. For both of the low energy feedback simulations (type A), SN feedback effects are extremely small and produce no relevant change to account for the observed densities in the bright dSphs, for the CDM runs this is consistent with the results of [Garrison-Kimmel et al.(2013)], in the SIDM halo small feedback translates into a negligible delay in the core formation, here the self-interactions are dominant and the halo is slowly thermalizing, the small effect is shown in Figure 5.4 noting that for this run the final value ends on top of the grey line.

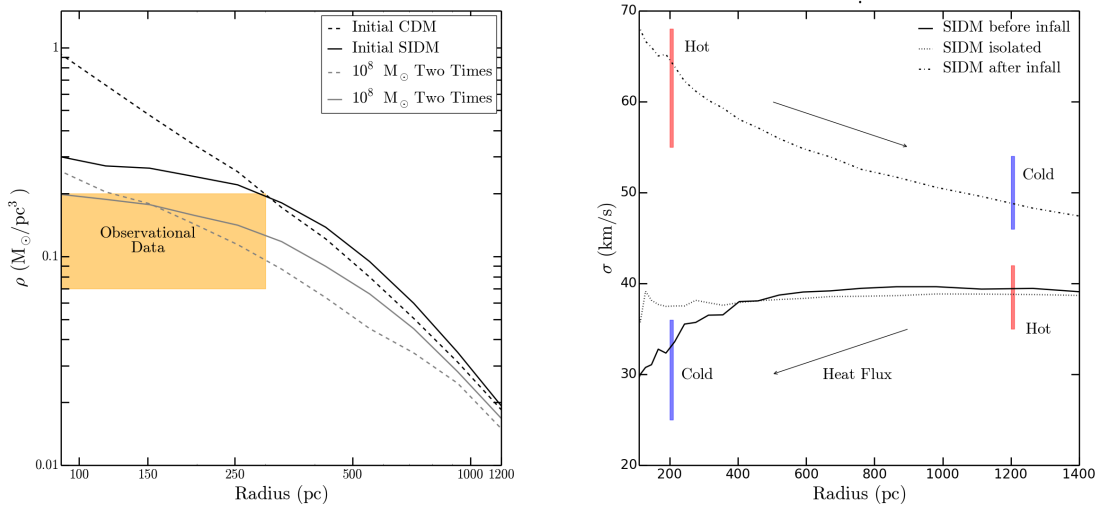


Figure 5.3: Left:Initial and final density profiles after two massive blowouts ejecting a total cumulative mass $1 \times 10^8 M_\odot$ for both SIDM (solid line) and CDM (dashed line). The shaded region shows observational data for bright dSphs with $r_{1/2}$ comparable to the one used in our simulations. Right:Velocity dispersion for SIDM in isolation, before and after the first infall of $10^8 M_\odot$. The arrows show the direction of the heat flux, before infall hotter particles transfer heat to cold ones in the center as expected from the SIDM scenario, however, at infall time there is an inversion of heat flux where the particles at the center, being now hotter, can move to the outer regions.

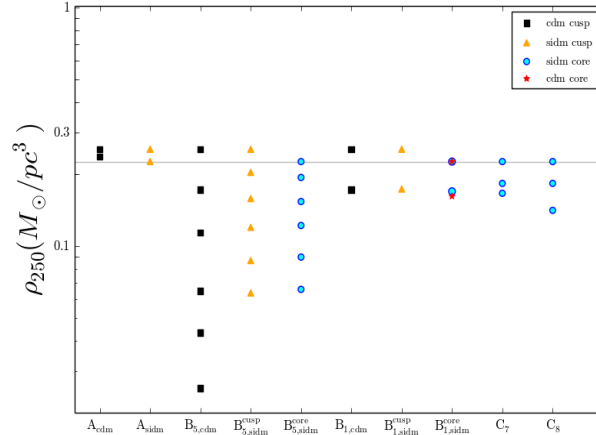


Figure 5.4: Densities at 250pc from the center for all the simulations. For simulations C_7 , C_8 , and all type B with 5 blowouts we plot the density after their respective blowouts. For all the other simulations we plot initial and final values only. The density always decreases after each blowout. The gray line represents the central density of a SIDM halo in isolation.

In fact, in case that observations confirm that low mass DM dominated systems possess large cores, SIDM would still be an attractive candidate, especially because low energy feedback events applied to collisionless particles cannot transform the characteristic cusp into a more constant density profile [Governato et al.(2012), Hopkins et al.(2014)]. Although we obtained that in the less massive SNe feedback scenario (blowouts of type A) the TBTF problem persists in both CDM and SIDM models, the result could change if we consider a full cosmological SIDM simulation, it has been seen that cosmological SIDM halos have lower central densities at the end of the simulations than our isolated run [Rocha et al.(2013), Zavala et al.(2013)], but it is possible that the difference is due to their lower numerical resolution, in fact, lately the increase in resolution could reopen the possibility of using larger values of $\sigma/m = 0.5 - 50 \text{ cm}^2/g$ and solve the TBTF issue and create cores of comparable sizes to those found in dSphs as suggested in [Elbert et al.(2014)]. Today, it seems clear that there is still work to be done in the SIDM model before it can be preferred over the standard paradigm.

CONCLUSIONS

In this thesis i have provided an overview of the current standing of the standard model of cosmology, also known as Cold Dark Matter(CDM). I have focused my study in the challenges at galactic scales that the model is currently facing and described some of the ideas in the literature that could bring the standard model to reasonable agreement with the newest observations. Being in the era of high-resolution observations, it is now possible to test some of the long standing theoretical predictions of the standard cosmological paradigm, so far the cosmological probes reveal an excellent agreement with the expected behavior in large scales. This seems to be continuously verified performing numerical simulations that include the relevant physical processes at those scales, at the same time these simulations also reveal the existence of discrepancies in the small scale regime, i.e. in galactic scales, some of the discrepancies treated in this thesis are the ubiquitous cusp-core problem, the missing satellite problem and the Too-Big-To-Fail issue.

In chapter 2 I have described in more detail solutions to these discrepancies in the cold dark matter model and their observational implications in dwarf galaxies. The most likely explanation seems to require modeling the interplay of astrophysical processes and the dark component in a self consistent way, seemingly only when the processes operate collectively is that we obtain the correct predictions. Although the latter is numerically plausible, there remains some skepticism of the results from hydrodynamical simulations, principally because the implemented routines that aim to describe the astrophysical process are in most cases approximations of our already incomplete understanding of baryonic processes.

Instead of blaming the stellar and gas physics for the apparent discrepancies of CDM predictions and observations in small scales, there exists the possibility that our assumptions on the dark matter are still missing something essential. Following the latter approach has

led to several proposals of dark matter models, two strong contenders were presented here, the scalar field dark matter(SFDM) and the self-interacting dark matter(SIDM) models. In Chapter 3 we described the status and conceptual bases of the SFDM model in the cosmological regime. We provided a classification of the models that assume an ultra light boson as dark matter to clearly identify the main properties of the dark matter particle under study. We propose that a spontaneous symmetry break in the early universe led to the decoupling of the scalar field, by means of the temperature corrections and the fact that the universe cools due to the expansion of the universe, at some time the temperature drops enough such that the symmetry break appears and we interpret that time when the scalar field decouples from the rest matter. Once the field is set in its new minimum, we can derive an explicit analytical approximation of the density distribution of a scalar field dark matter halo made of psyons(the corresponding bosonic dark matter particles) which is quite useful when dealing with observational tests in galactic scales.

We devote chapter 4 to evaluate the SFDM model in galactic scales. We focus our study in dwarf spheroidal galaxies, being the origin of the discrepancies found in CDM, they are suitable systems where we can test alternative models and possibly find clues to distinguish among the different DM proposals. We have found good agreement with the central shallow density slopes found in local dSphs, a consequence of the core profile predicted by the SFDM model whose origin lies in Heisenberg's uncertainty principle acting at $\sim 1\text{kpc}$ scales due to the small mass of the psyon. Assuming a mass of $m \approx 1 \times 10^{-22} \text{eV}/c^2$ for the psyon drastically decreases the formation of halos below $10^8 M_\odot$, additionally, we found that SFDM subhalos with $\sim \text{kpc}$ cores orbiting around MW-like hosts that also possess a SFDM halo, are more susceptible to be tidally disrupted when they closely interact with the host's disk, but that their stars can remain within the subhalos when the latter are in orbits whose pericenters are larger than the disk's length. If we assume one galaxy per halo the expected satellite abundance around Milky-Way-like galaxies should be smaller than the predicted value of CDM cosmological simulations, even the most massive ones, in the upcoming years identifying more satellites around massive hosts will help to set more stringent constraints on the SFDM model, in case the surveys increase the satellite abundance substantially we might need to reconsider the preference of the SFDM model over CDM, in the opposite case, the model offers a simpler explanation than the messy

baryonics physics to the missing satellite problem and possibly to the Too-Big-To-Big issue, although it is worth noticing that the value of the mass is constraint by observations and not predicted by the model.

Finally, in chapter 5 we discuss the status of the SIDM model regarding the cusp-core and TBTF issue. The appearance of high resolution hydrodynamical simulations, both cosmological and of isolated galaxies, have attracted the attention to the SIDM model of a large part of scientists in the past few years. The simulations imply that previous theoretical constraints on the cross-section per unit mass of $\sigma/m < 1 \text{ cm}^2/g$ can be modified and still give consistent results with the central masses of dwarf galaxies when baryons are included. There are increasingly more works suggesting that neither self-interactions with constant $\sigma/m < 0.5 \text{ cm}^2/g$ nor supernovae II feedback alone can account for the flattening of the central density profile in dSphs and simultaneously substantially reduce the missing satellite or the TBTF problem. In fact, we have shown that SIDM with constant $\sigma/m = 1 \text{ cm}^2/g$ (a preferential value to create core sizes comparable to the stellar half-mass radius in nearby dwarfs) and blowout feedback from SNe modeled by a time-varying potential that mimics the effect of a SNII explosion, produce very similar results to the CDM + baryons solution, and hence it is difficult to distinguish between these models when baryons are in the play. Slightly modifying the model to allow for a velocity dependent cross section has not reveal a substantial change to the predictions of constant σ/m , which can question the motivation to include the velocity dependence in the future. Despite SIDM being apparently indistinguishable from CDM for current constraints of the scattering cross section, it remains a viable model when astrophysical processes are accounted for in the simulations.

At this point, it seems that there is still much work to be done in SIDM and other models before they can become the new benchmark in cosmology, although there is a discouraging tone in the sentence, I have always found new ideas quite exciting. Even if it takes some time to develop them, they offer the opportunity for a great discovery, quoting the chinese philosopher Lao-tzu: “A journey of a thousand miles begins with a single step”.

Appendix

Publication List

- "Flat Central Density Profile and Constant DM Surface Density in Galaxies from Scalar Field Dark Matter" , Victor H. Robles, T. Matos, MNRAS, 422, 282-289 (2012)
- "Exact Solution to Finite Temperature SFDM: Natural Cores without Feedback", Victor H. Robles, T. Matos, ApJ , 763 , 19 (2013)
- "Strong Lensing with Finite Temperature Scalar Field Dark Matter" Victor H. Robles, T. Matos, 2013, Phys.Rev. D88, 083008 (2013)
- "Dwarf galaxies in multistate Scalar Field Dark matter halos" Martinez-Medina, L. A. , V. H. Robles, T. Matos, PRD 91, 023519 (2015)
- "Evolution of a dwarf satellite galaxy embedded in a scalar field dark matter halo" Victor H. Robles, V. Lora, T. Matos, F.J. Sanchez-Salcedo., arXiv:1404.3424, submitted to MNRAS
- "SFDM: A new formation mechanism of tidal debris" Victor H. Robles, L.A. Martinez-Medina, T. Matos 2015, arXiv:1503.00799, in revision.
- Victor H. Robles, James S. Bullock, Shea Garrison-Kimmel, O. Elbert, in preparation. (2015). I have included the main results from this work in Section 5.2.

Articles published in proceedings

- "Finite Temperature Density Profile in SFDM" Victor H. Robles, T. Matos, 2013. Published in Sources and Detection of Dark Matter and Dark Energy in the Universe, Ed. David Cline, Springer Proceedings in Physics, Vol. 148, Springer Netherlands, 2013, pp 17-24.

- "A Review on the Scalar Field Bose-Einstein Condensate Dark Matter Model" Abril Suarez, Victor H. Robles, Tonatiuh Matos, In: Accelerated Cosmic Expansion. Ed. By Claudia Moreno González, José Edgar Madríz Aguilar, and Luis Marina Reyes Barrera. Astrophysics and Space Science Proceedings, Vol. 38, Springer International Publishing, 2014, pp. 107-142.

Bibliography

- [Hogg et al. (2005)] Hogg D. et al., ApJ, 624, 54, (2005)
- [Komatsu et al. (2011)] Komatsu E. et al., ApJS, 182, 18 (2011)
- [Spergel et al. (2007)] Spergel D.N., et al., ApJS, 170, 377 (2007)
- [Page et al. (2007)] Page L., et al., ApJS, 170, 335 (2007)
- [Massimo(2008)] Massimo. G., A Primer on the Physics of the Cosmic Microwave Background, World Scientific, Singapore (2008)
- [Bertone et al. (2005)] Bertone et al., Physics Reports, 405, 279, (2005)
- [Taoso(2008)] Taoso M., Bertone G., Masiello A., JCAP 0803:022, (2008)
- [Sikivie & Yang (2009)] Sikivie P. & Yang Q., PRL, 103, 111301, (2009)
- [Dodelson (2003)] Dodelson S., Modern Cosmology, Academic Press, USA (2003)
- [Springel et al.(2006)] Springel V., Frenk C. S. & White S.D.M., Nature 440, 1137 (2006)
- [Feng (2010)] Feng J.L., Annual Review of Astronomy and Astrophysics, Vol. 48, 495 (2010)
- [Peccei & Quinn (1977)] Peccei R. D. and Quinn H. R., Phys. Rev. Lett. 38, 1440, 1977
- [Villaescusa-Navarro & Dalal (2011)] Villaescusa-Navarro F. & Dalal N., JCAP03, 024, (2011)

- [Viel et al.(2013)] Viel M., Becker G.D., Bolton J.S., Haehnelt M.G., PRD, 88, 043502, 2013
- [Souza et al.(2013)] de Souza R. S., Mesinger A., Ferrara A. et al., MNRAS, 432, 3218 (2013)
- [Macció et al.(2012)] Macció A.V., Paduroiu S., Anderhalden D., Schneider A. & Moore B.,MNRAS,424 (2), 1105 (2012).
- [Guo et al(2010)] Guo Q., White S., Li C., Boylan-Kolchin, M., MNRAS,404, Issue 3, 1111 (2010)
- [Guo et al(2011)] Guo Q. White S., Boylan-Kolchin M. et al., MNRAS, 413 (1): 101,(2011)
- [Hahn & Abel(2011)] Hahn O., Abel T., MNRAS, 415, 2101 (2011)
- [Seljak & Zaldarriaga(1996)] Seljak, U., & Zaldarriaga, M., ApJ, 469, 437 (1996)
- [Zaldarriaga, Seljak, & Bertschinger(1998)] Zaldarriaga, M., Seljak, U., Bertschinger, E., ApJ, 494, 491 (1998)
- [Zaldarriaga & Seljak(2000)] Zaldarriaga, M., & Seljak, U., ApJS, 129, pp 431-434 (2000)
- [Springel(2005)] Springel V.,MNRAS, 364, 1105 (2005)
- [Vogelsberger et al.(2014)] Vogelsberger M., Genel S., Springel V. et al., Nature,509, 177, (2014)
- [Vogelsberger et al.(2014b)] Vogelsberger M., Genel S., Springel V. et al.,arXiv:1405.2921 (2014b)
- [Genel et al.(2014)] Genel S., Vogelsberger M., Springel V.,et al. MNRAS, 445 (2): 175-200 (2014)
- [de Blok et al.(2001)] de Blok W. J. G., McGaugh S. S., Bosma A., & Rubin V. C., ApJ, 552, 23 (2001)

- [de Blok & Bosma(2002)] de Blok W. J. G. & Bosma A., *A&A*, 385, 816 (2002)
- [Swaters et al.(2003)] Swaters R. A., Madore B. F., van den Bosch F. C., & Balcells M., *ApJ*, 583, 732 (2003)
- [Navarro et al.(1996)] Navarro J. F., Frenk C. S., White S. D. M., *ApJ.*, 462, 563 (1996)
- [Navarro et al.(1997)] Navarro J. F., Frenk C. S., White S. D. M., *ApJ*, 490, 493 (1997)
- [Binney & Tremaine (2008)] Binney J. & Tremaine S., *Galactic Dynamics, Second Edition*, Princeton University Press, New Jersey,USA (2008)
- [Navarro et al.(2010)] Navarro J. F., Ludlow A., Springel V. et al., *MNRAS*, 402, 21 (2010)
- [Springel et al.(2008)] Springel V., Wang J., Vogelsberger M. et al., *MNRAS*, 391,1685 (2008)
- [Klypin et al.(1999)] Klypin A. et al., *ApJ*. 522,82 (1999).
- [Simon & Geha(2007)] Simon J. D., Geha M., *ApJ*, 670, 313 (2007)
- [Strigari et al.(2007)] Strigari L.E. , Bullock J.S., Kaplinghat M., et al. *ApJ* 669 676 (2007)
- [Spergel et al.(2007)] Spergel D. N., Bean R., Doré O. et al., *Astrophys.J.Suppl.* 170:377 (2007)
- [Ade et al. (2007)] Planck Collaboration: Ade P. A.R., Aghanim N., Alves M.I.R. et al., *A&A*, 571 (2014) A1
- [Boylan-Kolchin et al. (2014)] Boylan-Kolchin M., Bullock J.S., Garrison-Kimmel S., *MNRAS*, 443, L44 (2014)
- [Peñarrubia et al. (2012)] Peñarrubia J., Pontzen A., Walker M.G., Kroupa S. E., *ApJ* 759 L42 (2012)
- [Pawlowski et al.(2013)] Pawlowski M.S., Kroupa P., Jerjen H., arXiv:1307.6210 (2013)
- [Pawlowski & McGaugh (2014)] Pawlowski M. & McGaugh S., *ApJL*, 789, L2 (2014)

- [Tully (1982)] Tully B., *Astrophys. J.* 257: 389–422 (1982)
- [Garrison-Kimmel et al. (2014a)] Garrison-Kimmel S., et al., *MNRAS*, 438, 2578 (2014a)
- [Garrison-Kimmel et al. (2014b)] Garrison-Kimmel S., Boylan-Kolchin M., Bullock J.S., Kirby E.N., *MNRAS* 444, 222 (2014b)
- [Ibata et al.(2013)] Ibata R. et al. *Nature* 493, 62 (2013)
- [Brook et al.(2014)] Brook C. et al., *ApJL*, 784, L14 (2014)
- [Governato et al.(2012)] Governato F. et al., *MNRAS*, 422, 1231 (2012)
- [Di Cintio et al.(2013)] Di Cintio, Knebe, A., Libeskind, N. I., et al., *MNRAS*, 431, 1220 (2013)
- [Boylan-Kolchin et al.(2011)] Boylan-Kolchin M., Bullock J. S., Kaplinghat M., *MNRAS*, 415, L40 (2011)
- [Power et al.(2014)] Power C., Wynn G. A., Robotham A.S. G. et al., arXiv:1406.7097 (2014)
- [Sawala et al.(2014)] Sawala T., Frenk C.S., Fattahi A. et al. arXiv:1404.3724 (2014)
- [Vogelsberger et al.(2014)] Vogelsberger M., Zavala J., Simpson C., Jenkins A., *MNRAS*, 444, 3684 (2014)
- [Hopkins et al.(2014)] Hopkins P. F. et al., *MNRAS*, 445, 581 (2014)
- [Oñorbe et al.(2015)] Oñorbe J., Boylan-Kolchin M., Bullock J.S. et al. arXiv:1502.02036 (2015)
- [Hopkins (2014)] Hopkins P.F., arXiv:1409.7395 (2014)
- [Trujillo-Gomez et al.(2015)] Trujillo-Gomez S., Klypin A., Colin P. et al., *MNRAS*, 446, 1140 (2015)
- [Gallazzi et al.(2005)] Gallazzi A., Charlot S., Brinchmann J., White S. D. M., Tremonti C. A., *MNRAS*, 362, 41 (2005)

- [Kirby et al.(2013)] Kirby E. N., Cohen J. G., Guhathakurta P., et al., ApJ, 779, 102 (2013)
- [Peñarrubia et al.(2010)] Peñarrubia J. et al. MNRAS 406, 1290 (2010)
- [Łokas et al.(2012)] Łokas E. L., Majewski S.R., Kazantzidis S. et al. ApJ 751, 61 (2012)
- [Zolotov et al.(2012)] Zolotov A., Brooks A. M., Willman B., et al., ApJ 761 71 (2012)
- [Brooks & Zolotov (2014)] Brooks A. M. and Zolotov A., ApJ 786 87 (2014)
- [Hayashi & White (2006)] Hayashi E. & White S.D.M, MNRAS, 370, L38 (2006)
- [Lee & Komatsu (2010)] Lee J. and Komatsu E., ApJ.718,60-65 (2010)
- [Bullock et al. (2001)] Bullock J. S. et al. ApJ, 555, 240 (2001)
- [van den Bosch et al. (2001)] van den Bosch F. C., Burkert A., and Swaters R.A.,MNRAS, 326, 1205, 2001.
- [Peebles & Nusser (2010)] Peebles P.J.E. & Nusser Adi, Nature, 465, 565 (2010)
- [Taehyun et al. (2012)] Taehyun K., Sheth K., Hinz J.L. et al., ApJ, 753, 43 (2012)
- [Hau & Forbes (2006)] Hau G.K.T., & Forbes D.A., MNRAS, 371, 633 (2006)
- [Koprolin & Zeilinger (2000)] Koprolin, W., Zeilinger, W., A&A, 145, 71 (2000)
- [Goodman & Witten (1985)] Goodman M.W. & Witten E., Phys. Rev. D 31, 3059 (1985).
- [Scherrer & Turner(1986)] Scherrer R.J. and Turner M.S., Phys. Rev. D 33, 1585 (1986).
- [Drukier et al. (1986)] Drukier A. K., Freese K., and Spergel D.N., Phys. Rev. D 33, 3495 (1986).
- [Bauer et al. (2013)] Bauer et al., arXiv:1305.1605 (2013)
- [Griest & Kamionkowski (2000)] Griest K. & Kamionkowski M., Physics Reports 333, 167 (2000)

- [Aad et al.(2013)] Aad G. et al., Journal of High Energy Physics 10, 130 (2013)
- [Carroll (1998)] Carroll S. M., Physical Review Letters 81, 3067 (1998),
- [Arkani et al. (1999)] Arkani-Hamed N., Dimopoulos S., and Dvali G., Phys. Rev. D 59, 086004 (1999)
- [Hu, Barkana & Gruzinov(2000)] Hu W., Barkana R., Gruzinov A., Phys.Rev.Lett. 85, 1158 (2000)
- [Schive et al.(2014)] Schive H.-Y., Chiueh T., Broadhurst T., Nature Physics, 10, 496 (2014)
- [Goodman (2000)] Goodman J., New Astronomy,vol. 5, Issue 2, 103 (2000)
- [Slepian & Goodman (2012)] Slepian Z.,& Goodman J., MNRAS, 427, 839 (2012)
- [Peebles(2000)] Peebles P.J.E., ApJ, 534, L127 (2000)
- [Colpi,Shapiro,& Wasserman(1986)] Colpi M., Shapiro S. L., & Wasserman I., PRL, 57, 2485 (1986)
- [Matos & Ureña(2001)] Matos, T., & Ureña-López, L.A. PRD, 63, 063506 (2001)
- [Guzmán & Matos(2000)] Guzmán, F. S., & Matos, T., Class. Quant. Grav., 17, L9 (2000)
- [Bernal et al.(2010)] Bernal A., Barranco J., Alic D., & Palenzuela C., PRD, 81, 044031 (2010)
- [Robles & Matos(2013)] Robles V.H., & Matos T., ApJ, 763, 19 (2013)
- [Harko(2011)] Harko T., PRD, 83, 123515 (2011)
- [Chavanis(2012)] Chavanis P.H., A&A 537, A127 (2012)
- [Li et al.(2014)] Li B., Rindler-Daller T., & Shapiro P.R., PRD, 89, 083536 (2014)
- [Sikivie(2012)] Sikivie P., arXiv:1210.0040 (2012)
- [Davidson & Elmer(2013)] Davidson S., & Elmer M., JCAP12, 034 (2013)

- [Ureña-Lopez(2009)] Ureña-Lopez L.A., JCAP01, 014 (2009)
- [Kapusta (1981)] Kapusta I. Phys. Rev. D 24, 426 (1981).
- [Haber & Weldon (1982)] Haber H.E. & Weldon H.A., PRD 25, 502 (1982)
- [Erken et al.(2012)] Erken O., Sikivie P., Tam H. and Yang Q.,PRD 85, 063520 (2012)
- [Governato et al.(2010)] Governato F., Brook C., Mayer L. et al., Nature, 463, 203 (2010)
- [Pontzen & Governato(2012)] Pontzen A., & Governato F., MNRAS, 421, 3464 (2012)
- [Scannapieco et al.(2012)] Scannapieco C., Wadepuhl M., Parry O.H. et al., MNRAS, 423, 1726 (2012)
- [Magaña et al.(2012)] Magaña J., Matos T., Suárez A., Sánchez-Salcedo F. J. , JCAP,10,003, 2012
- [Matos et al.(2009)] Matos T., Vazquez-Gonzalez A., Magaña J., MNRAS, 393, 1359, (2009)
- [Pitaevskii & Stringari(2003)] Pitaevskii L.P. & Stringari S., Bose-Einstein Condensation, International Series of Monographs on Physics (Clarendon Press, 2003).
- [Woo & Chihue(2009)] Woo T.P.& Chiueh T., ApJ, 697, 850 (2009)
- [Dutta & Scherrer (2010)] Dutta S. & Scherrer R.J., Phys. Rev. D 82, 083501 (2010)
- [Steigman (2012)] Steigman G., arXiv:1208.0032 (2012)
- [Durrer (2008)] Durrer R., The Cosmic Microwave Background, Cambridge University Press, Cambridge (2008)
- [Liddle & Lyth (2000)] Liddle A. & Lyth D.H., Cosmological Inflation and Large-Scale Structure, Cambridge University Press, Cambridge (2000).
- [Malik(2001)] Malik K.A., Ph.D. Thesis, University, arxiv: astro-ph/0101563 (2001)
- [Ma & Bertschinger(1995)] Ma C.P. & Bertschinger E., ApJ, 455,7 (1995)

- [Ma et al. (1999)] Ma C.P., Caldwell R., Bode R. & Wang L., ApJ, 521, L1, (1999)
- [Hwang& Noh (2001)] Hwang J.C., & Noh H., PRD, 64, 103509, (2001)
- [Marsh & Silk(2014)] Marsh D.J.E., & Silk J., MNRAS, 437, 2652 (2014)
- [Marsh & Ferreira(2010)] Marsh D. J. E., Ferreira P.G., Physical Review D, 82, 103528 (2010)
- [Park et al. (2012)] Park C.G., Hwang J., Noh H., PRD, 86, 083535 (2012)
- [Suárez & Matos (2011)] Suárez A., Matos T., MNRAS, 416, 87 (2011)
- [Suárez & Chavanis (2015)] Suárez A., Chavanis P.H., arXiv:1503.07437
- [Bode et al.(2001)] Bode P., Ostriker J.P., Turok N., ApJ, 556, 93 (2001)
- [Press & Schechter (1974)] Press W. H., Schechter P., ApJ, 187, 425 (1974)
- [Sheth & Tormen (1999)] Sheth R. K., Tormen G., MNRAS, 308, 119 (1999)
- [Bozek et al.(2015)] Bozek B., Marsh D. J. E., Silk J., Wyse R.F.G., MNRAS 450, 209 (2015)
- [Bogolyubov & Shirkov (1980)] Bogolyubov N.N.& Shirkov D.V., Introduction to the theory of quantized fields, Wiley, New York (1980)
- [Coleman & Weinberg(1973)] Coleman S. & Weinberg E.J. PRD, 6, 1888 (1973)
- [Jackiw (1973)] Jackiw R., PRD, 9, 1686 (1973)
- [’t Hooft(1971)] ’t Hooft, Nucl. Phys. B35, No. 1, 167 (1971)
- [Slavnov & Faddeev (1980)] Slavnov A.A.& Faddeev L.D., Gauge Fields: Introduction to Quantum Theory, Benjamin-Cummings, London (1980)
- [Taylor(1976)] Taylor J.C., Gauge Theories of Weak Interactions, Cambridge University Press, Cambridge (1976)
- [Linde (1976)] Linde A.D., JETP Lett., 23, 73 (1976)

- [Linde (1979)] Linde A.D., Rep. Prog. Phys., 42, 389 (1979)
- [Landau & Lifshitz (1968)] Landau L.D. & Lifshitz E.M., Statistical Physics, Pergamon, London (1968)
- [Linde (1990)] Linde A.D., Particle Physics and inflationary cosmology, Harwood Academic Publishers, Switzerland (1990)
- [Weinberg (1974)] Weinberg S., PRD, 9, 3320 (1974)
- [Dolan & Jackiw (1974)] Dolan & Jackiw, PRD, 9, 3357 (1974)
- [Kirzhnits (1972)] Kirzhnits D.A., JETP Lett., 15, 529 (1972)
- [Kirzhnits & Linde (1972)] Kirzhnits D.A. & Linde A.D., Phys. Rev. Lett., 42B, 471 (1972)
- [Ureña-López (2009)] Ureña-López L.A., JCAP01, 014, (2009)
- [Robles & Matos (2013)] Robles V.H. & Matos T., ApJ, 763, 19 (2013)
- [Sin (1994)] Sin S.J., PRD,50, 3650 (1994)
- [Ureña-Lopez(2002)] Ureña-Lopez L.A., Class. Quant. Grav., 19, 2617 (2012)
- [Ureña-López & Bernal(2010)] Ureña-López L.A., & Bernal A., PRD, 82, 123535 (2010)
- [Ureña-Lopez,Valdez-Alvarado, & Becerril(2012)] Ureña-Lopez L.A., Valdez-Alvarado S., Becerril R., Class.Quant.Grav., 29, 065021 (2012)
- [Arbey et al.(2003)] Arbey A., Lesgourgues J., & Salati P., PRD, 68, 023511 (2003)
- [Balakrishna, Seidel, & Suen(1998)] Balakrishna J., Seidel E., & Suen W-M., PRD, 58, 104004 (1998)
- [Bernal et al.(2010)] Bernal A., Barranco J., Alic D., & Palenzuela C., PRD, 81, 044031 (2010)
- [Kaup (1968)] Kaup D. J., Phys. Rev. 172, 1331 (1968)

- [Ji & Sin (1994)] Ji S. U. and Sin S. J., Phys. Rev. D, 50, 3655 (1994)
- [Ruffini & Bonazzola (1969)] Ruffini R. & Bonazzola S., Phys. Rev., 187 ,1767 -1783 (1969)
- [Glesier (1988)] Gleiser M. Phys.;. Rev. D, 38, 2376 (1988)
- [Friedbeg (1987)] Friedbeg R. et al., Phys. Rev. D, 35, 3640 (1987)
- [Arbey et al.(2002)] Arbey A., Lesgourgues J., and Salati P., PRD 65, 083514 (2002)
- [Guzmán & Ureña-López(2004)] Guzmán F.S., & Ureña-López L.A., PRD, 69, 124033 (2004)
- [Guzmán & Matos(2000)] Guzmán, F. S., & Matos, T., Class. Quant. Grav., 17, L9 (2000)
- [Seidel & Suen(1991)] Seidel E., & Suen W.M., PRL, 66 , 1659 (1991)
- [Lee & Koh(1996)] Lee J.W, & Koh I.G., PRD, 53, 2236 (1996)
- [Lee & Lim(2010)] Lee J.W., & Lim S., JCAP01, 007 (2010)
- [Bray(2012)] Bray H.L., 2012, arXiv:1212.5745
- [Böhmer & Harko(2007)] Böhmer C.G., & Harko T., JCAP06, 025 (2007)
- [Robles & Matos(2012)] Robles V.H., & Matos T., MNRAS, 422, 282 (2012)
- [Rindler-Daller & Shapiro(2012)] Rindler-Daller T., Shapiro P.R., MNRAS, 422, 135 (2012)
- [Rindler-Daller & Shapiro(2014)] Rindler-Daller T., & Shapiro P.R., Mod. Phys. Lett. A, 29, 1430002 (2014)
- [Briscese(2011)] Briscese F., Phys.Lett.B, 696, 315 (2011)
- [Chavanis (2011)] Chavanis P.H., Phys. Rev. D 84, 043531 (2011)
- [Chavanis & Delfini (2011)] Chavanis P.H., Delfini L., Phys. Rev. D 84, 043532 (2011)

- [Chavanis & Harko (2012)] Chavanis P.H., Harko T., PRD 86, 064011 (2012)
- [Seidel & Suen(1990)] Seidel E., & Suen W-M., PRD, 42, 384 (1990)
- [Guzman et al.(2014)] Guzman F.S., Lora-Clavijo F. D. et al. PRD, 89, 063507 (2014)
- [Matos & Ureña-López(2007)] Matos T., Ureña-López L.A., Gen. Relativ. Gravit., 39, 1279 (2007)
- [Robles & Matos(2013b)] Robles V.H., & Matos T. Phys. Rev. D 88, 083008 (2013b)
- [Walter & Peñarrubia(2011)] Walker, M. G., & Peñarrubia, J., ApJ, 742, 20 (2011)
- [Madau et al.(2014)] Madau P., Weisz D.R., Conroy C., 2014, ApJ, 790, L17
- [Weisz et al.(2014a)] Weisz D. R. et al., ApJ 789 147 (2014a)
- [Weisz et al.(2014b)] Weisz D. R. et al., ApJ 789 148 (2014b)
- [Weisz et al.(2014c)] Weisz D. R., Skillman E.D., et al. ApJ, 789, 24 (2014c)
- [Weisz et al.(2015)] Weisz D. R. et al., ApJ 804 136 (2015)
- [Kuzio de Naray & Spekkens(2011)] Kuzio de Naray R.,& Spekkens K., ApJ, 741, L29 (2011)
- [Kuzio de Naray & Kaufmann(2011)] Kuzio de Naray R., & Kaufmann T., MNRAS, 414, 3617 (2011)
- [Kuzio de Naray et al.(2010)] Kuzio de Naray R. et al., ApJ, 710, L161 (2010)
- [Walker et al.(2009)] Walker M. G., Mateo M., Olszewski E. W., et al., ApJ, 704, 1274 (2009)
- [Lokas(2009)] Lokas, E. L., MNRAS, 394, L102 (2009)
- [Salucci et al.(2011)] Salucci P., Wilkinson M.I., Walker M.G., et al., MNRAS, 420 2034 (2011)
- [Walker et al.(2010)] Walker, M. G., McGaugh, S. S. et al., ApJ, 717, L87 (2010)

- [Lora & Magaña(2014)] Lora V. & Magaña J., JCAP, 09, 011 (2014)
- [Diez-Tejedor et al.(2014)] Diez-Tejedor A., Gonzalez-Morales A. X., Profumo S., PRD, 90, 043517 (2014)
- [Martinez-Medina, Robles, & Matos(2015)] Martinez-Medina L.A., Robles V.H., & Matos T., PRD, 91, 023519 (2015)
- [Navarro et al.(2010)] Navarro, J.F., Ludlow, A., Springel V., et al., MNRAS, 402, 21 (2010)
- [Merrit et al.(2006)] Merrit D., Graham A.W., Moore B., Diemand, J., & Terzić, B., ApJ, 132, 2685 (2006)
- [Graham et al.(2006)] Graham, A.W., Merrit, D., Moore, B., Diemand, J., & Terzić, B, AJ, 132, 2701 (2006)
- [Robles et al.(2014)] Robles V. H., Lora V., Matos T., Sanchez-Salcedo F. J., arXiv:1404.3424 (2014)
- [Martin et al.(2008)] Martin N. F., de Jong J. T. A., Rix H. W., ApJ, 684, 1075 (2008)
- [Odenkirchen et al.(2001)] Odenkirchen M., Grebel E. K., Harbeck, D., Dehnen, W. et al., AJ, 122, 2538 (2001)
- [Miyamoto & Nagai(1975)] Miyamoto M., & Nagai R., PASJ, 27, 533 (1975)
- [Collins et al.(2014)] Collins M. L. M., Chapman S. C., Rich R. M., et. al, ApJ, 783, 7 (2014)
- [Klimentowski et al.(2009)] Klimentowski, J., Łokas, E. L., Kazantzidis, S., Mayer, L., Mamon, G.A., MNRAS, 397, 2015 (2009)
- [Łokas et al.(2012)] Łokas E. L., Kazantzidis S., & Mayer L., ApJ, 751, L15 (2012)
- [Robles, Medina & Matos (2015)] Victor H. Robles, L.A. Martinez-Medina, T. Matos, arXiv:1503.00799 (2015)

- [Hayes et al.(2006)] Hayes J.C., Norman M.L., Fiedler R.A., ApJS, 165, 188 (2006)
- [Spergel & Steinhardt (2000)] Spergel D. N., Steinhardt P. J., Phys.Rev.Lett., 84,3760 (2000)
- [Burkert(2000)] Burkert, A., Astrophys. J. Lett., 534, L143 (2000)
- [Miralda-Escude(2000)] Miralda-Escude J., Astrophys. J., 564, 60 (2002)
- [Kochanek & White(2002)] Kochanek C. S., & White M., ApJ, 543, 514 (2002)
- [Rocha et al.(2013)] Rocha M., Peter A. H. G., Bullock J. S. et al. MNRAS, 430, 81 (2013)
- [Peter et al.(2013)] Peter A. H. G., Rocha M., Bullock J. S., & Kaplinghat M.,MNRAS, 430, 105 (2013)
- [Vogelsberger et al.(2012)] Vogelsberger M., Zavala J., & Loeb A., MNRAS, 423, 3740 (2012)
- [Newman et al.(2013a)] Newman A. B. et al., Astrophys. J., 765, 24 (2013a)
- [Newman et al.(2013b)] Newman A. B. et al., Astrophys. J., 765, 25 (2013b)
- [Markevitch et al.(2004)] Markevitch M. et al. ApJ 606 819 (2004)
- [Kaplinghat et al.(2014)] Kaplinghat M., Keeley R. E., Linden T., Yu H.B. , Phys. Rev. Lett. 113, 021302 (2014)
- [Bastidas Fry et al.(2015)] Bastidas Fry A., Governato F., Pontzen A. et al., arXiv:1501.00497 (2015)
- [Vogelsberger et al.(2014)] Vogelsberger M., Zavala J., Simpson C., Jenkins A., arXiv:1405.5216 (2014)
- [Clowe et al.(2006)] Clowe, D. et al., Astrophys.J. Lett., 648, L109 (2006)
- [Randall et al.(2008)] Randall, S. W. et al., Astrophys. J., 679, 1173 (2008)
- [Dawson et al.(2012)] Dawson W. A., et al., Astrophys. J. Lett., 747, L42 (2012)

- [Ackerman et al.(2009)] Ackerman, L., Buckley, M. R., Carroll, S. M., & Kamionkowski, M., Phys Rev D, 79, 023519 (2009)
- [Buckley & Fox (2010)] Buckley, M. R., & Fox, P. J., PRD, 81, 083522 (2010)
- [Feng et al. (2010)] Feng, J. L., Kaplinghat, M., & Yu H.-B., Physical Review Letters, 104, 151301 (2010)
- [Tulin et al. (2013a)] Tulin, S., Yu, H.-B., & Zurek, K. M., Physical Review Letters, 110, 111301 (2013a)
- [Tulin et al. (2013b)] Tulin, S., Yu, H.-B., & Zurek, K. M., arXiv:1302.3898 (2013b)
- [Zavala et al.(2013)] Zavala, J., Vogelsberger, M., & Walker, M. G. 2013, MNRAS, 431, L20 (2013)
- [Harvey et al.(2015)] Harvey D., et al., Science, volume 347 no. 6229, 1462 (2015)
- [Foot (2014)] Foot R., International Journal of Modern Physics A 29, 30013 (2014)
- [Boddy et al.(2014)] Boddy K. K. et al, PRD 89, 115017 (2014)
- [Cline et al.(2014)] Cline J. M. et al., PRD 90, 015023 (2014)
- [Vogelsberger et al.(2013)] Vogelsberger, M., Genel, S., Sijacki, D., et al., MNRAS, 436, 3031 (2013)
- [Springel (2010)] Springel, V., MNRAS, 401, 791 (2010)
- [Feng et al.(2009)] Feng, J. L., Kaplinghat, M., Tu, H., & Yu, H.-B., JCAP, 7, 4 (2009)
- [Loeb & Weiner(2011)] Loeb A., Weiner N., PRL, 106, 171302 (2011)
- [Garrison-Kimmel et al.(2013)] Garrison-Kimmel S. et al., MNRAS 433, 3539 (2013)
- [Boylan-Kolchin et al.(2012)] Boylan-Kolchin M., Bullock J. S., & Kaplinghat M., MNRAS, 422, 1203 (2012)
- [Amorisco & Evans (2012)] Amorisco N. C., & Evans N. W., MNRAS, 419, 184 (2012)

- [Kroupa (2002)] Kroupa, P., *Science*, 295, 82 (2002)
- [Yoshida et al.(2000)] Yoshida N., Springel V., White S. D. M., Tormen G., *ApJ*, 544, L87 (2000)
- [Davé et al.(2001)] Davé R., Spergel D. N., Steinhardt P. J., Wandelt B. D., *ApJ*, 547, 574 (2001)
- [Willman & Strader(2012)] Willman B. & Strader J., *The Astronomical Journal*, 144, 76 (2012)
- [Muñoz et al.(2005)] Muñoz R. R. et al., *ApJ*, 631, L137 (2005)
- [Wolf et al.(2010)] Wolf J., Martinez G. D., Bullock J. S. et al., *MNRAS*, 406, 1220 (2010)
- [Koch et al.(2007)] Koch A., Kleyna J. T., Wilkinson M. I., et al., *AJ*, 134, 566 (2007)
- [Power et al.(2003)] Power et al. *MNRAS* 338, 14 (2003)
- [Kauffmann (2014)] Kauffmann, G., arXiv:1401.8091(2014)
- [Mateo et al.(2008)] Mateo M., Olszewski E. W., Walker M. G., *ApJ*, 675, 201 (2008)
- [Elbert et al.(2014)] Elbert O.D., Bullock J.S. et al., arXiv:1412.1477 (2014)
- [Robles et al.(2015)] Robles V.H., Bullock J.S., et al., in preparation. (2015b)